Oscillation and non-equilibrium behaviour of supramolecular disulfides



A thesis submitted for the MSc by Research in Chemistry

Trinity Term 2025

Zhiheng Zhang

St Edmund Hall

Abstract

Chemical oscillation is a unique type of chemical reaction in which the reactants and products fluctuate rather than achieving a thermodynamic steady state. Due to their non-equilibrium, self-organisation, and energy dissipative characteristics, oscillating systems are considered to play a significant role in living behaviours.

This thesis investigates the emergence of oscillations from synthetic supramolecular disulfide systems through both experiments and mathematical modelling. Experimental efforts create a chemically fuelled, self-replicating vesicle system capable of exhibiting oscillations in both molecular concentrations and supramolecular structure. These oscillations are driven by a physical autocatalytic network and sustained through continuous fuel input, resembling biological cycles such as replication, growth, and collapse.

Complementing the experimental study, a theoretical framework is developed to explain the mechanism of supramolecular chemical oscillation. A delayed-differential kinetic model is created and validated through numerical simulations. It captures the key features of chemical kinetics and bifurcation in the oscillating system. Moreover, the model provides some quantitative insights into the control of oscillations through parameters such as fuel supply rates, stirring rates, and catalysts. Lastly, a model for mixed oscillators is formulated to simulate the synchronisation and competition between two surfactants, offering a theoretical framework for constructing more complex reaction networks.

Overall, the thesis connects experimental and theoretical approaches to enhance the understanding of how non-equilibrium chemical systems can exhibit oscillation and life-like behaviour, providing conceptual and practical insights for origin-of-life research and the design of artificial life-like complex systems.

Table of Contents

1. General Introductions 1

1.1 The origin of life 1

1.1.1 Definitions of life 2

1.1.1.1 Metabolism 2

1.1.1.2 Responsiveness 4

1.1.1.3 Reproduction 5

1.1.1.4 Summary 6

1.1.2 Theories and research methods on the origin of life 6

1.1.2.1 Synthetic systems with fuel and metabolism 8

1.1.2.2 Artificial chemical reaction networks 10

1.1.2.3 Self-replicating systems and autocatalysis 12

1.2 Chemical oscillation 17

1.2.1 Basic principles of chemical oscillation 18

1.2.1.1 Oscillations based on feedback loops 18

1.2.1.2 Oscillations based on time delays 20

1.2.1.3 The thermodynamic view of chemical oscillations 21

1.2.2 Classifications of chemical oscillators 24

1.2.2.1 Chemical oscillators on the molecular scale 24

1.2.2.2 Chemical oscillators on the macromolecular and supramolecular scale 26

1.2.2.3 Chemical oscillators on the macroscopic scale 27

1.2.3 Applications of chemical oscillators 29

2. A Chemical Reaction Network Drives Complex Population Dynamics in Oscillating Self-Reproducing Vesicles 30

2.1 Introduction 30

2.2 Results and discussion 33

2.2.1 Molecular oscillations 33

2.2.2 Supramolecular oscillations 36

2.2.3 Non-equilibrium supramolecular behaviour during oscillations 40

2.3 Conclusions 42

3. Mathematical Models for Self-Catalytic Supramolecular Chemical Oscillators 43

3.1 Introduction 43

3.2 A mathematical model of the oscillating supramolecular self-replicator 44

3.2.1 The reaction kinetic model 44

3.2.2 The simulation of oscillation experiments 46

3.2.3 The role of the fuel supply 47

3.2.4 Control of oscillations 49

3.3 The modelling of the mixed oscillators 52

3.3.1 Two-surfactant kinetic model 52

3.3.2 Competition and synchronisation 53

3.4 Conclusions 55

4. Conclusions and Future Works 56

5. Experimental and Simulation Details 58

5.1 Supplementary methods and data of Chapter 2 58

5.1.1 Oscillation experiments 58

5.1.2 Sampling and UPLC measurements 58

5.1.3 iSCAT measurements 59

5.1.4 DLS measurements 60

5.1.5 Synthesis of compounds 61

5.1.6 UPLC Calibration 65

5.1.7 Contrast-to-mass calibration of iSCAT 68

5.1.8 DLS measurements of 1 69

5.1.9 Replications of iSCAT measurements shown in Fig 5 70

5.1.10 iSCAT of the vesicles of 1 in steady state 72

5.1.11 Replication of chemical oscillation with extended time 74

5.1.12 Cryo-TEM measurements of vesicles of 1 74
5.1.13 NMR spectra 77
5.2 Supplementary methods and data of chapter 3 83
5.2.1 Derivation of non-dimensionalised rate equations 83
5.2.2 The time-delayed kinetic model 84
5.2.3 Simulation details 85
5.2.3.1 The parameter settings in 3.2.2 86
5.2.3.2 The parameter settings in 3.2.3 86
5.2.3.3 The parameter settings in 3.2.4 86
5.2.3.4 The parameter settings in 3.3.2 87
5.2.4 Derivations of the kinetic model of mixed oscillators 88
6. References 90

Abbreviations

°C	degrees Celsius
bpy	2,2’-bipyridine
B-Z reaction	Belousov–Zhabotinsky reaction
cat.	catalytic
CIMA	chlorite-iodide-malonic acid
CMC	critical micelle concentration
CRNs	chemical reaction networks
cryo-TEM	cryogenic transmission electron microscopy
CSTR	continuously stirred tank reactor
DLS	dynamic light scattering
DMAP	4-dimethylaminopyridine
DTNB	(5,5'-dithiobis(2-nitrobenzoic acid))
eq.	equivalents
g	grams
h	hours
Hz	hertz
iSCAT	interferometric scattering microscopy
J	coupling constant
L	litre
LCST	lower critical solution temperature
LSODA	Livermore solver for ordinary differential equations with automatic stiffness detection
M	molar concentration
MGSG	methylene glycol–sulfite–gluconolactone
min	minute
mol	mole

NMR	nuclear magnetic resonance
ODEs	ordinary differential equation
Ph	phenyl
pH	decimal logarithm of the reciprocal of the hydrogen ion activity
rpm	revolutions per minute
TFA	trifluoroacetic acid
TLC	thin layer chromatography
TRIS	tris(hydroxymethyl)aminomethane
UPLC	ultra high performance chromatography
UV	ultraviolet
δ	chemical shift
λ	wavelength

Acknowledgement

I would like to thank Professor Stephen Fletcher for providing me with the invaluable opportunity to work in the challenging yet profound field of origin-of-life research. He offered me considerable assistance whenever I needed it and encouraged me to explore different directions, including experiments and theories, freely. Without him, I would not possess such a deep and comprehensive understanding of the complex chemical systems.

I also wish to thank all my group members for creating a wonderful experience while I worked in the group. In particular, I would like to express my gratitude to Michael for teaching me everything about the oscillation project and to David for guiding me in chemical synthesis when I joined the group initially. I am grateful to Michael and Lukas for providing valuable experimental data for the simulation.

Many people outside the Fletcher group have provided me with essential assistance. I wish to thank the Kukura group, especially Samuel T. Cahill and Manish Kushwah for their help with iSCAT experiments, and Daohe Yuan for his help with DLS. I also thank Rishi Matadeen, Edward Lowe, and Borut Rozman at the COSMIC cryo-EM facility (University of Oxford) for their support with microscope maintenance and data storage. Additionally, I would like to thank Dr. Fernando Temprano-Coleto and Professor Howard A. Stone for their significant help with the simulations.

Lastly, I want to express my gratitude to the China Oxford Scholarship Fund for providing a studentship. Their support serves as a financial foundation for me to pursue my academic goal at Oxford.

1. General Introductions

1.1 The origin of life

Understanding the origin of life is regarded as one of the most important scientific problems of the 21st century, which has attracted a lot of theoreticians and experimentalists for decades.[1] The central topics in the origin of life (Figure 1) can be summarised as identifying the simplest structure that can sustain life-like behaviour in the early Earth, which made us different from the "inorganic substances" such as rocks and air.[2] If we capture a set of necessary conditions at the origin of life, we could better understand all life forms, propose universal pictures for life science and even search for potential alien life.[3,4] However, these tempting outlooks are still facing extreme challenges. The core concept in the origin of life research, the definition of life, is not well-defined and remains controversial.[5,6] There is also no standard research method, because it is impossible to really "witness" the emergence of the earliest life. In this chapter, the basic concepts and research methods will be reviewed.

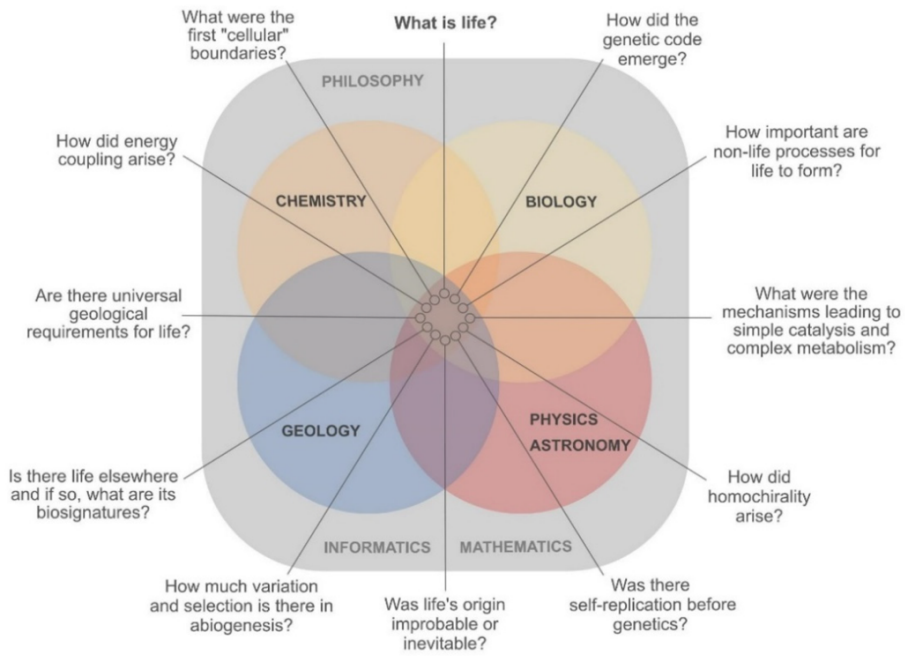


Figure 1. Current central questions in the origin of life research. The figure is from M. Preiner et. al.[2]

1.1.1 Definitions of life

Life, or life-like behaviour, is remarkably hard to define. It is often described through a combination of observable features rather than a single and universal definition.[7] This section will review three perspectives: metabolism,[8] responsiveness[9] and reproduction[10] (Figure 2), which represent the core pillars of life: energy, network kinetics and information transfer.

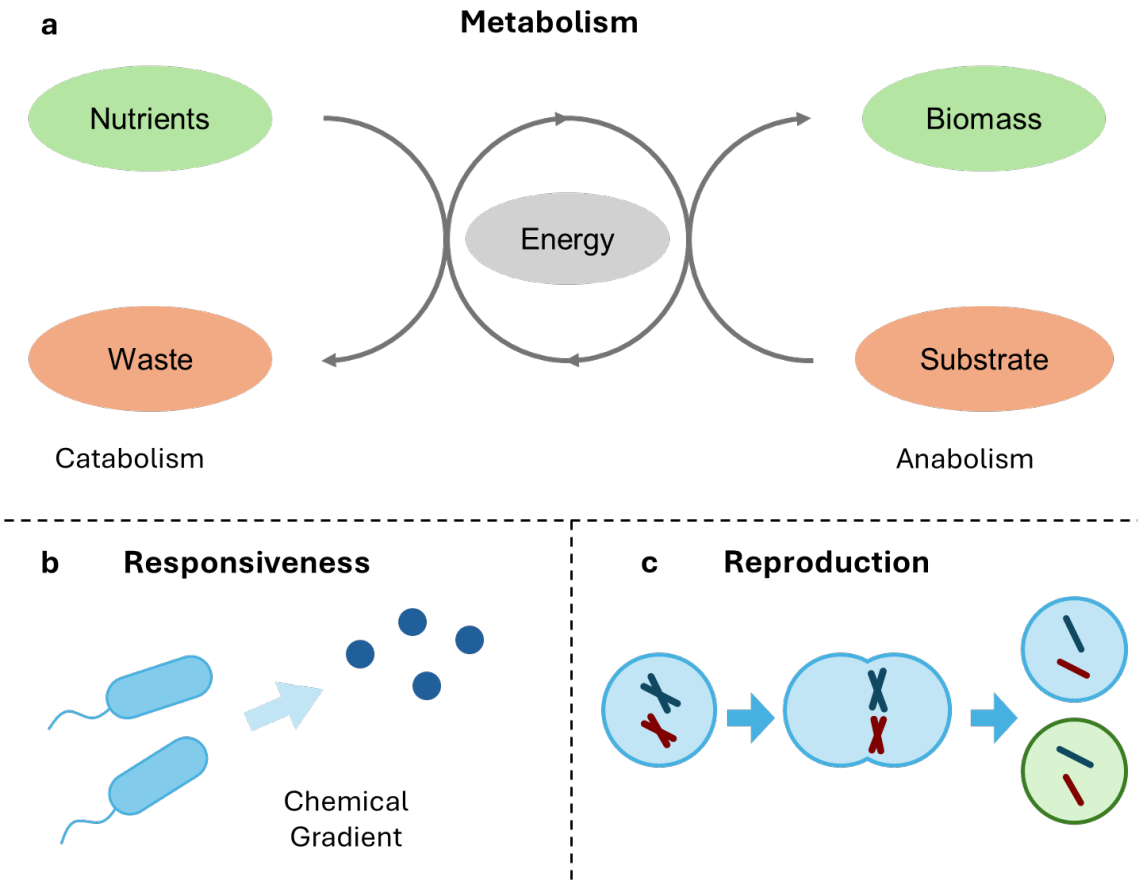


Figure 2. Three core features of life. a) Metabolism breaks down external nutrients and utilises the energy to sustain biological functions and produce biomass. b) Responsiveness is the capability to react to changes, such as chemotaxis is a form of responsiveness towards chemical gradients. c) Life can replicate and transfer its information to the offspring. The diagram illustrates the process of mitosis in a cell. The offspring may inherit features from their parents (blue) or have new features through mutation (green).

1.1.1.1 Metabolism

As a fundamental characteristic of life, metabolism is the capability of matter and energy transformation, typically from nutrients or sunlight to biologically useful forms. Metabolism

can be broadly divided into two categories[11]: catabolism, the breakdown of molecules to release energy, and anabolism, the synthesis of complex molecules from simpler ones by utilising energy (Figure 2a). These processes support all kinds of features of life, including growth, responsiveness and reproduction.

From a physical view, Erwin Schrödinger proposed that life maintains internal low entropy by dissipating external matter and energy, which is also called feeding by negative entropy.[8] According to the second law of thermodynamics, everything tends to reach a state of maximum entropy and equilibrium. The capability of life to maintain an ordered state and low entropy seems to contradict the second law. Ilya Prigogine explained this phenomenon in the concept of dissipative structure, which is a far-from-equilibrium and ordered system sustained through enough chemical and energy flux (Figure 3).[12–14] Thus, metabolism is both a biochemical necessity and a thermodynamic strategy for life to persist in a universe governed by the second law of thermodynamics.

This view has profound implications for the origin of life research. The emergence of living behaviour may not only require highly specific components, such as nucleic acids and amino acids, but could also be driven by general far-from-equilibrium features, which expands the perspective of searching for prebiotic systems.

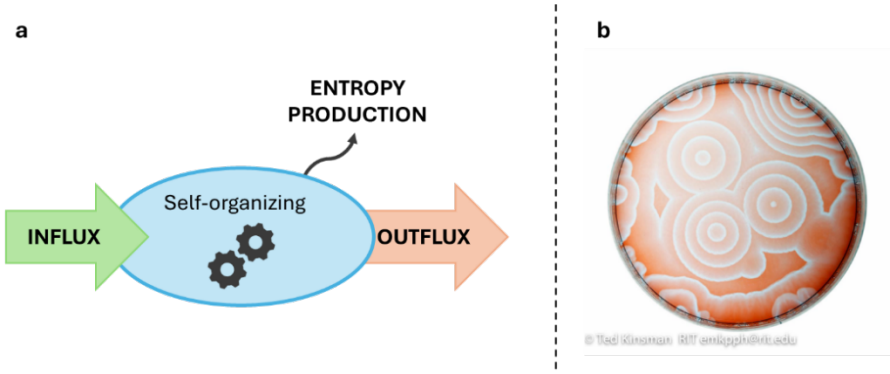


Figure 3. a) A diagram of a typical dissipative structure. It is an open system with influx and outflux of matter and is capable of maintaining self-organisation through releasing entropy to the environment. b) Chemical wave produced by Belousov-Zhabotinsky (BZ) reaction, which is one of the known simple chemical systems belonging to a dissipative structure.[15]

1.1.1.2 Responsiveness

Responsiveness refers to the ability to detect and react to changes in its internal or external environment. This feature allows living systems to maintain homeostasis, avoid harm and utilise resources in a changing environment. For example, bacteria exhibit chemotaxis - moving toward or away from chemical gradients (Figure 2b).

In simple organisms, the basis of responsiveness is chemical reaction networks (CRNs). The networks always include feedback loops,[16,17] which are capable of switching between states,[18] suppressing the noise,[19] and processing the environmental information.[20]

In a broader view of populations, responsiveness manifests as adaptation and evolution, which could also result from reproduction in 1.1.1.3. For example, pests can develop resistance when insecticides are intensively used.[21] Populations respond to environmental pressures not only through immediate biochemical changes but also over generational timescales via mutation, inheritance and selection.[22]

In summary, whereas metabolism reflects the flow of energy and matter, responsiveness represents the kinetics of life – how systems dynamically relocate themselves in a fluctuating environment and maintain an ordered state.

1.1.1.3 Reproduction

Reproduction is the process by which living systems produce new individuals, which occurs through two basic forms: inheritance and mutation. The former one is passing on their structural and functional characteristics to the offspring, while the latter one is creating new heritable features (Figure 2c). This capacity ensures both the continuity and diversity across generations and is the basis of evolution in natural selection.

Apart from the metabolism and responsiveness, the core of reproduction is the encoding and processing of information. In modern organisms, this role is played by nucleic acids such as DNA and RNA, the "blueprint" of life. We know that nucleic acids store and self-replicate their information by complementary bonding between bases, and process the information through gene regulation and repair.[23] These processes are different from other self-organising phenomena, such as crystals, which mostly do not carry inheritable and processable information.

Some researchers claim that the emergence of self-replicating molecules marks the threshold between life and non-life.[24,25] Some simpler species, such as viruses, are regarded as having animate features even without cellular structure and an independent metabolic system.[26] In the origin of life research, this view shows that the formation of self-replicating molecules and autocatalytic systems may be the starting point of life, and then more complicated features could emerge through selection and evolution.

1.1.1.4 Summary

Together, these three features, metabolism, responsiveness and reproduction, represent three different aspects of life: energy, kinetics and information. Energy flux enables the kinetics to operate in a non-equilibrium state and support reproduction. At the same time, kinetic networks shape and allocate energy flow through feedback mechanisms. Information, stored in nucleotides, ensures energy and kinetics operate in a regulated manner, while the information is dynamically regulated by gene networks. Life is not only defined by a single feature, but rather as a comprehensive entity emergent from the complicated interplay of the three aspects (Figure 4).

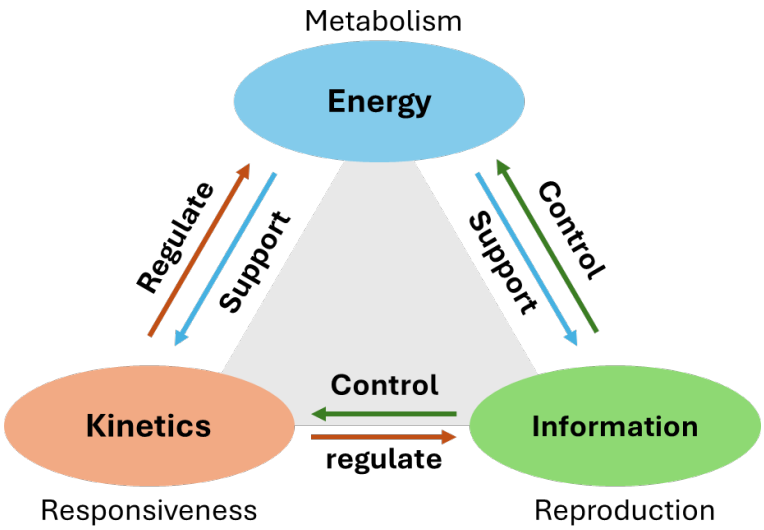


Figure 4. Relationship between the three perspectives of life.

1.1.2 Theories and research methods on the origin of life

It is impossible to observe the operation mechanisms of the earliest life directly, so they must be studied indirectly through simplified experimental models. Two complementary paradigms in the origin of life research exist: “top-down” and “bottom-up” (Figure 5).[27,28]

The top-down strategy aims to identify the minimal requirements for life based on existing organisms, including creating an artificial cell and determining the smallest set of components necessary to sustain life. The ultimate goal of this approach is the development of minimal artificial cells.

The bottom-up strategy works from the opposite side. It begins with non-living chemically synthesising components and aims to build life-like systems. This includes synthetic protocells composed of lipids, nucleic acids, peptides, and other small molecules, which aim to recreate fundamental biological features such as compartmentalisation, replication, metabolism, and adaptive behaviour. Bottom-up research is more directly relevant to understanding how life could have arisen spontaneously from abiotic conditions on early Earth.

A major challenge in bottom-up research is determining when a synthetic system can be considered "alive". Given that the definition of life remains elusive, finding a clear criterion is thus difficult. One criterion is to evaluate whether the system exhibits some or all key life-like features—metabolism, responsiveness, and reproduction—and whether it follows similar physical principles, such as far-from-equilibrium thermodynamics, nonlinear kinetics in networks, and information transfer.[29,30]

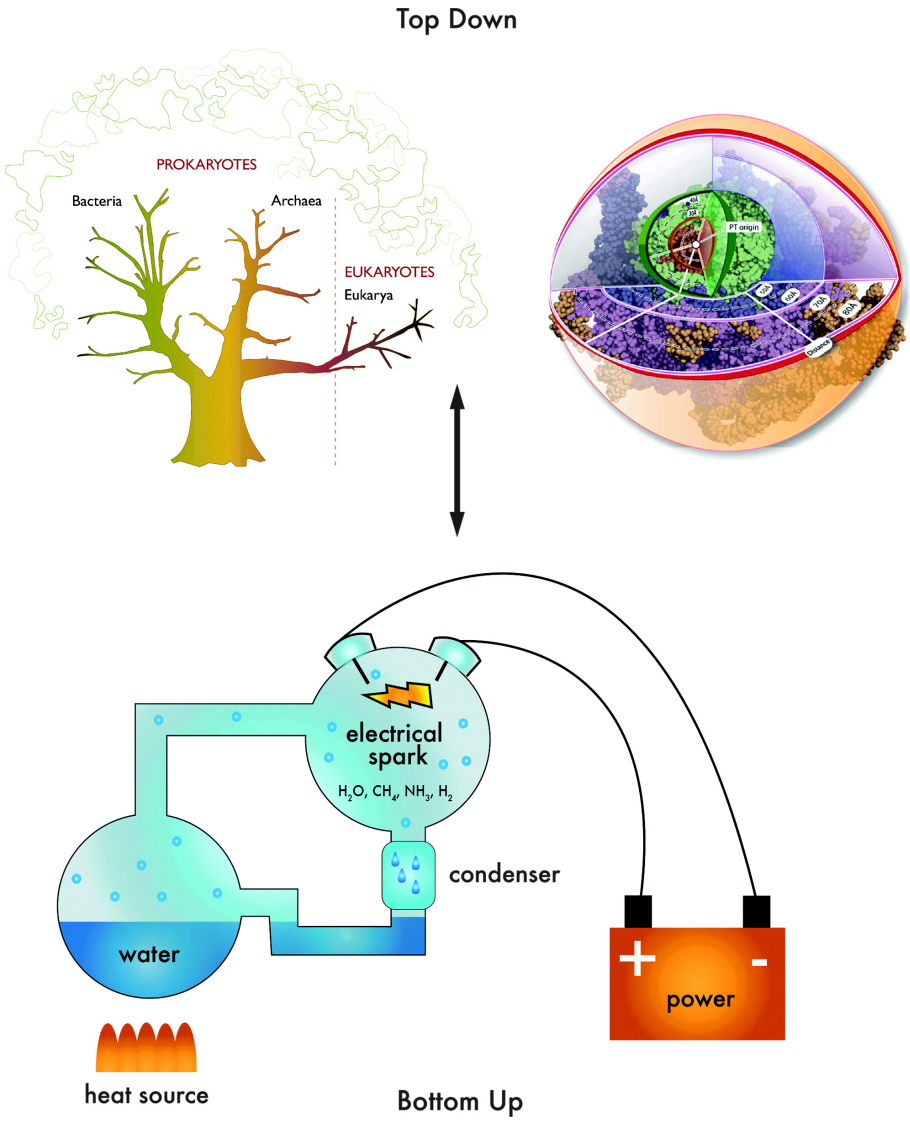


Figure 5. Top-down and bottom-up paradigms in the origin of life research. Here, the "top-down" strategy is shown by a phylogenetic tree and ribosome structure, illustrating that the goal of this strategy is to reveal the earliest and simplest life form from existing life. The "bottom-up" Strategy is shown by the Miller-Urey experiment, showing that it begins with non-living small molecules. The figure is from J. W. Peters et. al.[27]

1.1.2.1 Synthetic systems with fuel and metabolism

The biological behaviour of countering the maximisation of entropy by consuming chemical energy has inspired many synthetic systems (Figure 6a). A typical biological example is the microtubule that uses guanosine-5'-triphosphate (GTP) as an energy source to maintain its self-assembly (Figure 6b). This feature is called dynamic instability.[31,32] In general, the systems consist of inactive building blocks which are activated by external energy, assemble into

ordered structures, are called dissipative self-assembly (DSA) systems. It maintains an ordered low-entropy state through the flux of energy.[33,34]

An artificial counterpart of the DSA system has been developed by J. Boekhoven et. al., which consists of building blocks based on dibenzoyl-(l)-cystine (DBC) that can be activated by iodomethane, the chemical fuel. Then the activated building blocks can self-assemble into filament-like structures and revert to monomers (equilibrium state) when the fuel is depleted (Figure 6c).[35] Another system reminiscent of microtubules has been developed based on carboxylic gelators and exhibits transient assembly under the input of fuel.[36] A dissipative system with a highly complicated order structure is also reported by Juan Perez-Mercader et. al.,[37] showing multicompartmental features driven by Belousov-Zhabotinsky (B-Z) reaction as chemical fuel.

Apart from chemical fuel, light-driven systems are also widely studied as analogues of photosynthesis.[38–40] Nanoparticles modified by light-sensitive ligands, such as azobenzene derivatives, are transformed to an unstable high-energy conformation when activated by light and form aggregates (Figure 6d). These non-equilibrium properties can drive multiple macroscopic dynamic behaviours such as colour changing[41] and selective self-assembly.[42,43]

While the DSA system focuses on the formation and maintenance of ordered structures, another dissipative system can transform chemical energy into mechanical work, which is classified by molecular motors (Figure 6e).[44,45] Canonical natural examples include myosin[46] and kinesin.[47] Such systems are fundamental to life, enabling the microscopic motion to be controlled and biased in the presence of thermodynamic noise. Inspired by these systems, researchers have developed a range of artificial molecular motors. Early examples include light-driven molecular rotors based on aromatic hydrocarbons,[48] azobenzene[49] and chiral dithienylethene.[50] More recently, chemically-fuelled molecular motors have been created, such as chemical-

fuelled rotors[51,52] and pumps,[53,54] allowing translational motion along circular and straight "tracks" (Figure 6f).

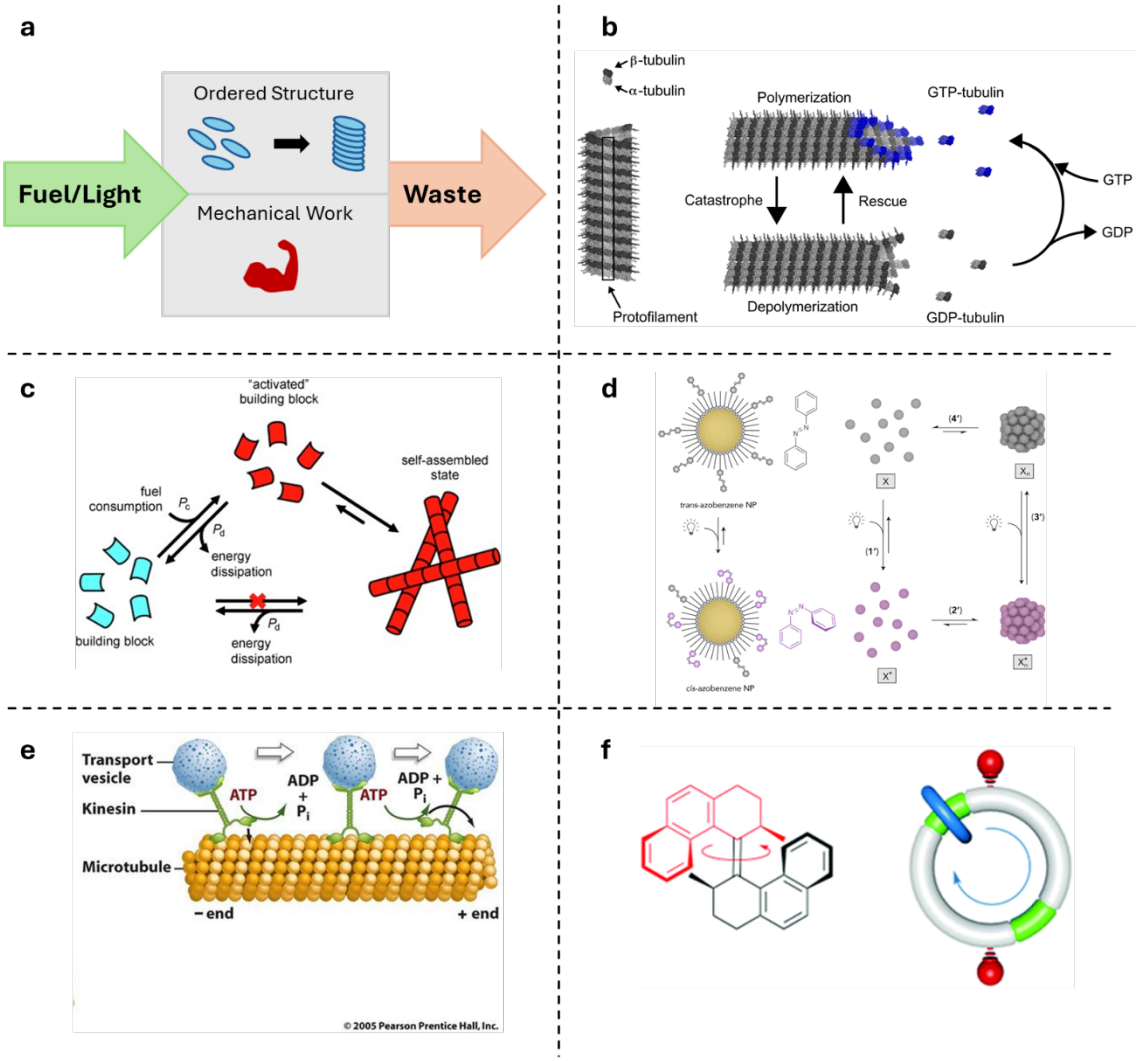


Figure 6. a) Summary of two fuelled systems, dissipative self-assembly (DSA) and molecular motor. b) Microtubule assembly/disassembly. The polymerisation of microtubules relies on GTP as chemical fuel.[55] c) An artificial DSA system. The inactive "building block" is activated by chemical fuel and self-assembles into the filament-like structure.[35] d) A light-controlled self-assembly nanoparticle.[41] e) Structure and "walking" mechanism of kinesin.[56] f) Two examples of light and chemical-fuel-driven molecular motors.[44] The left one is rotation along an axis, and the right one is translational motion along a circular molecular track.

1.1.2.2 Artificial chemical reaction networks

Complicated life behaviours such as responsiveness and regulation not only rely on the input of energy but also the intricate organisation of matter and energy flux. The core of the

organisation is CRNs. A typical and well-studied natural example is the citric acid cycle (Krebs cycle). This highly sophisticated eight-step reaction network efficiently oxidises acetyl-CoA to CO_2, releasing energy in a controlled and stepwise manner (Figure 7a). The intermediates of the cycle are not isolated to energy production alone - they are also interconnected with numerous biosynthetic pathways, serving as precursors for amino acids, nucleotides, and lipids.[23] The tight coupling of energy release and molecular synthesis in CRNs supports a wide range of cellular functions.

The construction of artificial CRNs has become another central goal in the bottom-up origin of life research.[57] Inspired by biological networks, researchers have developed cell-free biological circuits using microfluidic devices,[58,59] which can be used in designing customised in vitro networks (Figure 7b). Some reported Artificial CRNs consist of positive (autocatalysis) and negative (inhibition) feedback loops with well-tuned energy inputs that allow the system to exhibit nonlinear features, including bifurcation, bistability and oscillation.[60] Such features are essential for mimicking the biological regulatory mechanisms.

Artificial CRNs have also become an essential tool for investigating spatial organization and morphogenesis in prebiotic chemistry. A fundamental concept in this area is Turing's reaction-diffusion (RD) model,[61] which proposes that CRNs with short-range activation and long-range inhibition exhibit a Turing Pattern, a type of asymmetric pattern such as spots, strips, and waves (Figure 7c).[62] In artificial systems, there have been a few theoretical designs[63,64] and experiments[65–67] for pattern formation based on specific CRNs.

To expand the function of artificial CRNs, a set of general strategies for designing CRNs is developed based on the continuously stirred tank reactor (CSTR).[68] CSTRs constantly replenish starting materials and remove products while maintaining a fixed volume, and are a major experimental tool for developing out-of-equilibrium networks.[69] Based on these features,

lots of CRNs with variable dynamics have been developed (Figure 7d).[68,70–75] A network based on the formose reaction shows highly self-organising behaviour and is able to perform information processing and computing tasks.[76]

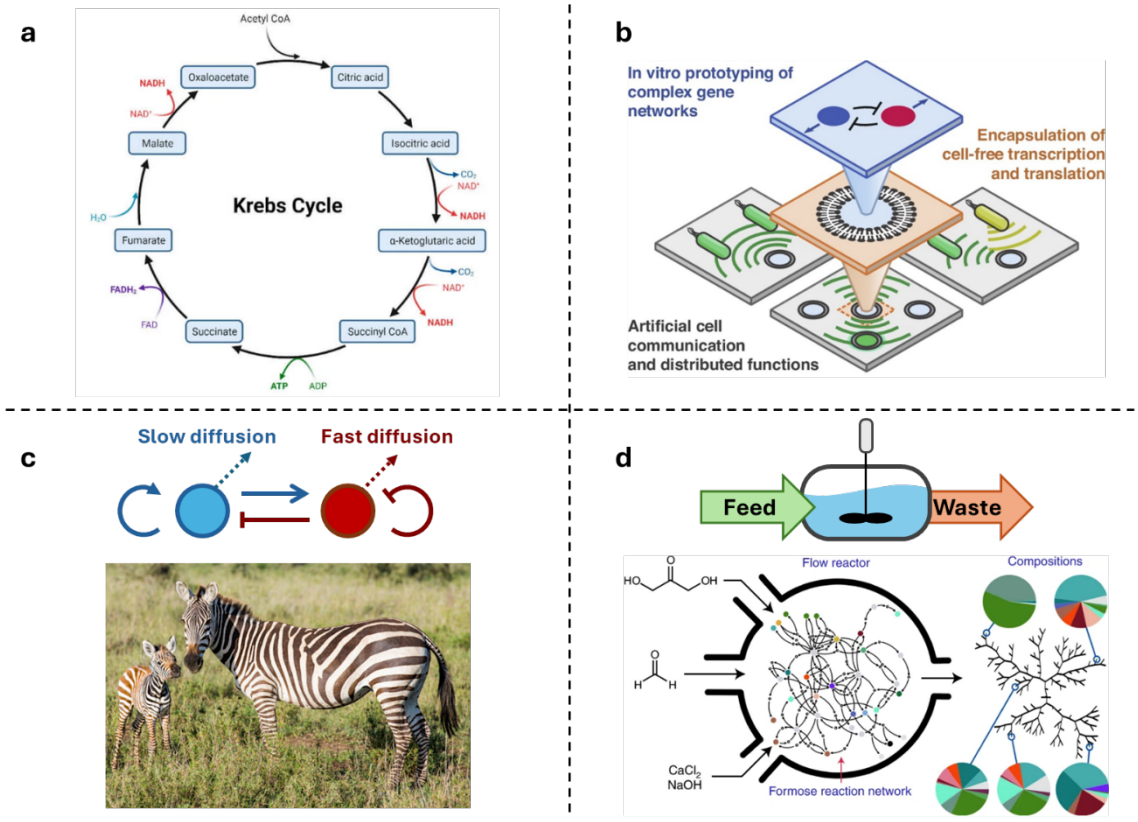


Figure 7. Natural and artificial CRNs. a) Reaction networks in the citric acid cycle.[77] In the cycle, Acetyl-CoA is converted to ATP, NADH and $FADH_2$. b) A diagram of artificial CRNs in microfluidic devices.[59] c) A classical CRN topology in Turing patterns. The blue dot represents a chemical signal for producing pigments with slow diffusion, and the red dot represents an inhibitor with fast diffusion. The network participates in the formation of stripes of animals such as zebras. The photo of zebras is from Discover magazine.[78] d) A diagram of CSTR and its application in designing artificial CRNs.[79]

1.1.2.3 Self-replicating systems and autocatalysis

Another milestone in the emergence of life is the development of self-replicating capability. Living organisms can be viewed as complex chemical systems organised to replicate and change their structures and functions. By generating offspring, the populations can propagate, mutate and evolve.[80] Modern life uses highly complicated molecular bases such as DNA and

RNA (Figure 8a) to achieve self-replication, but in the early stage, there must be primal and simple self-replicators.

In the realm of probiotic chemistry, Alexander Rich first proposed that RNA might be the first self-replicating molecule before the emergence of DNA and proteins.[81] This idea was expanded to RNA world theory in the following decades, which stated that rudimentary RNA fragments were produced by inorganic molecules such as hydrogen, methane, ammonia and water.[82] Then the small fragments were able to catalyse the formation of themselves, and some offspring started to have enzymatic functions after hundreds of replication cycles.[83,84,25] However, this "RNA-first" view has become controversial in recent years, such as the instability of nucleotides in an aqueous environment and statistical difficulties in the formation of complex polymers from simple fragments.[85,86]

An alternative idea is that compartmentalisation comes first, an assumption grounded in the self-assembly of amphiphilic lipids into aggregates, such as micelles and vesicles.[87] Once the amphiphilic aggregates are formed, they could then serve as autocatalysts, concentrating molecules and promoting reactions that would be too inefficient in bulk solution (Figure 8b).[87–89] These self-replicating lipid aggregates could be the earliest protocells, capable of producing offspring, providing an active micro-environment and regulating chemical reactions.[90] These occasional functions enable the synthesis of more complex structures, which may give certain individuals selective advantages.[29,91,92] Through the cycle of replication and competition, individuals with more complex functions would survive and become the basis of modern organisms with genomes. This framework is formalised in the "Lipid World" hypothesis,[93] which stresses that lipid-like molecules played a central role in the earliest stages of life.

For artificial systems, both the imitation of nucleotide and lipid are extensively studied. The former one is template autocatalysis[94,95] and the latter one is physical autocatalysis.[92,95,96] The

key distinction between template and physical autocatalysis is that, in template autocatalysis, autocatalytic species have defined structures and facilitate reactions through molecular interactions like base pairing. In contrast, in physical autocatalysis, autocatalytic species lack a defined size or shape and promote reactions via phase-based mechanisms. These two mechanisms can be easily distinguished by the seeding experiment, in which the reaction rate increases with the concentration of product in the template autocatalysis, whereas the rate shows little increase in physical autocatalysis below the critical aggregation concentration of the autocatalytic species. To note that there is another type of autocatalytic reaction that does not rely on templates or produce complex mesoscopic structures, such as the Soai reaction,[97] are not the main focus of "self-replication" and origin of life articles. They are simply described as autocatalysis or amplification instead. Otto group reported a few templated self-replicators based on macrocycles with benzene-1,3-dithiol core (Figure 8c). These self-replicators are an imitation of pairing replication of DNA and RNA, showing mechanosensitive self-replication,[98] selection,[99,100] diversity[101] and catalytic activity.[102]

Early physical autocatalysis systems were reported by the Luisi group in 1990. The system ran a hydrolysis reaction of octyl octanoate and aqueous LiOH in isooctane/1-octanol mixture. Sodium octanoate was added as a surfactant in the solution. Reverse micelles were observed to promote their own formation, whereas experiments conducted in the absence of sodium octanoate yielded no hydrolysis.[88] This work supported the autocatalytic role of the micelles. In the following years, a variety of micellar self-replicators were developed by the Luisi team, including self-replicating micelles encapsulating enzymes[103] and an autopoiesis system in the absence of pre-formed micelles.[89]

In recent years, the Fletcher group has conducted broad and systematic research on a variety of micelle- and vesicle-forming surfactants, enabling the rational design of physical autocatalytic

systems. In 2014, self-reproducing protocells based on thiol-ene reaction were developed.[104] The formation of autocatalytic surfactants depends on an irreversible reaction on specific functional groups (thiol group and carbon-carbon double bond) of the precursors. Such reactions allow the design of diverse protocells and the investigation of far-from-equilibrium systems.[96] A similar example is developed based on the click reaction between alkyne and azide.[105,106]

However, not all self-replication systems should be considered "life-like", as life is a non-equilibrium state rather than a thermodynamic steady state. In 2018, A transient self-assembling self-replicator was built based on olefin metathesis reaction.[107] The micellar replicator is formed in a thermodynamically unstable state and decomposes once the reactants are depleted. From this idea, a chemically fuelled self-replicator which operates in an open system is developed (Figure 8d).[108] It relies on thiol-disulfide exchange reactions and is sustained by continuous addition of a chemical fuel, hydrogen peroxide. A similar vesicular version was later designed using a double-tailed disulfide surfactant.[109]

These systems combine features of self-replication and dissipative self-assembly (DSA), distinguishing them from the thermodynamically stable lipid assemblies reported over the past decades.[110] Because they are maintained in a metastable state, these replicators exhibit complex dynamic behaviours such as selection and competition when multiple precursors are present.[111,112] Such systems provide promising artificial models for exploring natural selection and evolutionary dynamics in non-equilibrium chemical environments.

The self-replicators can be visualized by interferometric scattering microscopy (iSCAT).[113–115] Using iSCAT, nanoscale particles binding to a glass surface can be monitored and quantified to achieve the real-time, label-free analysis of supramolecular structures (Figure 9). Compared to static analysis methods, such as cryogenic transmission electron microscopy (Cryo-TEM),

iSCAT can capture dynamic details in chemical reactions, making it particularly suitable for monitoring physical autocatalysis systems.

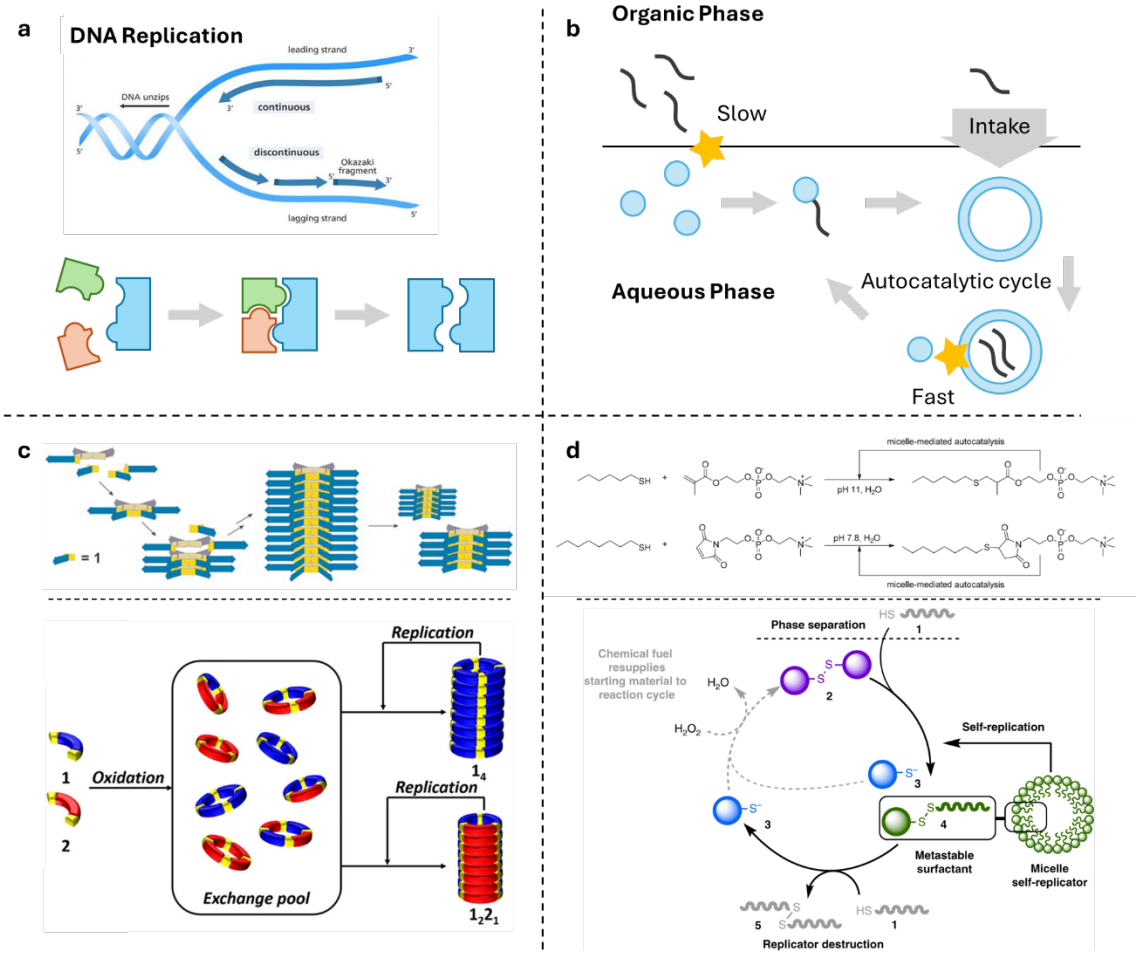


Figure 8. Self-replicating and autocatalytic systems. a) Templated replication of DNA (up) and a diagram of template autocatalysis. A template in blue can recruit reactants in green and orange and catalyse the formation of the template itself. b) Process of physical autocatalysis. The hydrophilic heads and hydrophobic tails react and form surfactants on the interface. The surfactants self-assembly into micelles and take in more hydrophobic reactants in the aqueous phase, promoting the formation of itself. c) Examples of artificial template autocatalysis. Different replicators show exchange and selective features.[98,100] d) Examples of non-fuelled[96] (up) and fuelled[108] (down) physical autocatalysis.

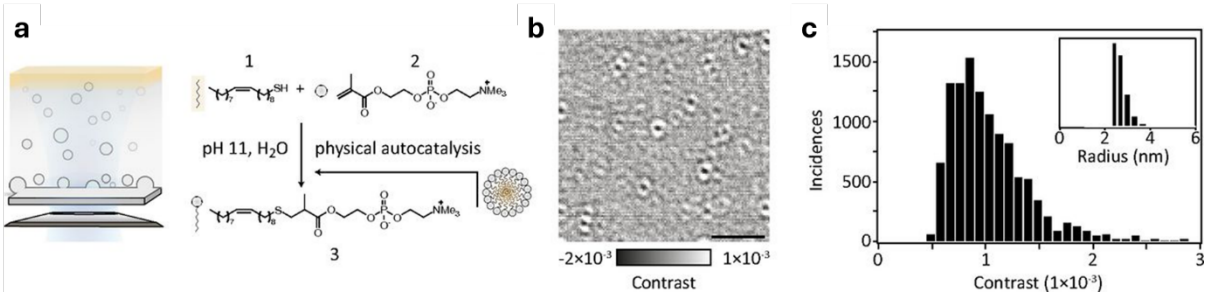


Figure 9. Visualising physical catalysis by iSCAT.[113] a) Diagram for iSCAT measurement. The chemical reaction is running in the solution on the coverslip. iSCAT relies on illuminating the sample with a coherent light source and imaging the reflected and backscattered light from the sample. b) An iSCAT image of micelles. Particles on the coverslip are shown by dark spots (scale bar: 2 μm). c) iSCAT contrast histogram of micelles. The contrast can be used to calculate the molecular mass distribution.

1.2 Chemical oscillation

Chemical oscillations are a distinct class of chemical reactions in which the concentrations of reactants and products fluctuate periodically over time. Unlike typical chemical reactions that start from reactants and proceed toward a thermodynamically stable endpoint, oscillatory systems stay in a far-from-equilibrium state and are sustained by an energy supply.

Chemical oscillations play a vital role in living systems by enabling temporal control over biochemical processes. Periodic and cyclic processes driven by chemical oscillators are universal in living systems, such as circadian rhythms driven by oscillatory gene circuits,[116] and calcium ion oscillations in cells.[117] It provides a timing mechanism for life activities and helps to keep accuracy and robustness in a noisy chemical environment.[118]

In the context of origin of life research, oscillatory systems participate in all three features of life discussed in 1.1.1 and bring the complexity to the next level. In terms of energy, oscillation systems require chemical fuels and produce waste, exhibiting metabolic-like behaviour. The operation of chemical oscillation relies on nonlinear kinetics, including autocatalysis and feedback loops. These kinetic mechanisms also enable the responsiveness and robustness of the systems. The frequency, amplitude and phase of oscillation can encode information and

allow temporal regulation in early biological functions such as the cell cycle, which may provide genetically-free timing mechanisms with simple structures. Studying chemical oscillators thus provides insight into how periodic features emerged naturally as part of life's earliest organisational strategies.

1.2.1 Basic principles of chemical oscillation

To achieve a periodic change in a dynamical system, certain essential requirements must be met. In summary, oscillations are caused by two general mechanisms – feedback loops and time delays.[119]

1.2.1.1 Oscillations based on feedback loops

We can begin with a simple example, predator-prey models.[120] Imagine rabbits and foxes living in a forest with population densities as x for rabbits and y for foxes. The per capita birth rate of rabbits is a constant; however, foxes must catch and consume rabbits to support their growth, or they will starve to death. The encounter rate between rabbits and foxes, the prey and predator, is xy, which causes an increase in foxes and a decrease in rabbits. So, the changing rate of each population is shown in the equation (1.1). All rate parameters are set to 1 for simplicity.

$$\begin{aligned} \frac{dx}{dt} &= x - xy \\ \frac{dy}{dt} &= -y + xy \end{aligned} \tag{1.1}$$

These nonlinear ordinary differential equations (ODEs) show simple feedback loops. When x and y are small, the increment rate of x is dominated by x, showing positive feedback (The more rabbits there are, the faster they produce rabbits). As x increased, the magnitude of xy overtakes $-y$ and supports an increment of y (Foxes can eat more rabbits), which leads to

further growth of xy and finally causes a decrement of x when $-xy$ overtakes x. This is another negative feedback on the high density of x and y. The alternative operation of increasing and decreasing states makes the populations oscillate. The network topology is shown in Figure 10a. In the numerical simulations, the change of time derivatives of x and y are shown as a vector plot in Figure 10b. The blue arrows show the vector $(dx/dt, dy/dt)$, which reflects the direction of movement of species populations in the phase space. The greylines show the state where x or y is not changing (nullcline), and the red point is a fixed point. Figure 10c shows the time evolution of the density of rabbits and foxes, which is consistent with the analysis above.

This simplified model shows the importance of feedback loops in an oscillatory system. In feedback-driven oscillations, at least one negative feedback is essential because it controls the increasing steps and pushes the system back to its original state. The participation of more components and feedback loops (including negative and positive) is also possible and may result in diverse peak shapes in oscillations.[119]

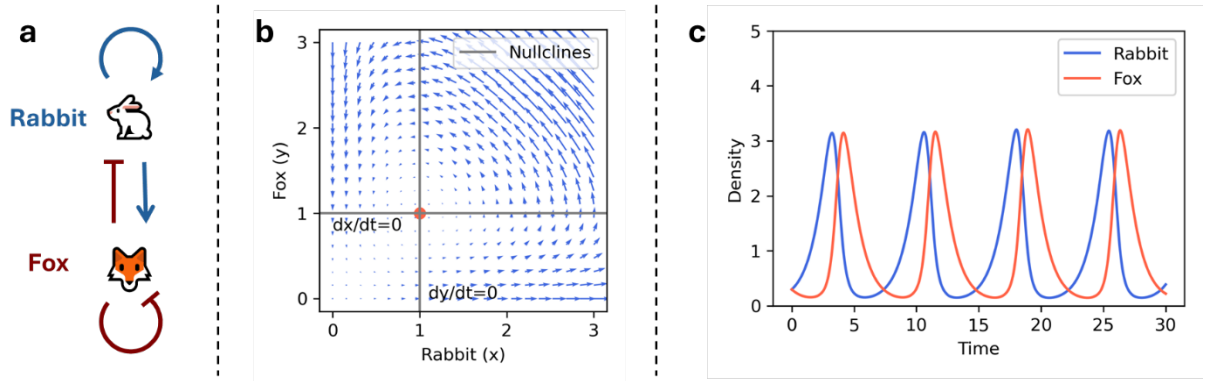


Figure 10. a) Network topology of a simple predator-prey model. The arrow means promotion and the blunt arrow means inhibition of the population increment. b) A vector plot of time derivatives of rabbit and fox densities. A blue arrow at (x, y) notes a vector (dx/dt, dy/dt) at this (x, y) value. The grey lines and red points are the nullclines ($dx/dt = 0$ or $dy/dt = 0$) and fixed points ($dx/dt = dy/dt = 0$). c) The time evolution of the density of rabbits and foxes. The results show oscillation in both species. The initial value of the numerical simulation is (0.30, 0.30).

1.2.1.2 Oscillations based on time delays

Another oscillatory system is driven by a different mechanism – time delay, which can be demonstrated by another simple model in equation (1.2).

$$\frac{dy(t)}{dt} = y(t) - y^2(t) \tag{1.2}$$

Obviously, this system has one stable fixed point $y = 1$ on $y > 0$. So all the starting points will move toward to this state. However, if the time derivative dy/dt is not dependent on $y(t)$ at time *t*, but on its history ($y(t - t_d)$), it becomes a time-delayed model. The dynamic properties of time-delayed models change significantly compared with non-delayed ones, including from non-oscillatory systems to oscillatory systems.

$$\frac{dy(t)}{dt} = y(t - t_d) - y^2(t - t_d) \tag{1.3}$$

Figure 11 shows numerical simulations of the non-delayed system and the delayed system (equation (1.2) and (1.3)). If there is no delay at all (Figure 11a), y will increase for all $0 < y < 1$ and decrease for all $y > 1$. So the trajectory $y(t)$ asymptotically reaches $y = 1$ for any starting points (Figure 11c). However, in the presence of the time delay, the changing rate dy/dt depends on the history of y, allowing y continue to increase for a while when $y > 1$ or decrease for a while when $0 < y < 1$ (Figure 11b). This behaviour is called overshooting and causes oscillation (Figure 11d). The explicit time delays are commonly found in biological systems. The delays can be caused by bioelectronic signal transmission or cell migration and play important biological roles.[121,122]

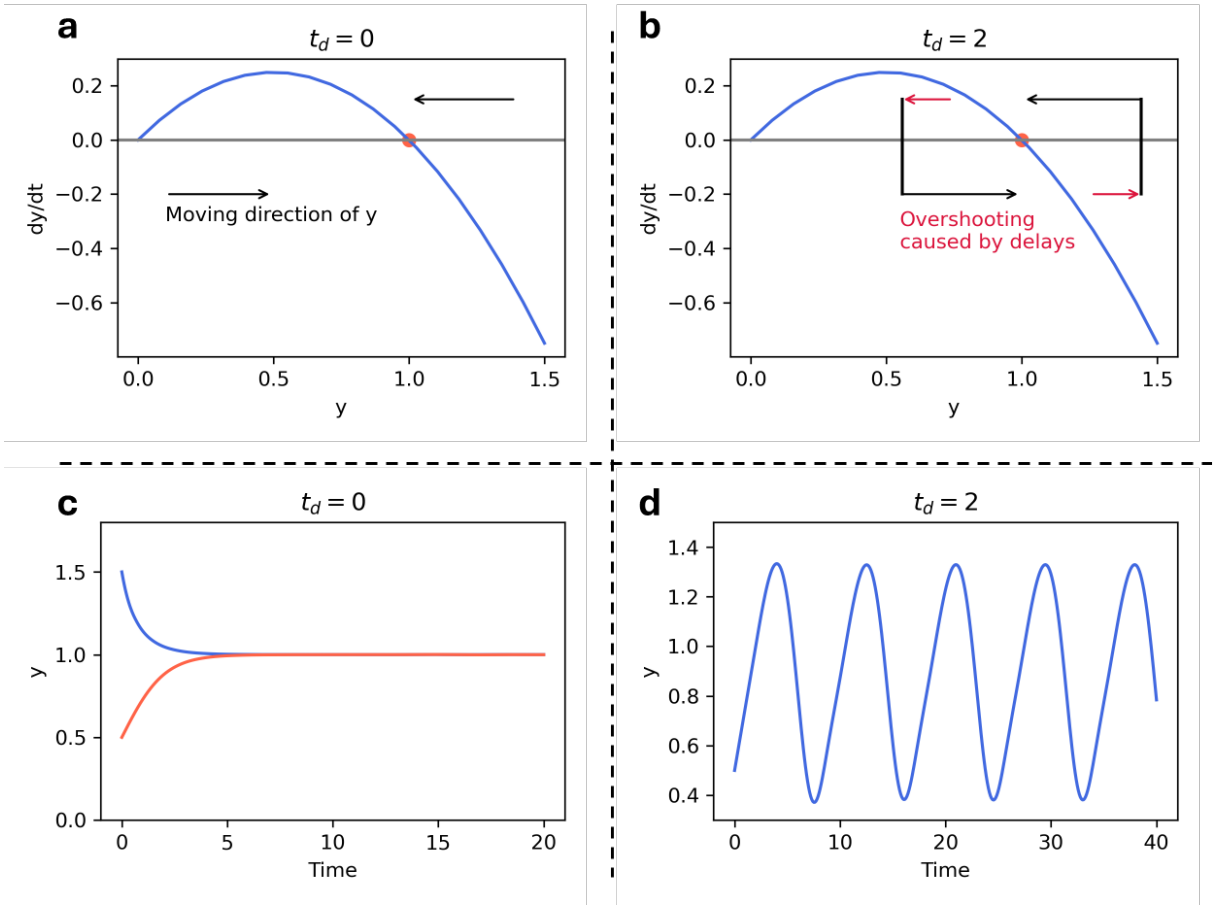


Figure 11. Time-delayed oscillator. a) $dy/dt - y$ plot of a non-delayed model. The arrows show the movement on the y-axis at different y values. b) $dy/dt - y$ plot of a delayed model. The red arrows show the "overshooting" caused by delays. The trajectories keep the moving directions when it comes across $y = 1$. c) Time evolution of y in the non-delayed model. The initial values of the two trajectories are 0.5 and 1.5. d) Time evolution of y in the oscillatory delayed model. The time delay t_d is set to 2. The initial value is 0.5.

1.2.1.3 The thermodynamic view of chemical oscillations

The previous sections discussed chemical oscillations from a kinetic perspective, focusing on nonlinear feedback loops and time delays. However, from this viewpoint, oscillatory and non-oscillatory behaviours are simply different types of solutions to ordinary differential equations (ODEs), without addressing their chemical and physical significance and the connections between living systems. In this section, a thermodynamic perspective will be presented to address these questions.

For oscillatory autocatalytic systems, a more complex model called the Brusselator is introduced, which was proposed by I. Prigogine and collaborators in 1967.[123] The reaction equations of the Brusselator can be written as (1.4), in which A and B are reactants, X and Y are intermediates, and D and E are products.

$$\begin{aligned} &\mathrm{A} \rightarrow \mathrm{X} \\ &\mathrm{B} + \mathrm{X} \rightarrow \mathrm{Y} + \mathrm{D} \\ &2\mathrm{X} + \mathrm{Y} \rightarrow 3\mathrm{X} \\ &\mathrm{X} \rightarrow \mathrm{E} \end{aligned} \tag{1.4}$$

Assume A and B are quickly replenished, so their concentrations A and B are constant. All rate constants are 1. The rate equation is the equation (1.5), where x and y are the concentrations of X and Y. It is in the steady state when $B < A^2 + 1$ (Figure 12a) and oscillates when $B > A^2 + 1$ (Figure 12b).

$$\begin{aligned} \frac{dx}{dt} &= A + x^2 y - (B+1)x \\ \frac{dy}{dt} &= Bx - x^2 y \end{aligned} \tag{1.5}$$

Now we can track the thermodynamic features in the steady and oscillating states. From the Second Law, the change in entropy (S) in a system is (1.6), where $d_e S$ is the flow of entropy due to the change with the surroundings and $d_i S$ is the entropy production inside the system due to irreversible processes such as chemical reactions and diffusions.

$$\frac{dS}{dt} = \frac{d_e S}{dt} + \frac{d_i S}{dt} \tag{1.6}$$

For simplicity, only the entropy production from chemical reactions is considered. The free energy dissipation of a chemical reaction is $\Delta_r G = \sum_j \nu_j \mu_j = -A_r$, where ν_j is the

stoichiometric number of the chemical j (positive for reactants, negative for products) and A_r is the affinity potential of the chemical reaction. From the definition of Gibbs free energy $G = H - TS$, the sum of the entropy production rate of r reactions is (1.7). Using the diluted solution approximation, the chemical potential μ_j can be written as $\mu_j^0 + RT \ln c_j$.

$$\frac{d_i S}{dt} = \frac{1}{T} \sum_r A_r r_r \tag{1.7}$$

The entropy production rate of the Brusselator is calculated in Figure 12c. The value of A is set to 1. In the steady state regime ($B < 2$), the system exhibits a low and gradually increasing entropy production rate as the parameter B increases. However, when the system enters the oscillatory regime ($B > 2$), the entropy production rate rises quickly. This result indicates that oscillatory states are characterised by higher entropy production compared to steady states, suggesting they dissipate more energy and release greater entropy to their surroundings. This thermodynamic characteristic mirrors a fundamental feature of living systems. Like chemical oscillators, life sustains its far-from-equilibrium and organised structure through constant energy dissipation and exports entropy to the environment.

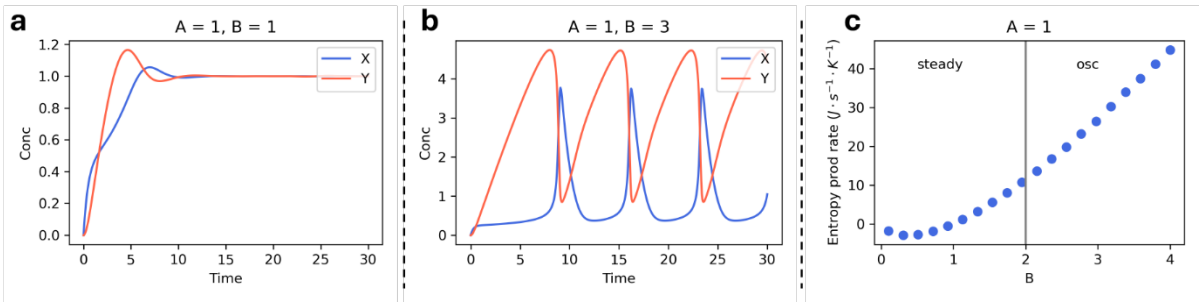


Figure 12. a) The Brusselator in a steady state. b) The Brusselator in an oscillatory state. c) The change of the entropy production rate with the change of *B*. The grey line indicates the bifurcation between the steady and oscillatory states. The initial values of (*X*, *Y*) are (0, 0) in all simulations.

1.2.2 Classifications of chemical oscillators

In the past century, various chemical oscillators have been developed. In this section, oscillators with different designs and scales will be reviewed.

1.2.2.1 Chemical oscillators on the molecular scale

A series of the earliest discovered chemical oscillators are driven by homogeneous chemical reactions in aqueous solution. In 1921, Bray[124] discovered an autocatalytic oscillator in the mixture of H_2O_2, KIO_3 and H_2SO_4, where the concentration of I_2 increases and decreases periodically. The mechanism of this reaction was further investigated by H. A. Liebhafsky, hence named Bray–Liebhafsky reaction,[125] and is also called "iodine clock" by later researchers.[126] A second case of oscillatory reaction was reported by Belousov in 1958.[127] In this reaction, citric acid is oxidised by potassium bromate under the catalysis of the Ce^{3+}/Ce^{4+} couple. A few years later, Zhabotinsky expanded the organic substrate and catalyst to a series of organic acids and metal ions.[128] These reactions were named Belousov-Zhabotinsky (B-Z) reaction, which is the most famous and widely-studied chemical oscillator. Other halogen-based oscillators include the arsenite-iodate-chlorite system[129] and the chlorite-iodate-malonic acid (CIMA) system.[130] In some more contemporary examples, the oscillating species were extended beyond the realm of halogens. Jensen[131] reported oscillation of benzaldehyde with oxygen in the presence of catalytic Br^- and Co^{2+}. More halogen-free oscillators were also discovered by Burger and Field[132] (SO_3^{2-}, S^{2-} O_2 and methylene blue) and I. R. Epstein[133] (S^{2-} and H_2O_2) in the following years. More recently, an organic-based pH oscillator is reported in 2007, which is built by Methylene glycol–sulfite–gluconolactone (MGSG) mixture.[134] This reaction provides controlled and dramatic changes in pH, which creates new potential for coupling with pH-sensitive materials.

The early homogeneous versions of chemical oscillators are closed systems and solely sustained by the intrinsic kinetics of the reactions. In such systems, the ability of oscillation is

limited by the natural reaction rates and will decay once the reactants are depleted. This makes oscillators rare and short-lived. To overcome these limitations, the use of CSTRs is a more contemporary strategy for making chemical oscillators.[135] By constantly replenishing and removing certain components in the reactor, CSTRs maintain the system far from equilibrium and precisely control the chemical flux. Unlike traditional batch reactors, such as beakers, CSTR is a more practical experimental platform for the rational design of chemical oscillators.[136]

I. R. Epstein and his team systematically developed a few strategies for CSTR-driven chemical oscillators from the 1980s. A family of iodate-based reaction network are studied under controlled flow of reactants in CSTR, leading to different complex dynamic behaviours, including bistability[137,138] and oscillation.[129,130,138] Additionally, more complicated feedback networks can be created by sensors within CSTRs, such as ion-selective electrodes, which connect with a computer and control the pumps in the reactor to alter the flow of substrates and provide positive or negative feedback.[139,140]

As more oscillating regulatory motifs in biochemical networks have been revealed by theoretical analyses,[119,141,142] a variety of CSTR-based oscillating counterparts have been designed by W. T. S. Huck and S. N. Semenov in recent years.[57,70,71,73,143–146] In these works, feedback motifs are imitated by enzymes and small organic molecules. By using a CSTR, these motifs are under precise control and are combined into a complex network, which can result in various oscillators. The reaction networks can also be modulated by external signals such as light[147,148] and temperature,[149] making the responsiveness and self-adaptation of oscillators possible.

1.2.2.2 Chemical oscillators on the macromolecular and supramolecular scale

Oscillatory behaviour not only occurs on molecular scales, but also can be coupled with macromolecular and supramolecular systems such as self-assembly and microdroplets. These systems always have much more complex multi-scale behaviours, as they combine chemical kinetics with physical processes such as diffusion, phase separation, and mechanical deformation.

Based on the MGSG oscillator, a vesicle-micelle oscillator is developed by B. A. Grzybowski et. al.[150] A pH-sensitive fatty acid precursor is introduced, which forms micelles at high pH and forms vesicles at low pH. In the pH oscillation, the cyclic vesicle-to-micelle transition can be observed, and striped patterns are formed when chemical reactions are coupled with particle diffusion (Figure 13a). A similar design also used pH oscillation to control periodic aggregation and dispersion of nanoparticles.[151]

In the past 20 years, R. Yoshida has developed different kinds of self-oscillators from polymers to gels (Figure 13b).[152] The basic design is to use ruthenium catalyst ($Ru(bpy)_3^{2+}$) to replace the cerium in the B-Z reaction,[153] and the bipyridine (bpy) ligands are covalently bonded to the polymers. This strategy can convert the chemical energy in the B-Z reaction to various dynamical supramolecular events, including cyclic swelling/shrinking of polymers,[154] making/breaking of vesicles[155] and mechanical movement in gels.[156] These studies show that the chemical energy in molecular chemical oscillations can be extracted in a time-controlled way and drive periodic events on different scales.

The oscillators discussed above rely on the coupling of molecular oscillators with external macromolecular materials. In these cases, the oscillatory behaviour is from the response, instead of an inherent property of the supramolecular structure. In 2022, the Fletcher group reported a notable advance, a self-replicating system with intrinsic chemical oscillation, based

on a physically autocatalytic network (Figure 13c).[157] In this system, a surfactant molecule catalyses its formation, providing positive feedback at low concentrations. At higher concentrations, the surfactant undergoes decomposition, introducing negative feedback necessary for oscillation. This work shows that oscillation can emerge intrinsically from a supramolecular system.

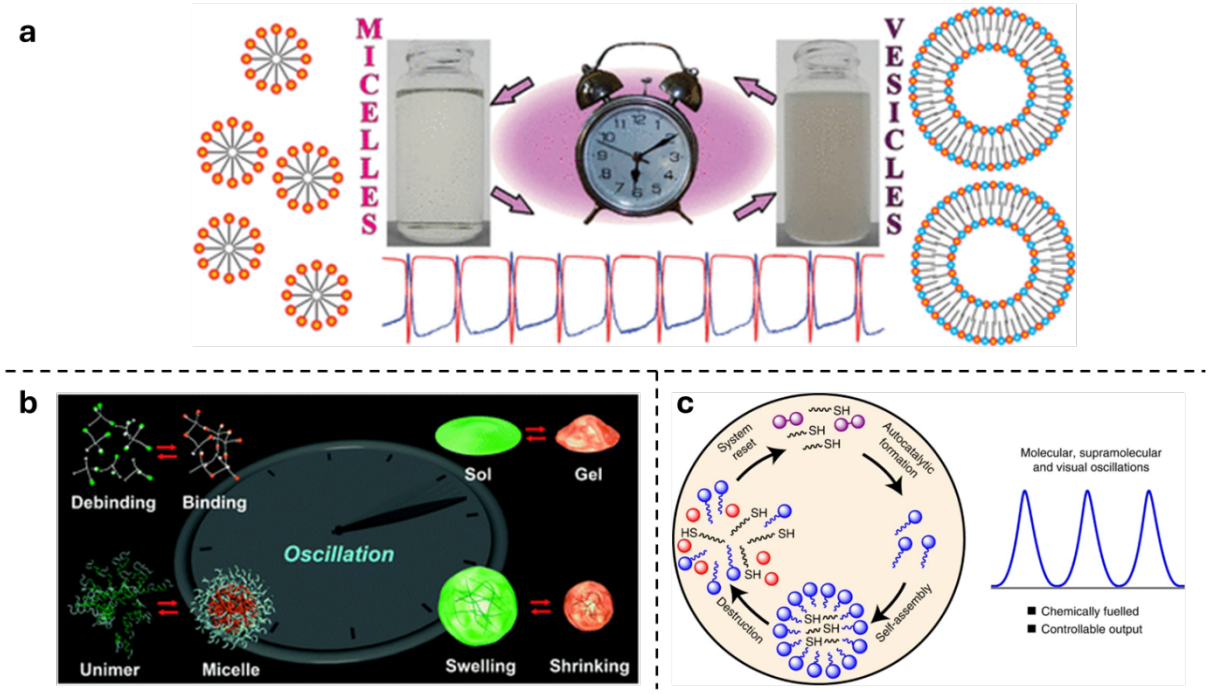


Figure 13. Macromolecular and supramolecular oscillators. a) A pH oscillator is coupled to and controls vesicle-to-micelle oscillations.[150] b) Oscillating gel and micelle coupled to the B-Z oscillation.[154] c) Supramolecular self-replicating oscillator.[157]

1.2.2.3 Chemical oscillators on the macroscopic scale

From the examples above, we can see that chemical feedback loop (both positive and negative) drives oscillations. However, the feedback is not only from microscopic chemical reactions, but also from the coupling of chemical, electrochemical and mechanical effects. A famous macroscopic example is the "Mercury heart" reported by Gabriel Lippmann in 1873.[158] In this experiment, a mercury drop is submerged in H_2SO_4 and $K_2Cr_2O_7$, when an iron needle touches the drop, it pulsates like a beating heart (Figure 14a). Two possible mechanisms drive the

oscillation of this system. One is that the dichromate oxidises mercury, forming an oxide layer. In this process, the surface tension of the mercury drop decreases and flattens its shape to contact with the needle. Then the iron needle reduces the oxide film and reverses the surface tension, making the surface of mercury drop leave the needle and restart the oxidation step again.[158] Lin et. al. proposed another mechanism without an oxide film.[159] A uniform electrical double layer forms between the electrolyte and the surface of the mercury drop. When the iron needle is introduced, a redox reaction begins, causing the electrical double layer and surface tension to become non-homogeneous, which results in mechanical oscillations.

Another more contemporary version of chemical-mechano coupling oscillator is developed by He et. al,[160] which is called SMARTS (self-regulated mechanochemical adaptively reconfigurable tunable system). Microfins made of hydrogel are modified by a catalyst on their top and sink in a bilayer solution, where the lower layer is water and the upper layer is reagents for an exothermic reaction. When the temperature of the microfins is below the lower critical solution temperature (LCST), the hydrogel swells and comes into contact with the reagents in the upper layer, triggering the chemical reaction and releasing heat to raise the temperature above the LCST. Then, the hydrogel shrinks and returns to its original state. The negative feedback loop drives oscillation in temperature and shape of the hydrogel.

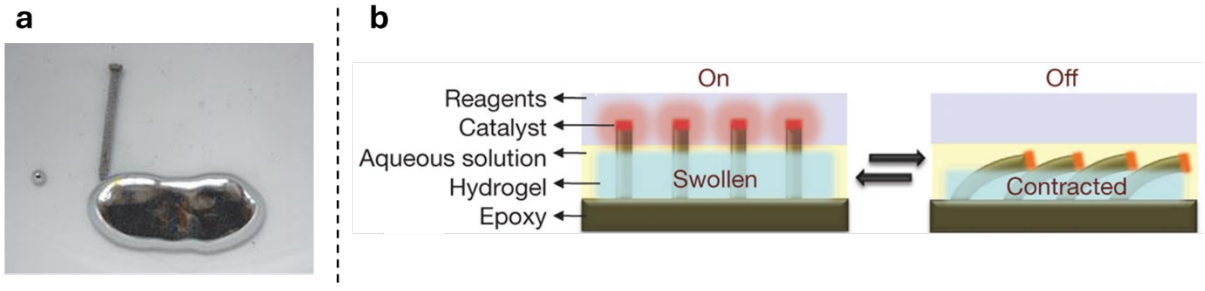


Figure 14. a) An example of "Mercury Heart". The reductant is the iron nail on the top left. b) The oscillation mechanism of SMARTS.[160]

1.2.3 Applications of chemical oscillators

As a relatively well-studied chemical complex system, chemical oscillators have many scientific applications. A typical example is making Turing patterns such as strips and waves,[161] which are similar to the patterns of animals and plants. In 1982, wave-like patterns were observed in the CIMA oscillator on a thin solution layer.[162] Still based on the CIMA, an experimental realisation of controlled Turing patterns was achieved in 1990, showing dot-like patterns in a gel reactor.[163] In the following studies, lots of shapes of Turing patterns, including hexagons, dots, strips and eye-like patterns, were generated by tuning the proportion of the reactants in the CIMA system.[164] Another similar example of a Turing pattern formation was also observed in the B-Z reaction in microemulsions.[165] These works provide a practical method to imitate and study the biological morphogenesis from a simple chemical basis, which builds a bridge from molecules to macroscopic orderliness.

Apart from their role in pattern formation, chemical oscillators also offer applications in information storage and processing. In particular, M. G. Howlett et. al. encoded chemical (oxidant) and physical (stirring) information into the waveforms of a physical autocatalytic oscillator.[166] The waveforms may serve as information transducers, allowing applications in molecular sensing and data storage.

Due to their inherent feedback mechanisms, chemical oscillators can also be used to construct chemical computing systems. An early example was image processing using chemical waves from the B-Z reaction, where grayscale information was processed through the movement and interactions of the chemical waves.[167] Since then, the computation methods based on chemical oscillations have been expanded in theory and experiment. Systems capable of performing logic operations, such as chemical logic gates[168] and Boolean circuits[169] have been designed by incorporating the B-Z reaction in microfluidic devices. A more complex example is the

"chemical processor" developed by L. Cronin and co-workers,[170,171] in which the B-Z reaction is implemented in a grid-like array of cells. The starting phases of the oscillator in each cell are inputs, and the outputs are the form of chemical waves in the grid. The outputs are then interpreted using a convolutional neural network (CNN). These developments highlight the potential of chemical oscillators as non-traditional computing platforms that operate without electronics, relying instead on reaction-diffusion dynamics and chemical feedback.

2. A Chemical Reaction Network Drives Complex Population Dynamics in Oscillating Self-Reproducing Vesicles

The work in this chapter was undertaken in joint collaboration with Michael G. Howlett, Emma Silvester, Philipp Kukura and was published in Journal of the American Chemical Society, 2024: "A Chemical Reaction Network Drives Complex Population Dynamics in Oscillating Self-Reproducing Vesicles".

2.1 Introduction

The complexity and intricacy of living systems inspire scientists to understand how molecular structures may achieve life-like dynamics and functions.[8,172] Despite numerous hypotheses regarding the origins of life,[83,93,173–175] it is still unclear how simple molecules can give rise to the dynamics observed in living systems, which can control functions across the molecular, microscopic and macroscopic scales.

Among the diverse behaviours characterised in living systems, those that are periodic in time are particularly fascinating. Oscillations are seen in events as disparate as glycolysis,[176] expression of the tumour suppressor protein p53,[177] circadian rhythms,[178] and the reproductive cycle of cells.[179]

Living cells have the ability to perform complex, time-controlled functions to sustain themselves, synchronize, and respond to external stimuli. Many models have been developed in order to simulate and better understand the operations of living cells.[180,181] However, most artificial cells are either static structures, or need repeated or continuous stimulation to maintain their structures and control functions.[182–185] In living cells, various feedback mechanisms enable autonomous cellular processes, and many internal biochemical reactions exhibit periodic behaviour.[186]

Designing oscillating chemical reactions may be relevant to understanding periodicity in biology. The mathematical and physical foundations of non-equilibrium systems have been extensively discussed,[14,119] but it is not at all well understood how to incorporate the specific design elements required to observe non-equilibrium systems into chemical reaction networks so that novel systems may oscillate and show complex dynamic behaviour.

Multiple approaches have been used to hold chemical systems out-of-equilibrium, including the addition of chemical fuels,[36] light[48] and electrical energy.[187] Our group has also developed several out-of-equilibrium supramolecular systems,[92] including chemically-fuelled self-reproducing micelles[108] and vesicles,[109] and we have observed competition and selection in systems containing mixtures of protocells[110] and characterized lipid populations that evolve in time.[112]

Several oscillating chemical reactions have been discovered over the last 200 years.[188] While classical oscillators feature electrochemical and inorganic components,[124,126,189,190] more contemporary examples are based on chemo-mechanical systems,[160] supramolecular polymers[191] and there are several systems where continuous-flow stirred tank reactors (CSTRs) are used to drive oscillations.[68,70,72–74] CSTRs constantly replenish starting materials and

remove products while maintaining a fixed volume, and are the major experimental tool for developing out-of-equilibrium systems and rationally designed oscillators.[69,192]

In 2022, our group reported oscillating micelles (Figure 15a).[157] This system depends strongly upon non-linear feedback mechanisms between micelles and their phase separated precursors.[95] Rather than mechanical flow, our system uses a chemically fuelled reaction network to regenerate reactive starting materials from a waste product of the reaction, in a manner that is similar to the metabolic cycles seen in biology.

Vesicles are widely regarded as basic compartments that may be relevant to the origins of life, and are likely closer to living systems than micelle-based systems.[193,194] Light-driven oscillations in a vesicle-forming system have been previously reported by Perez-Mercader and co-workers.[195,196] In that system, light-induced radical polymerisation led to the formation of giant polymer vesicles which showed "Phoenix behaviour" (growth, collapse and regrowth) and phototaxis.

We previously reported that self-reproducing metastable vesicles could be kept in a steady state.[109] Here we set out to develop a system of vesicles that could oscillate in time (Figure 15b).

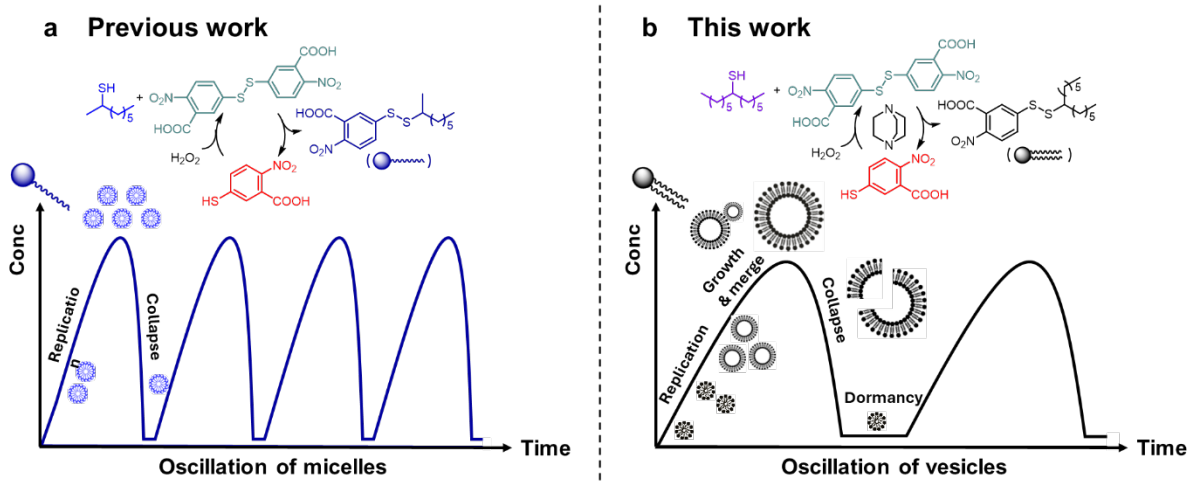


Figure 15. a) Previous work on oscillating self-replicating micelles. b) This work: oscillating self-replicating vesicles.

2.2 Results and discussion

2.2.1 Molecular oscillations

The key to observing oscillations in the self-replicating vesicles shown here is a metabolic cycle (Figure 16a) which replenishes starting material from a waste product of the reaction. We assume that the metabolic cycle features autocatalytic steps for both the formation and decomposition of **1**, which is similar to the assumption for the micelle oscillator.[157]

Surfactant **1** is formed when **2** reacts at the interface with **3**. Molecular **1** aggregates to form vesicles in aqueous buffer at pH 9.0. The formation of **1** is autocatalytic because aggregates of **1** transport **2** from the organic layer to locations where it can more readily react with **3** to produce more **1**. This physical autocatalytic mechanism operates on the principle that the products of the reaction increase the reaction rates between phase-separated precursors.[92,95,109]

The system is biphasic, with thiol **2** initially comprising the organic layer, and **4** and 1,4-diazabicyclo[2.2.2]octane (DABCO) initially dissolved in aqueous buffer. The continuous addition of H_2O_2 via a syringe pump forms **3** from **4** and keeps the system out of equilibrium.

Electrophilic **3** is the limiting reagent in the autocatalytic formation of **1**. When **3** is depleted, nucleophilic **2** (solubilised by aggregates of **1**), reacts with electrophilic **1** and the decomposition of **1** causes the vesicles to collapse and forms waste products **4** and **5** in a second auto-catalytic process. While the asymmetry of the peak shapes in the kinetics of **1** shows that vesicle collapse is a highly non-linear process, the autocatalytic mechanism at play here is not necessarily obvious. At this stage we believe that the reason the decomposition of **1** is autocatalytic is because the partial collapse of the supramolecular structure releases thiol **2** into the aqueous phase, which is more active than phase separated thiol and reacts readily with **1** to further promote vesicle destruction.[157]

We propose that both the formation and destruction phases of surfactant **1** exhibit autocatalytic characteristics, though by distinct mechanisms. Formation is driven by physical autocatalysis: aggregates of **1** promote the mixing of precursors **2** and **3**, enhancing their own production. In contrast, the decomposition of **1** and associated vesicle collapse represent a different form of autocatalysis—one in which supramolecular disassembly triggers molecular reactivity. Specifically, when vesicles collapse, thiol **2** is released into the aqueous phase, where it is more reactive. The released thiol then causes more micelles to decompose, resulting in the release of more thiol. This mechanism makes the micelles decompose in an autocatalytic way.

The formation and decomposition phases alternate in dominance, causing the molecular concentrations of reactants **1**-**4** to oscillate (Figure 16b). As well as constantly supplying peroxide and stirring, the presence of a nucleophilic catalyst (DABCO) is also required to see oscillations (at least on the timescales examined), as oscillations require a balance of reaction rates in the formation and decomposition of the reaction components, and while this maybe obtainable by other means (for example stirring speed) we found the use of a nucleophilic catalysis convenient, and possibly relevant to how relative reaction rates may be fine-tuned in

biological systems. While DABCO likely catalyses both the formation (Figure 16a i) and decomposition (Figure 16a ii) of **1**, we propose that it plays a key role in the oscillations by catalysing the decomposition of **1**, as the formation of **1** is still observed in the absence of DABCO (Figure 16c).

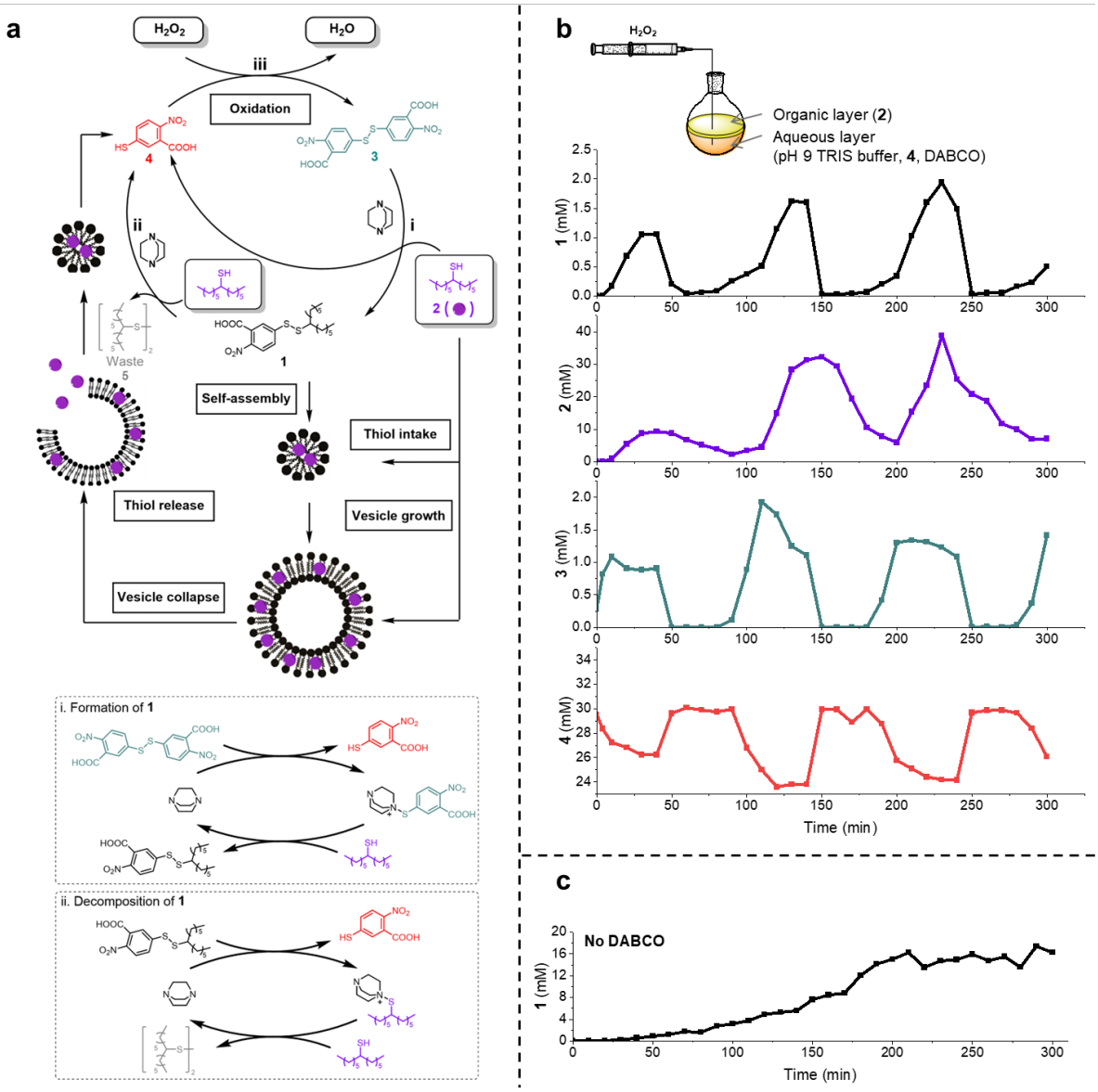


Figure 16. a) Chemical reactions and supramolecular events in the cycle of oscillating vesicles. Surfactant **1** is formed in the reaction of phase separated thiol **2** and disulfide **3**; waste product **4** is also formed (step i). Surfactant **1** aggregates to form supramolecular species; the formation of **1** is autocatalytic because aggregates of **1** allow **2** and **3** to mix. Disulfide **3** is the limiting reagent in the system and in the absence of **3**, surfactant **1** and disulfide **2** react (step ii) to give waste products **4** and **5**. The decomposition of molecular **1** also decomposes aggregates of **1** and this step is also non-linear. The constant addition of hydrogen peroxide converts waste **4** back into electrophilic disulfide **3** (step iii). As shown in boxes (bottom) for steps i and ii, DABCO mediates both the formation (i) and decomposition (ii) of **1**. b) Top: cartoon picture of the oscillating biphasic reaction, where a mixture of **2** and aqueous **4** are stirred while H_2O_2 is added at a constant rate. Bottom: Aqueous phase concentrations of **1**, **2**, **3**, and **4** as determined by removing aliquots of the reaction, quenching with 0.06 M aqueous maleimide and measurement by ultra-performance liquid chromatography (UPLC). The molecular concentration of surfactant **1** oscillates. We assume some **1** is present in the organic phase, which is undetected when the aqueous layer is sampled and analysed. The concentration of **2** is largely in phase with **1**, but lags somewhat, consistent with **1** carrying **2** into the aqueous phase. The concentrations of **3** and **4** are out of phase. DABCO adducts (a, steps i and ii) are expected to be undetected and lower the measured concentration of **4**. The concentration of **4** returns to ~30 mM after every pulse and so appears to be completely regenerated. c) In the absence of DABCO **1** forms slowly and the system did not oscillate on the timescale examined. Lines are drawn to guide the eyes.

2.2.2 Supramolecular oscillations

We used interferometric scattering microscopy (iSCAT) to detect supramolecular species in real-time during oscillations. iSCAT can measure the change in refractive index caused by particles landing or unbinding on a surface, with the change in contrast being proportional to particle mass.[197] This powerful method has been used to analyse micelles and vesicles in situ.[109,115,157] Dynamic light scattering (DLS)[198] was used to measure the average size of the vesicles during oscillations, and cryo-TEM was used to observe the vesicles at equilibrium.

In a typical oscillation experiment, the average particle count and contrast were measured by iSCAT every 20 minutes (See 5.1.3). The contrast values, whether positive or negative, signify unbinding and binding events of particles, with binding predominating in this experiment. The approximate particle mass is determined through the calibration curve in Figure S 2.

The iSCAT images clearly suggest that vesicles form, grow and decay within one pulse of an oscillation (Figure 17a shows one pulse from 200 to 280 min). Vesicles appear as dark circles with a white boundary, with larger and brighter particles representing higher mass aggregates.

The change in contrast distribution over time is shown in Figure 17b (one pulse) and Figure 17d (overall), where all the distributions are calculated based on a 60-second video at each time point. Low contrast values such as 0.0 – (–)0.1 indicate smaller assemblies such as micelles whereas greater values such as > (–)0.2 support the presence of larger aggregates such as vesicles.[109,115] Initially in the reaction, mostly very low contrast values < (–)0.05 are seen, alongside a growing broad peak with medium contrast (~ (–)0.1). Over time the contrast distribution broadens and shifts to higher contrast (> (–)0.25) during each oscillation pulse, and in comparison to subsequent pulses. This supports the formation of larger and heterogeneous vesicle-scale aggregates during each pulse (in line with increasing **1**), similar to that previously observed[109] and is compared with a symmetric distribution and lower contrast seen for the analogous, smaller and more homogeneous micellar systems.[115] Interestingly, the overall increase in average contrast shows that, in this particular experiment (vida infra), larger aggregates are preferentially formed as the oscillation progresses, despite the apparent decay of aggregates between pulses.

In Figure 17c, the counts of all landing particles within 60 seconds are recorded, while the approximate average mass is calculated based on the average particle contrast. Simultaneously monitoring oscillations with iSCAT and UPLC revealed a correlation between the count and mass of the particles and the solution concentration of **1**. However, initially, the growth of count and mass lags slightly because the self-assembly process requires accumulation of sufficient building blocks **1** to reach the critical assembly concentration (Figure S 3). A cartoon interpretation of the supramolecular dynamics - where the aggregates change during the course of a single pulse - is shown in Figure 17e.

While iSCAT provides a measure of the amount of material in a nanoscopic object, extracting the size is difficult for sub-diffraction objects in the absence of other measures, such as

diffusion. To track changes in vesicle size we monitored a reaction using dynamic light scattering (DLS). Like with iSCAT experiments discussed below, reaction aliquots were taken every 10 min. and then diluted to measure the particle size distribution over time. Figure 18 shows how the mean particle diameter (top) and the molecular concentration of **1** (bottom) fluctuates. Both DLS and iSCAT observations show the growth and decay of vesicles. However, DLS measures hydrodynamic diameter, while iSCAT measures the amount of material, which are not necessarily trivially correlated. cryo-TEM images (see Figure 19 and SI Figure S 9) provide insight into how vesicles can increase in mass, but not size, as they show the formation of vesicles within vesicles, and illustrate that a wide variety of vesicles with different sizes and complexities can easily be formed from examining **1** in a simple buffer solution.

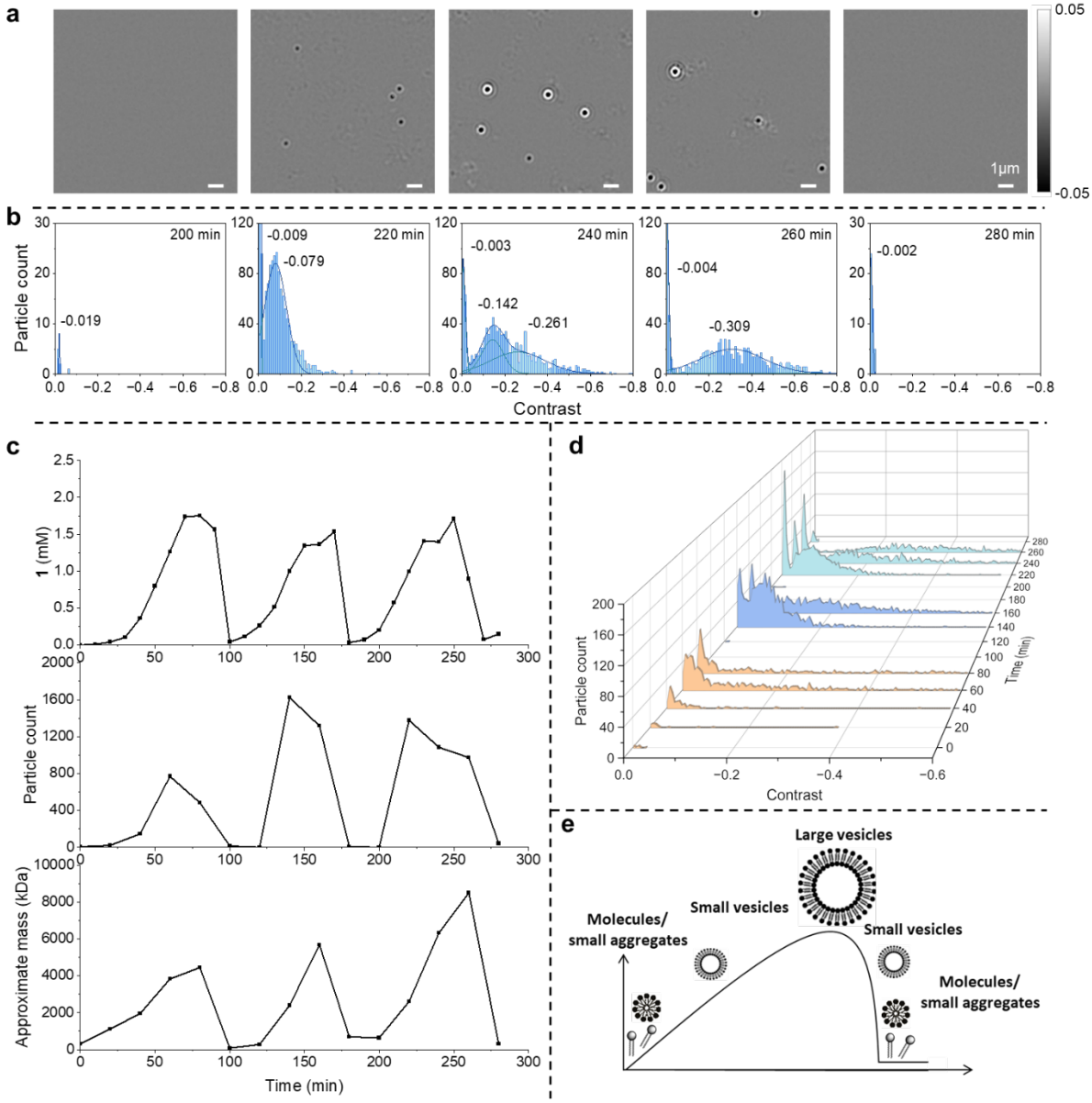


Figure 17. a) iSCAT photos corresponding to the timepoint shown in b with contrast threshold of ±0.05 showing that micelles or small vesicles are first formed, then large vesicles are observed before the supramolecular aggregates decay. The scale bar is 1 μm. b) The fitted Gaussian curve of contrast distribution within one oscillation pulse where the changes in distribution suggest vesicles are growing. c) The change in the concentration of **1**, particle count, and the approximate average mass of particles over time during an oscillation experiment. Particle data was obtained from iSCAT movies. d) Waterfall plot of contrast distribution over time, showing the change in particle count and contrast distribution over time. The data from 3 peaks are labelled by different colours. e) Cartoon diagram of the supramolecular species observed during a single pulse of an oscillation. Lines are drawn to guide the eyes.

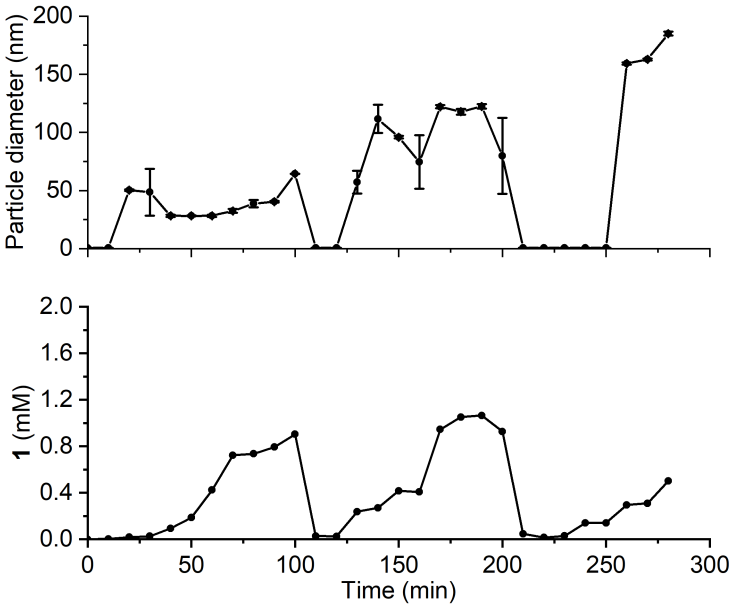


Figure 18. Number mean diameter of vesicles in time as measured by DLS. Lines are drawn to guide the eyes.

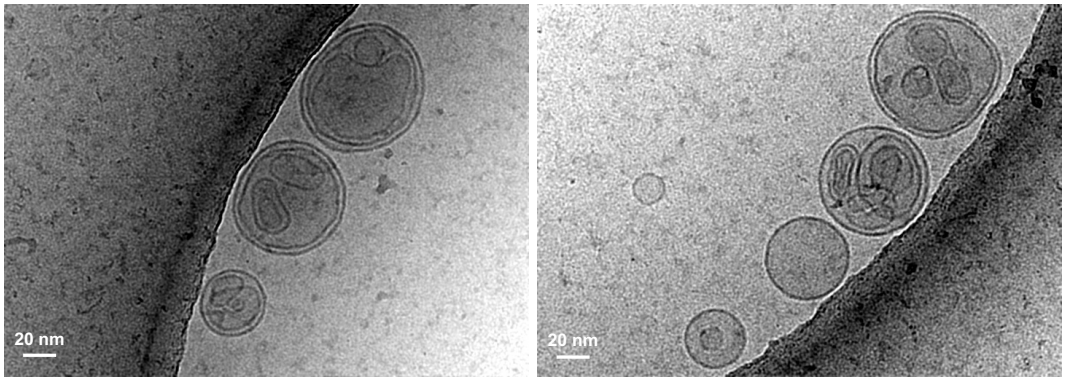


Figure 19. Cryo-TEM images of vesicles of **1**. Images were recorded for 2.5 mM samples of **1** in TRIS buffer (0.5M, pH 9.00). The images show vesicles, including oligolamellar and multivesicular vesicles with a wide distribution of sizes. More photos can be found in Figure S 9.

2.2.3 Non-equilibrium supramolecular behaviour during oscillations

Our data shown in Figure 17c, d and Figure 18 show that larger aggregates are favoured in later pulses during these oscillation experiments, but this effect is not always observed, and at this stage it is not clear why this can be inconsistent. It is observed in the data shown in Figure 20, but not in some repeats of that experiment shown in Figure S 4.

To further reveal the details of the molecular and supramolecular behaviour of **1** during oscillations, a series of reactions were conducted which were monitored by UPLC and iSCAT every 10 minutes. As seen in Figure 20 (and three repeats of this experiment in Figure S 4), the change in particle count and mass varies throughout the experiment and the oscillations exhibit four distinct phases.

First, there is a "replication phase" (red shaded) where the number and mass of aggregates both increases, suggesting the vesicles are both simultaneously replicating and growing. Then the system enters a "growth phase" (blue shaded) where the mass of vesicles increases while the particle count begins to drop. During the growth phase the molecular concentration of **1** does not decrease, so the decreased particle count is likely due to the merging of micelles or small vesicles into larger aggregates. Although we cannot be certain, we suspect that replication and growth processes happen simultaneously, but dominate the system at different stages, and that the 'transition' from the 'replication phase' to 'growth phase' occurs when the number of aggregates in the system makes the probability of collision (and merging) between aggregates more likely, which would cause some vesicles to grow while simultaneously consuming smaller aggregates. It may be that nucleation of supramolecular structures by existing vesicles plays a role in this effect as well, as oligolamellar and multivesicular vesicles[199] can both be seen from cryo-TEM imaging of **1** in buffer (see Figure 19 and Figure S 9), which would increase the mass of measured particles while potentially offering a mechanism for them decreasing in number without the decomposition of **1**.

The third phase, "vesicle collapse" (purple shaded) occurs when **1** decomposes, which (as discussed above) is an autocatalytic process initiated by the depletion of electrophile **3**, and both the particle count and mass rapidly decrease in a non-linear fashion.

Finally, the system then reaches a "dormant phase" (shaded green), which starts when the concentration of **1** reaches its minimum and almost no particles are seen. During the dormant phase the molecular **1** increases in concentration until it begins to aggregate and then re-enters the replication phase.

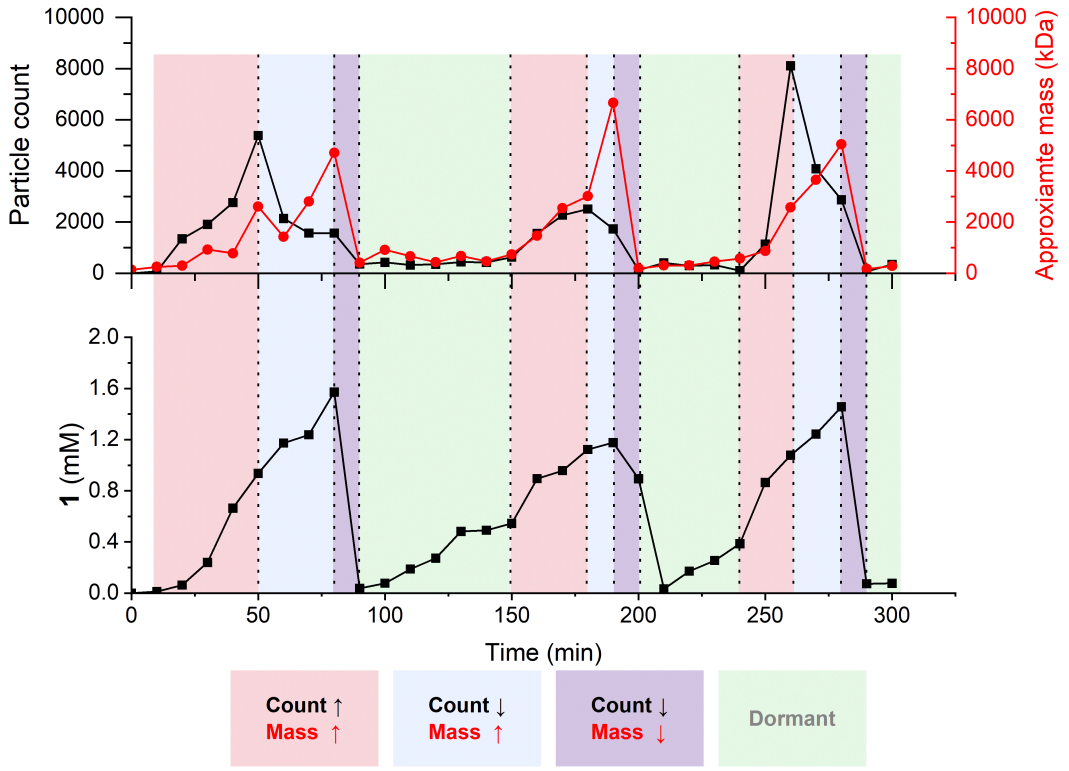


Figure 20. Following the oscillations in **1** where a sample is taken every 10 min and examined by iSCAT and UPLC. Four supramolecular stages of the oscillation have been identified and are highlighted by different colours: A “replication phase” (red), a “growth phase” (blue), a “vesicle collapse” phase (purple) and finally a “dormant phase” (green). Lines are drawn to guide the eyes.

2.3 Conclusions

We have developed a system of oscillating vesicles based on a chemically fuelled autocatalytic reaction network. Autonomous oscillations in both monomeric concentrations of amphiphilic disulfide **1** and its aggregates can be observed. The vesicle population undergoes repeating phases of replication, growth, collapse and dormancy. These dynamic events roughly imitate cell cycles. Rationally designed supramolecular oscillators are rare, but could shed light on

how biology operates, and our work here shows that consuming chemical energy can drive biologically relevant rhythms and responses that may be relevant to complex dynamic structures at the origins of life and/or early evolutionary processes.

3. Mathematical Models for Self-Catalytic Supramolecular Chemical Oscillators

The work in this chapter was undertaken in joint collaboration with Fernando Temprano-Coleto and Howard A. Stone from the Department of Mechanical and Aerospace Engineering, Princeton University.

3.1 Introduction

Understanding chemical oscillators requires more than qualitative descriptions – these systems involve complex and nonlinear structures that are difficult to intuitively predict. In history, the research on chemical oscillators was extensively restricted by the lack of mathematical and physical tools. Belousov had discovered the oscillation in 1950, but his work was rejected by other USSR scientists immediately because they thought his discovery "contradicted the Second Law of Thermodynamics" and was "Theoretically impossible".[200] After his discovery was published in 1958, it was unnoticed for years since the principle of chemical oscillators was not widely recognised in the USSR then. In the following decades, Prigogine, Field, and Noyes studied the kinetics and thermodynamics of the B-Z reaction, making the mathematical and physical basis solid gradually.[201,202] By the 1970s, a comprehensive understanding of the B-Z reaction was finally achieved thanks to the wide application of theoretical tools such as differential equations and non-equilibrium statistical mechanics. The most accepted mechanism today is the FKN mechanism, whose kinetic model is called Oregonator.[203]

The theoretical study on chemical oscillators is not only for a better understanding, but also is important for the rational design of new oscillating and self-organising dissipative systems. In

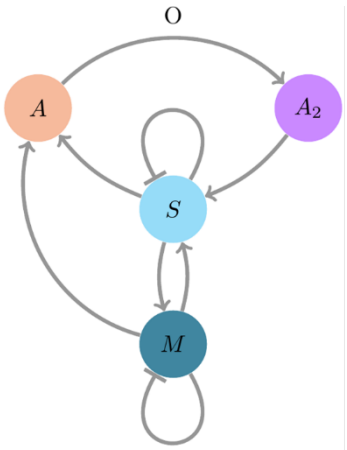
2015, W. T. Huck's group reported a tunable oscillating network by rational design of network topologies and kinetics simulations based on ODEs.[70] The oscillating behaviour of the system is well predicted by the mathematical model and highly tunable by changing the kinetic parameters. Another rationally designed example is the Fmoc-piperidine oscillation.[72] The differential kinetic model can not only precisely predict the oscillating features, but also explain the catalytic selectivity to piperidine-catalysed reactions.

In this chapter, we present the mathematical and physical principles to explain the mechanism of the physical autocatalysis supramolecular oscillators. We begin with basic kinetic models with positive and negative feedback loops, then introduce biphasic properties such as time delays. We also examine the bifurcation, responsiveness, and synchronisation of these models and adapt the models to experimental findings. By doing so, we aim to show a quantitative understanding of the supramolecular oscillators and advance the design of new oscillatory systems.

3.2 A mathematical model of the oscillating supramolecular self-replicator

3.2.1 The reaction kinetic model

The reaction kinetic model is made from the oscillating supramolecular self-replicator reported by our group in 2022.[157] The reaction networks and elementary reactions in the oscillation are shown in Scheme 1. In the network diagram and reaction equations, the 5,5'-dithiobis (2-nitrobenzoic acid) is noted as A_2, the 5-mercapto-2-nitrobenzoic acid is noted as A, the surfactant and micelle are noted as S and M, the oxidant (hydrogen peroxide) is noted as O, and the aliphatic thiol and the waste product (aliphatic disulfide) are noted as T and W. Because of the aliphatic thiol T is far excess, its concentration can be regarded as constant and omitted in the network diagram. The waste product W can also be omitted because it cannot participate in the oscillations.



$$A_2 + T \xrightarrow{k_S} S + A$$
$$S + T \xrightarrow{k_{dS}} A + W$$
$$nS \underset{k_{dM}}{\overset{k_M}{\rightleftharpoons}} M$$
$$M + A_2 + T \xrightarrow{k_S^*} M + S + A$$
$$M + nT \xrightarrow{k_{dS}^*} nA + nW$$
$$O + 2A \xrightarrow{k_O} A_2$$

Scheme 1. The reaction networks (left) and elementary reactions (right) in the oscillating supramolecular self-replicator. The arrows mean conversion and catalysis, and the blunt arrows mean inhibition in the network. The rate constants are noted as *k*.

We also assume all steps obey the law of mass action, which means the reaction rates of all steps are directly proportional to the product of the reactants. The rate equation is (1.8). The concentration of thiol T is constant and merged into the rate constants. r_{ext} is the constant injection rate of hydrogen peroxide. It is unlikely that the concentration of free surfactant and micelle can be measured separately. In the experiments, all the surfactants are fully dissolved in the UPLC sample solvent (ACN-water), so the measured surfactant concentration is $c_{S,sum} = c_S + nc_M$. In the following simulations, $c_{S,sum} = c_S + nc_M$ is used when comparing the simulations with experiments.

$$\begin{aligned}
\frac{dc_{A_2}}{dt} &= k_O c_O c_A - k_S c_{A_2} - k_S^* c_M c_{A_2} \\
\frac{dc_A}{dt} &= k_S c_{A_2} + k_S^* c_M c_{A_2} + k_{dS} c_S + n k_{dS}^* c_M - 2k_O c_O c_A \\
\frac{dc_O}{dt} &= r_{ext} - k_O c_O c_A \\
\frac{dc_S}{dt} &= k_S c_{A_2} - k_{dS} c_S + k_S^* c_M c_{A_2} + n k_{dM} c_M - n k_M c_S^m \\
\frac{dc_M}{dt} &= k_M c_S^m - k_{dM} c_M - k_{dS}^* c_M
\end{aligned} \tag{1.8}$$

By choosing proper units and using matter conservation, the equation (1.8) is reduced and non-dimensionalised for the simulations, the derivation is in 5.2.1. When the micelles form, transferring the thiol T from the organic phase to the aqueous phase takes time, thus, all steps with the participation of M and T have time delays (see 5.2.2). Due to the difficulties in analysing the time-delayed differential equation, the bifurcation analysis is performed on the non-delayed versions, and the other numerical simulations are performed on the delayed models.

3.2.2 The simulation of oscillation experiments

The differential reaction kinetic model is tested on the reported oscillation experiments.[157] The injection rate of hydrogen peroxide r_{ext} is obtained directly from the experiment. Due to the oxidation rate of A to A_2 and the micellisation/dimicellisation rate of micelles being very fast, the related constant terms are set to a very large constant value (10^4) and other parameters are optimised to make the experimental oscillation close to the simulation. Figure 21a shows an oscillating state at selected parameters. At the very beginning (0 - ~0.2 time units), there is a very high and sharp peak of S, because this trial starts from the A_2 and leads to a very fast formation of S. Then, the system reaches a stable oscillation. The simulation is partly quantitatively consistent with the experiments (Figure 21b), and captures most experimental kinetic features.

The reaction rates of A_2, S and M are shown in Figure 21c. The initial rates in the first 0.25 time units are truncated because it is transient and strongly fluctuate. The change of reaction rates is tracked in one oscillation peak (grey dotted lines in Figure 21a and Figure 21c). At the beginning, the changing rate of A_2 (dc_{A_2}/dt) is nearly a constant, so the concentration of A_2 (c_{A_2}) increases at a constant rate. The changing rates of both S (dc_S/dt) and M (dc_M/dt) are very slow at the beginning and then grow exponentially when enough A_2 accumulates, showing

the autocatalytic formation of S and M. The changing rate of S and M then decreases at their high concentrations, causing the concentrations of S and M to decrease and return to the beginning state. This result quantitatively shows the positive and negative feedback loops in the oscillation.

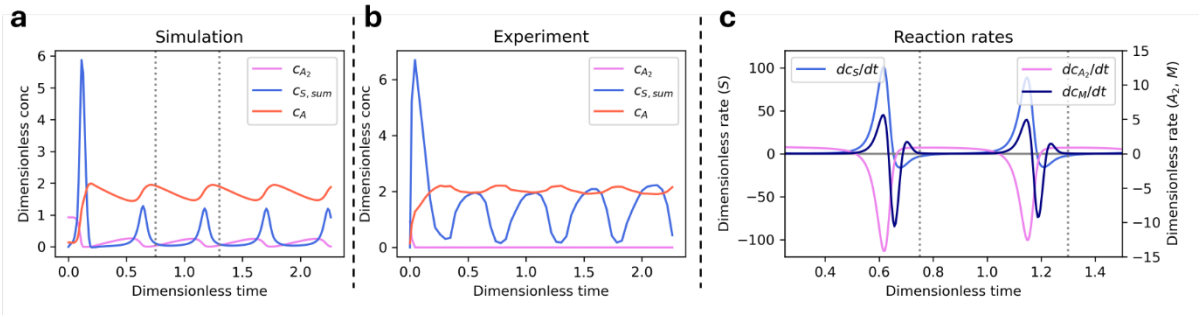


Figure 21. a) The numerical simulation of the oscillating kinetic model. b) The experimental oscillation. The experimental conditions are from M. G. Howlett et. al.[157] c) The changing rates of S, A_2 and M. The grey lines show the region within one peak, as well as in figure 21a.

3.2.3 The role of the fuel supply

The supply rate of the chemical fuel, hydrogen peroxide, is an important control factor of the chemical oscillator. It controls the conversion rate from A to A_2 and is very easy to tune in the experiments. So, the time-evolution of the chemical oscillator model is calculated at different hydrogen peroxide injection rates r_{ext} to study the role of the fuel in the chemical oscillator. In this part, a non-delayed model is used.

Numerical simulations show that the oscillator stays at a non-equilibrium steady state (Figure 22a) at a low injection rate, the concentration of A_2 and S remains unchanged at a low level after a transient increment. When the injection rate goes higher, the system is switched to an oscillating state (Figure 22b). We have discussed in 1.2.1.3 that oscillating states have higher entropy production and free energy dissipation. Thus, a higher fuel input is required to maintain

the oscillating state. Both the steady and oscillating states are reported in our group; the steady state is achieved at a slower fuel input, and the oscillating state needs higher inputs.[108,157]

However, the oscillation also stops when the injection of hydrogen peroxide continues rising (Figure 22c). An overhigh injection rate converts all A to A_2 in the beginning, then the decomposition of S is suppressed by the strong oxidising driving force, and the system finally stops at a complete conversion to S.

To visualise the global effect of hydrogen peroxide injection rates, a bifurcation analysis is performed (Figure 22d). The rate equations (1.10) has a pair of conjugate eigenvalues with negative real parts at low injection rates, indicating that the steady states are preferred. As the injection rate increases, the eigenvalues across the imaginary axis spontaneously show a typical Hopf bifurcation, a transition between steady states and oscillating states. When the injection rate continues to increase, another Hopf bifurcation happens, and the system returns to the steady state. These results show the oscillation only occurs at a specific window of the fuel supply rate. This indicates the importance of maintaining the balance of the energy and matter flux in the chemical oscillation.

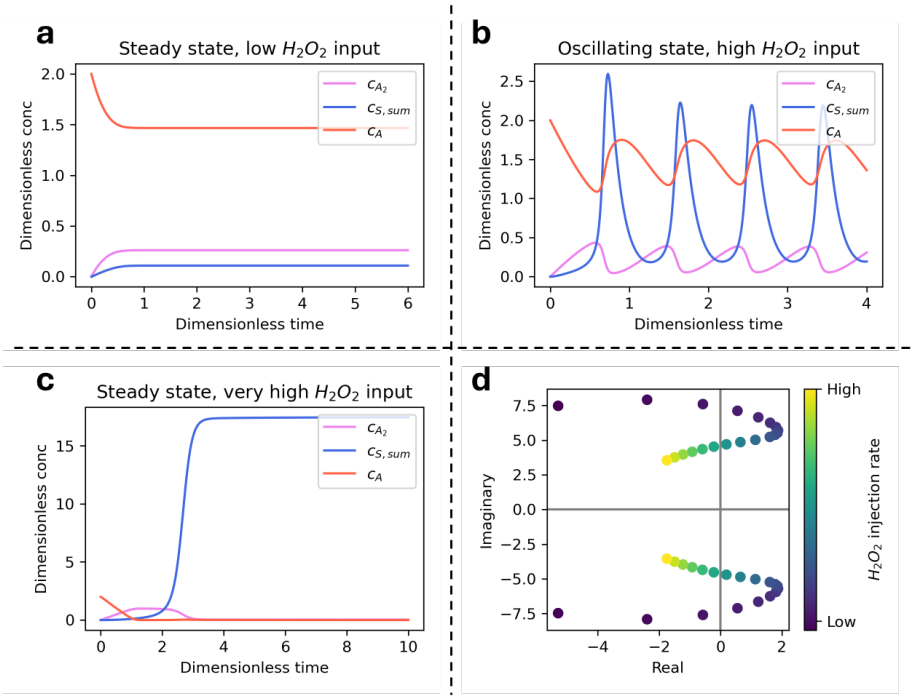


Figure 22. a) A non-equilibrium steady state at low H_2O_2 input. Both the A and S experience a transient increment and stay at the steady state. b) An oscillating state at a higher H_2O_2 input. c) The system returns to the steady state at a very high H_2O_2 input. d) The change of conjugate eigenvalues of the differential rate equations. The low and high injection rates are coloured in dark blue and bright yellow. The negative real part means that the steady states are preferred, while the positive real part means that oscillations are preferred.

3.2.4 Control of oscillations

The oscillation system is highly tunable by varying the conditions, including H_2O_2 injection rates, stirring speeds, and catalyst concentrations.[157,166]

The H_2O_2 injection rate is expressed explicitly in the model. Three different rates are used in the simulations, which are compared with the experiments. The higher injection rates increase the heights and decrease the periods of the peaks, so the peaks look taller and sharper at high injection rates (Figure 23).

The other two control factors, stirring rates and catalyst (DMAP) concentrations, are not explicitly included in the kinetic model. However, their effects can be evaluated by changing the delays and rate constants. Figure 24 shows the impact of the stirring rate on the oscillation

peaks. Increasing the stirring rate can accelerate the diffusion of all components, thus increasing the rate parameters and decreasing the delays. The amplitude decreases as the stirring rate increases, showing that the decomposition rates of the surfactant and micelle are affected more than the formation rates. Figure 25 shows the oscillations at different DMAP concentrations. The impacts on the rate constants are similar to increasing the stirring rate. DMAP activates the disulfide bonds and accelerates all the rate constants related to the formation and decomposition of the surfactants. However, it cannot affect the time delays. So, the addition of DMAP not only decreases the oscillation amplitudes but also decreases the periods significantly.

In summary, the simulations for the three types of control factors are qualitatively consistent with the experiments. What needs to be emphasised is that our model does not fully capture the shapes of the peaks at low DMAP concentrations (Figure 25, top 2 figures). In experiments, the peaks are very broad and flat, but the simulations are sharp at the maximum of the surfactant concentrations. We are still trying to figure it out in the next step.

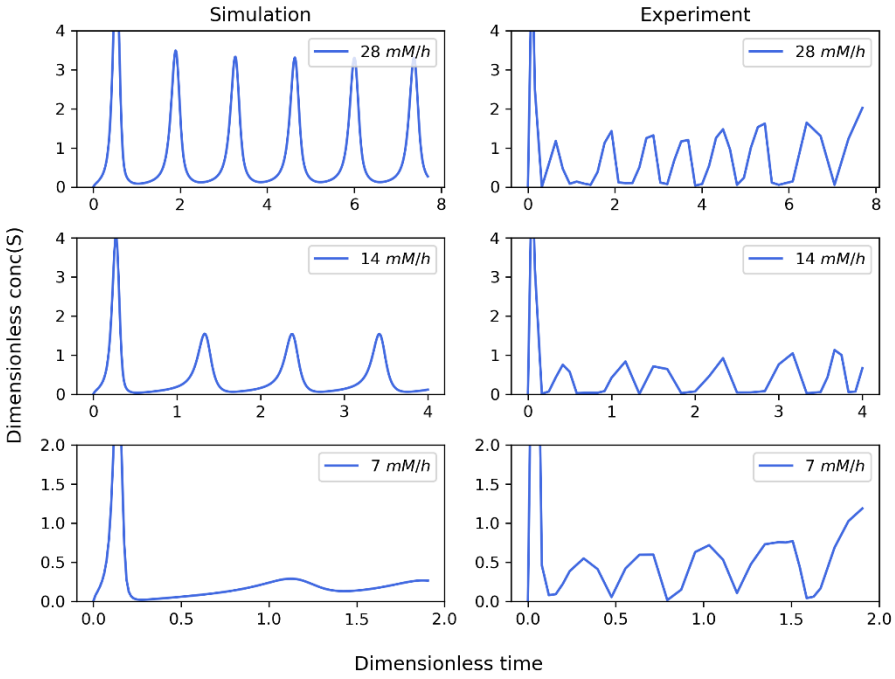


Figure 23. The effect of H_2O_2 injection rate on the chemical oscillation. The injection rates at 7, 14 and 28 mM/h are evaluated. When the injection rate increases, the peaks' periods decrease and the peaks' heights increase. So, the H_2O_2 injection rate controls the "sharpness" of the peaks. The simulation results are qualitatively consistent with the experiments.

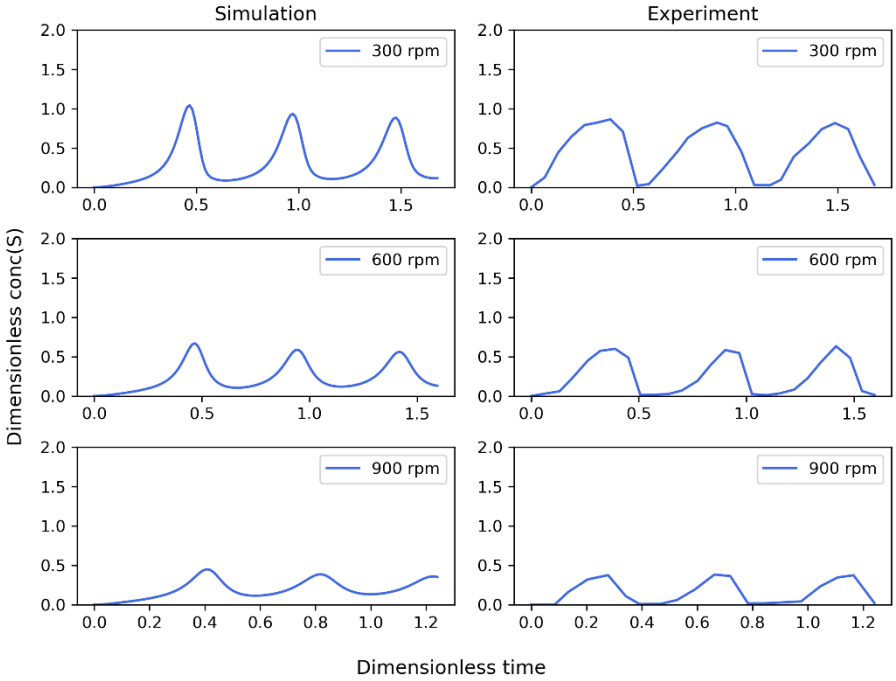


Figure 24. The effect of stirring rates on the chemical oscillation. The stirring rates are evaluated at 300, 600 and 900 rpm. The increment of stirring rates causes a decrease in the amplitudes and a slight decrease in the periods.

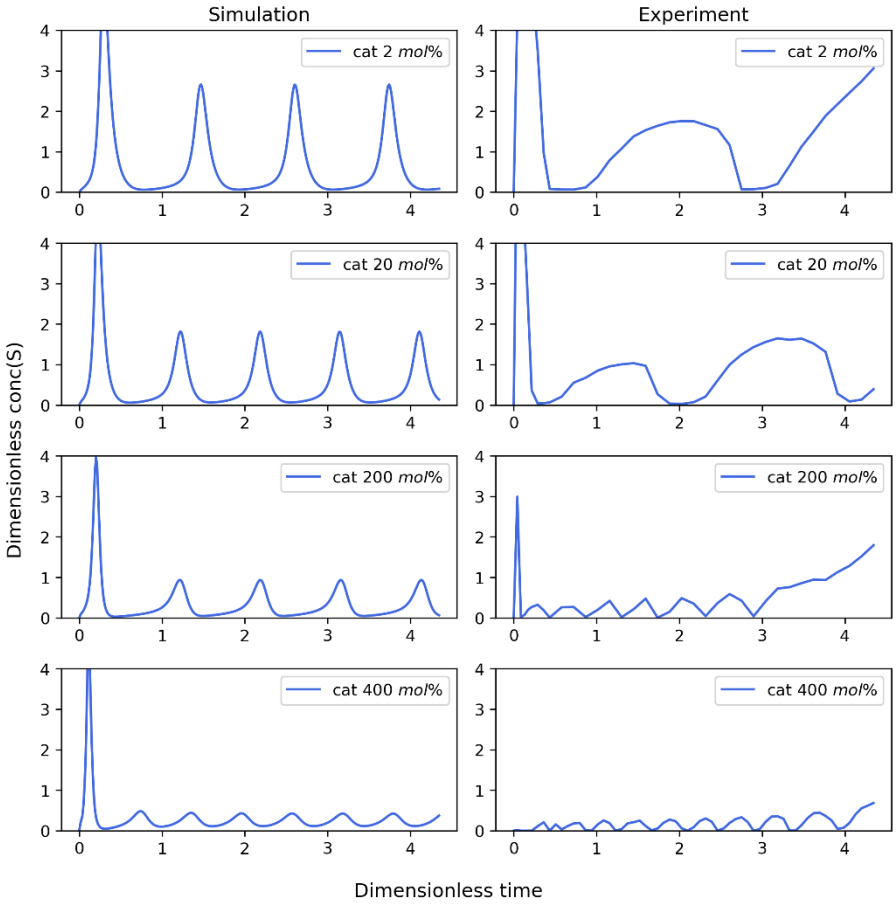


Figure 25. The effect of DMAP concentrations on the chemical oscillation. The DMAP are evaluated at 2%, 20%, 200% and 400% in mole fraction. The increment of DMAP causes a significant decrease in amplitudes and periods.

3.3 The modelling of the mixed oscillators

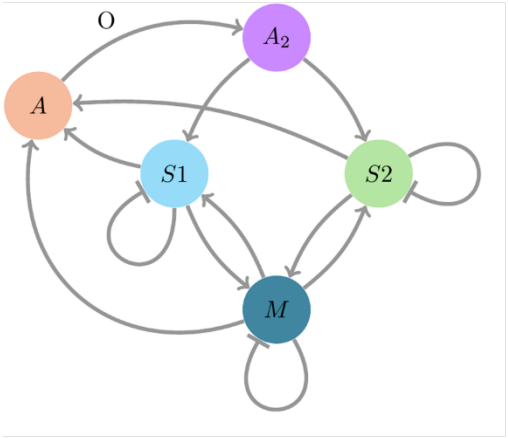
3.3.1 Two-surfactant kinetic model

We have explored the selection and competition behaviours in lipid systems.[112] In this section, we aim to explore the non-equilibrium dynamic behaviours when two chemical oscillators are mixed. So, a kinetic model for mixed oscillators is made (Scheme 2).

In this system, two different thiols T_1 and T_2 are mixed in the oscillation, which then convert to two surfactants S_1 and S_2. We assume the surfactants co-assemble to a mixed micelle M, whose concentration equals the sum of the concentrations of micelles at same surfactant

concentrations in separate ($c_M = c_{M_1} + c_{M_2}$). The micelle can catalyse the formation of both S_1 and S_2, and the catalytic capability of co-assembled micelles is the same as pure micelles. S_1, S_2 and M are decomposed by T_1 and T_2.

The co-assembly assumption plays a critical role in the reaction networks. The formation of both S_1 and S_2 contributes to the micelle formation, and the micelles M also catalyse the formation of both surfactants. In this network, the micelles mediate the synchronisation of concentration changes between the two surfactants. The kinetic equations for the mixed oscillator are (1.15).



$$A_2 + T1 \xrightarrow{k_{S1}} S1 + A$$
$$A_2 + T2 \xrightarrow{k_{S2}} S2 + A$$
$$S1 + T1 \xrightarrow{k_{dS11}} A + W$$
$$S1 + T2 \xrightarrow{k_{dS12}} A + W$$
$$S2 + T1 \xrightarrow{k_{dS21}} A + W$$
$$S2 + T2 \xrightarrow{k_{dS22}} A + W$$
$$n_1S1 + n_2S2 \underset{k_{dM}}{\overset{k_M}{\rightleftharpoons}} M$$
$$M + A_2 + T1 \xrightarrow{k^*_{S1}} M + S1 + A$$
$$M + A_2 + T2 \xrightarrow{k^*_{S2}} M + S2 + A$$
$$M + nT1 \xrightarrow{k^*_{dS1}} nA + nW$$
$$M + nT2 \xrightarrow{k^*_{dS2}} nA + nW$$
$$O + 2A \xrightarrow{k_O} A_2$$

Scheme 2. The reaction networks (left) and chemical reactions (right) of the 2-surfactant mixed oscillator. The arrows mean conversion and catalysis, and the blunt arrows mean inhibition in the network. The rate constants are noted as *k*.

3.3.2 Competition and synchronisation

The 1:1 mixture of 2-octanethiol (T1) and 2-nonanethiol (T2) is studied in the mixed oscillation. Both the experiment and the numerical simulation show that two chemical oscillators with different periods will synchronise when being mixed (Figure 26). This can be

explained by the concentration changes of the two surfactants S1 and S2 are “connected” by the co-assembly.

The competition can also be observed in the mixed oscillation. The amplitudes of S1 and S2 are similar when not mixed in the experiment. However, in the mixture, the amplitude of S1 remains almost unchanged while the amplitude of S2 decreases significantly. This happens in the simulations when the kinetic parameters of 1 are higher than those of 2. It means that the oscillator with a higher reaction rate can utilise the chemical fuel more efficiently and acquire advantages in the oscillation. So, the oscillator 1 occupies almost all fuel and remains unchanged, while the oscillator 2 is more difficult to sustain the oscillation under the competition.

These results show a good insight into how two different networks interact and compete mutually, and provide mechanistic explanations for competition and synchronisation in oscillators. Synchronised oscillation is widely discovered in living systems, such as circadian rhythms and firing neurons.[204] This study helps us to construct more complicated coupled oscillatory networks and simulate these live behaviours from bottom-up strategies.

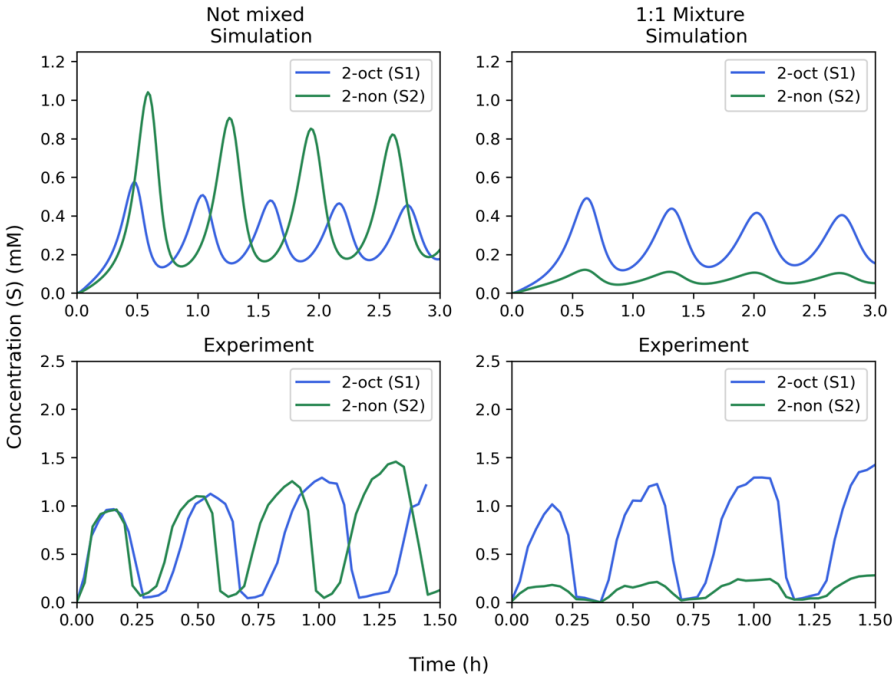


Figure 26. The simulations and experiments for the mixed oscillation. The left side shows the simulation and experiment of two oscillators with different periods. The right side shows the mixture of the two oscillators. The periods are synchronised, and the amplitudes show competition. The experimental data are from Lukas Marrow's Part II thesis "Exploring the reaction space of a supramolecular chemical oscillator".

3.4 Conclusions

In this chapter, we developed and analysed mathematical models for self-catalytic supramolecular chemical oscillators. Starting from the experimental system of a fuel-driven disulfide-based micellar replicator, we constructed a kinetic network based on the law of mass action and incorporated autocatalytic feedback and phase-transfer delays. Through simulations, we showed that the model successfully reproduces key features of the experimental oscillations, including periodic kinetics, asymmetric growth and decay phases and tunability.

Bifurcation analysis further revealed the critical role of the fuel supply rate in governing the transition between steady-state and oscillatory behaviour, with oscillations only occurring within a narrow window of fuel input.

A mathematical model for mixed oscillators is developed in the following step, demonstrating that synchronisation and competition arise through the interaction of networks. This study offers a theoretical tool for constructing diverse chemistry networks and simulating more complex life-like systems.

These results demonstrate that mathematical modelling serves not only as a tool for comprehending experimental data but also as a predictive framework for designing new oscillatory systems. The close alignment between the model and the experimental results reinforces the idea that chemical oscillators can be engineered in a rational way, guided by thermodynamic and kinetic principles.

4. Conclusions and Future Works

This thesis has explored how supramolecular disulfide chemical oscillators can act as minimal models for non-equilibrium and life-like dynamics. Starting with foundational concepts in the origin of life, the study constructed a conceptual bridge between biological features—metabolism, responsiveness, and reproduction—and their physical counterparts: energy dissipation, kinetic feedback, and information transfer. These three aspects converge in our self-replicating supramolecular oscillating systems, providing a rich framework for examining the emergence of order and function in non-equilibrium chemistry.

The experimental study of a self-replicating vesicle oscillator demonstrates that dynamic, out-of-equilibrium behaviours can be achieved in synthetic supramolecular systems through well-designed reaction networks. The periodic growth and collapse of vesicles mirror key biological cycles and suggest potential pathways for prebiotic compartmentalisation and self-organisation.

Theoretical modelling played a complementary role by helping to quantify the feedback mechanisms responsible for oscillation, identifying parameter regimes that support dynamic

behaviour, and predicting how experimental factors, such as fuel flow rate, stirring rate, and catalyst concentration, control the overall dynamics. A model for the mixed oscillators also simulated complex behaviours, including synchronisation and competition, arising from the interactions of multiple oscillatory networks. Together, these approaches provide a unified view of how chemical oscillators can be used to simulate and study life-like phenomena.

Both the experiments and the mathematical models possess the potential to be utilised in constructing more complex life-like systems. In the future, numerous extensions, both chemical and biological, can be explored. The packing parameters of the monomers can control the shape of the oscillatory aggregates, so the different shapes, including cylindrical micelles and lamellar phases, can be created by rational design.[205] Coupling oscillatory chemical systems with spatial gradients and diffusion may result in pattern formation reminiscent of biological morphogenesis. The advantages of oscillation control in our systems can effectively create different patterns. Beyond synthetic chemistry, the interaction and competition could provide an ideal simulation for natural selection and reveal how complexity increases autonomously under stress. These studies will make a significant contribution to understanding the origin of life.

In summary, chemical oscillators are fascinating non-equilibrium phenomena and powerful tools for understanding and engineering the fundamental principles of life. Their continued development may bring us closer to constructing artificial systems that blur the line between chemistry and biology.

5. Experimental and Simulation Details

5.1 Supplementary methods and data of Chapter 2

5.1.1 Oscillation experiments

All biphasic oscillation experiments were conducted in TRIS buffer (0.5 M, pH 9.00). The pH was adjusted by adding 0.1 M aq. HCl and measured using a Jenway 3510 benchtop pH meter. The final pH was recorded at RT while stirring, to an accuracy of ± 0.01 pH units. For kinetic experiments, an internal standard (3-methyl-2-nitrobenzoic acid, 4 mM) was used to calibrate the concentration measured by UPLC. All aqueous solutions were prepared by ultrapure Milli-Q water and/or HPLC grade organic solvents. A 10 mL round-bottom flask and oval stirring bars (L= 15 mm, ø= 5 mm) were used in oscillation experiments in order to keep stirring consistent from run to run.

In a typical oscillation experiment, 23 mg of compound **4** and 100 mg of 1,4-diazabicyclo [2.2.2] octane (DABCO) were dissolved in 4.0 mL of 0.5 M TRIS buffer. The solution was sonicated for 20 s to break any undissolved particles. The solution was stirred at 1200 rpm and heated to 50 °C. After the solution was fully heated and in equilibrium, 0.5 mL of compound **2** was added, while 0.3 M H_2O_2 was injected using an AL-1000 syringe pump at 120 µL/h. During the injection, the needle tip was kept within the stirred aqueous layer.

5.1.2 Sampling and UPLC measurements

Samples were taken every 10 or 20 minutes. by extracting 20 µL of the aqueous layer. The extracted solution was immediately quenched by 0.6 mL maleimide solution (62 mM, 3:1 H_2O: MeCN).

A Waters Acquity ultra performance liquid chromatography (UPLC) was used to analyse the samples. An Acquity UPLC BEH C18 column (130 Å, 1.7 µm, 2.1mm× 50 mm) was used as the stationary phase, and the mobile phase was a mixture of water, MeCN and 2% TFA. The

proportion is shown in Table 1. The proportion of solvents changes at a constant rate between different stages. 0.6 mL/min flow speed was used. The concentration of UV-active components of the reaction was monitored using a built-in photodiode array (PDA) detector. Peak areas were integrated at a wavelength of 240 nm. Instrument control and data processing were performed using Empower software.

Time	Water	MeCN	2% TFA
0.00-0.05 min	93%	2%	5%
0.06-0.40 min	70%	25%	5%
1.60-2.20 min	0%	95%	5%
2.45-3.00 min	93%	2%	5%

Table 1. The UPLC method

5.1.3 iSCAT measurements

The iSCAT experimental set-up is similar to that described by Young et al[197], with a 520 nm diode laser used as the incident light source. Frames were recorded at 1 kHz with an exposure time of 0.98 ms, using a CMOS camera. Focus in the z axis is maintained using an autofocus system relying on the total internal reflection (TIRF) of a 638 nm beam. Instrument control was performed using the custom software written in LabView.

Data processing was performed using the Refeyn Discover MP and Python 3. In brief, differential imaging was achieved by subtracting sets of images temporally offset by a time Δt. The signal-to-noise ratio was then improved by spatially (3 x 3 binning) and temporally averaging the differential images (3 images). Particle detection was performed as described by Young et al[1]. Briefly, diffraction-limited spots were identified by the software, and fitted to

the 2D Gaussian function to give the ratiometric contrast value. The possibility of each diffraction limited spot being attributed to more than one particle was excluded by considerations of landing rates similar to those described by Ortega-Arroyo et al.[113] In each 30 s video, the number and contrast of fitted particles corresponding to binding events was counted to quantify reaction kinetics. The mean and median of contrast were calculated by Python 3.

Glass coverslips (24 x 50 mm, VWR) and gaskets were cleaned by sequential sonication in MQ water and 1:1 MQ water: isopropanol (5 min each), and dried under the nitrogen flow. All coverslips and gaskets were made in the same day of measurement.

A typical oscillation experiment was run and 10 μL of sample was taken every 10 or 20 mins. The samples were diluted by 0.5 mL TRIS buffer immediately and filtered through a syringe filter (PTFE, 0.22 μm, VWR). 5 μL of TRIS buffer was loaded in the gasket before the measurement. 15 μL of diluted sample was loaded in the gasket and mixed with the pre-loaded TRIS buffer and 30 s iSCAT videos were recorded immediately.

5.1.4 DLS measurements

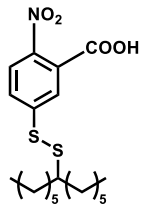
The size of aggregates in oscillation reactions was measured by dynamic light scattering (DLS). A typical oscillation experiment was run and 10 μL of sample was taken per 10 minutes. The samples were diluted by 0.5 mL TRIS buffer (0.5 M, pH 9.00) immediately and filtered through a syringe filter (PTFE, 0.22 μm, VWR). The filtered samples were injected into disposable plastic cuvettes (ZEN0040). All samples were equilibrated for 30s before measurement.

Analyses were performed using a Malvern Zetasizer Nano ZEN5600 recording particle and molecule size. Instrument control and data processing were performed using Zetasizer software. Measurements were made using an equilibrated heating probe at 25 °C, setting the following parameters for 0.5 M TRIS buffer (calculated internally using the software's complex solvent builder): refractive index = 1.339, viscosity = 1.0780 mPa s. The parameters

of POPC were used to approximate the surfactant **1**. Three repetitions of 12 measurements were taken for every sample.

5.1.5 Synthesis of compounds

All commercial chemicals were purchased from Sigma-Aldrich and were used without further purification. Reactions were followed using thin layer chromatography (TLC) on silica gel-coated plates (Merck 60 F254). Detection was performed with UV-light (254 nm), and/or by charring at ~150 °C after dipping into a solution of $KMnO_4$ (1 g/100 mL in ethanol). NMR spectra were recorded on a Bruker 400 (400 MHz) spectrometer in $CDCl_3$. Chemical shifts are given in ppm with respect to tetramethylsilane (TMS) as internal standard. Coupling constants are reported as J-values in Hz. Column chromatography was carried out using Acros silica gel (43-60 μm).



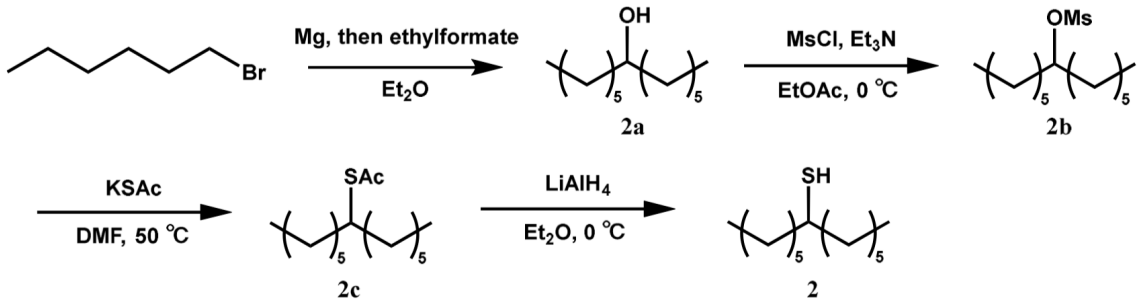
2-nitro-5-(tridecan-7-yldisulfaneyl)benzoic acid (**1**):

5,5'-Dithiobis-(2-nitrobenzoic acid) (332 mg, 0.84 mmol) and trimethylamine (0.36 mL, 0.84 mmol) were dissolved in 4 mL DCM. To this solution was added 7-tridecanethiol (200 mg, 0.92 mmol, 1.1 equiv.). The mixture was stirred for one hour, after which 20 mL of a 1M HCl solution was added. The aqueous layer was extracted with DCM, the organic fractions combined and dried using $MgSO_4$. After removal of the solvent, the crude product was purified using flash chromatography (2% AcOH in DCM), yielding 2-nitro-5-(tridecan-7-yldisulfaneyl)benzoic acid as a light yellow solid (52%)

^{1}H NMR (400 MHz, $CDCl_3$) δ 10.39 (s, 1H, CO_2H), 7.99 (d, J = 2.0 Hz, 1H, $CHCNO_2$), 7.92 (d, J = 8.5 Hz, 1H, SCC*H*CO_2H), 7.82 (dd, J = 8.5, 2.0 Hz, 1H, SCC*H*CH), 2.81 (p, J = 6.5 Hz, 1H, CHS), 1.62 (q, J = 7.5 Hz, 4H, C*H*$_2$CHS), 1.50 – 1.36 (m, 4H, alk-CH_2), 1.31 – 1.24 (m, 12H, alk-CH_2), 0.90 (t, J = 7.0 Hz, 6H, CH2C*H*$_3$).

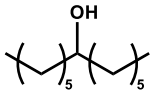
^{13}C NMR (101 MHz, $CDCl_3$) δ 170.5 (CO_2H), 147.0 (CNO_2), 145.8 (*C*SSCHCH$_2$), 128.8 (*C*CO$_2$H), 127.1 (*C*CNO$_2$), 126.8 (CSS*C*CO$_2$H), 124.5 (*C*CSSCHCH$_2$), 53.6 (*C*HSS), 33.8 (*C*H$_2$CHSS), 31.6 (alk-*C*H$_2$), 29.1 (alk-*C*H$_2$), 26.7 (alk-*C*H$_2$), 22.6 (alk-*C*H$_2$), 14.0 (CH$_2$*C*H$_3$).

Compound **2** was synthesised according to scheme reported by Anthonius et al.[109] with a few improvements.



Scheme S 1 Synthesis route for the preparation of **2**.

7-tridecanol (**2a**):

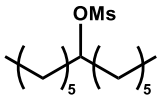


A solution of 1-bromohexane (30.0 mL, 213 mmol) in dry THF (300 mL) in a flame dried flask was cooled to –10 ºC (salt-ice bath), after which magnesium turnings (5.6 g, 230 mmol) were added portionwise (over about 3 min). A solution of ethyl formate (7.05 mL, 87 mmol) in THF was added dropwise (over about 3 min.), while maintaining the temperature below 10 ºC. The reaction mixture was then allowed to warm to RT after which it was stirred for an additional 6 hours. The reaction was quenched with sat. aq. NH_4Cl and then acidified using 1 M aq. HCl. The product was extracted using diethyl ether (3 x 50 mL) and the combined organic extracts were washed with brine and dried ($MgSO_4$). After removal of the solvent, the crude product was purified using flash chromatography (7% EtOAc in hexane) which yielded (after solvent removal) 7-tridecanol as colourless crystals (94%). NMR spectra were in agreement with literature[206].

^{1}H NMR (400 MHz, $CDCl_3$) δ 3.67 – 3.57 (m, 1H, C*H*OH), 1.52 – 1.35 (m, 4H, alk-CH_2), 1.35 – 1.17 (m, 16H, alk-CH_2), 0.87 (t, J = 7.0 Hz, 6H, CH_2CH_3).

^{13}C NMR (101 MHz, $CDCl_3$) δ 72.2 (COH), 37.8 (*C*H_2COH), 32.0 (alk-CH_2), 29.5 (alk-CH_2), 25.8 (alk-CH_2), 22.8 (alk-CH_2), 14.4 (CH_2*C*H_3).

Tridecan-7-yl methanesulfonate (**2b**):

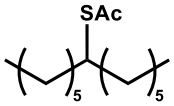


Methanesulfonyl chloride (8.2 mL, 102 mmol) was slowly added to a mixture of triethylamine (26.9 mL, 193 mmol) and 7-tridecanol (19.3 g, 96.4 mmol) in ethyl acetate (250 mL) cooled to 0 ºC. The resulting suspension was stirred for 2 h before dilute HCl (1 M, 100 mL) was added, after which the organic layer was separated, washed with brine and dried using $MgSO_4$. Solvent removal yielded tridecan-7-yl methanesulfonate as a colourless oil (96%).

^{1}H NMR (400 MHz, $CDCl_3$) δ 4.70 (quintet, 1H, CHOMs, J = 6.5 Hz), 2.99 (s, 3H, S(O)2OCH_3) 1.73 – 1.64 (m, 4H, alk-CH_2), 1.46 – 1.23 (m, 16H, alk-CH_2), 0.88 (t, J = 7.0 Hz, 6H, CH_2C*H*$_3$).

^{13}C NMR (101 MHz, $CDCl_3$) δ 84.5 (COMs), 38.9 ($CHOSO_2$*C*H_3), 34.6 (*C*H_2COH), 31.8 (alk-CH_2), 29.2 (alk-CH_2), 25.1 (alk-CH_2), 22.7 (alk-CH_2), 14.2 (CH_2*C*H_3).

S-(tridecan-7-yl) ethanethioate (**2c**):



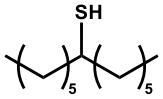
Potassium thioacetate (22.5 g, 198 mmol) was added to DMF (60 mL) and then heated to 50 ºC to dissolve all of the solid. The solution was then cooled to room temperature before tridecan-7-yl methanesulfonate (25.7 g, 92 mmol) was added in 3min. The mixture was heated to 50 ºC and vigorously stirred for 5 hours, after which the reaction was allowed to cool to RT. Brine (150 mL) and then diethyl ether (150 mL) were added and the aqueous phase extracted with diethyl ether (3 x 100 mL) and washed with brine (3 x 100 mL). After drying ($MgSO_4$)

and removal of the solvent, the crude product was purified using flash chromatography (5% EtOAc in hexane) to yield S-(tridecan-7-yl) ethanethioate as a dark red oil (99%).

^{1}H NMR (400 MHz, $CDCl_3$) δ 3.54 – 3.46 (tt, 1H, CHOAc, J = 5.5 Hz, 7.8 Hz), 2.31 (s, 3H, $SC(O)CH_3$) 1.64 –1.45 (m, 4H, alk-CH_2), 1.42 – 1.21 (m, 16H, alk-CH_2), 0.88 (t, J = 7.0 Hz, 6H, CH_2CH_3).

^{13}C NMR (101 MHz, $CDCl_3$) δ 196.3 ($SC(O)CH_3$) 44.9 (CSAc), 35.0 (*C*H2COH), 31.9 (alk-CH_2), 30.9 ($SC(O)CH_3$) 29.3 (alk-CH_2), 26.9 (alk-CH_2), 22.8 (alk-CH_2), 14.2 (CH_2CH_3).

7-tridecanethiol (**2**):

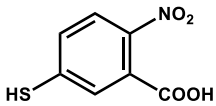


S-(tridecan-7-yl) ethanethioate (6.31 g, 26 mmol), dissolved in dry diethyl ether (20 mL), was added dropwise to a stirred suspension of $LiAlH_4$ (1.98 g, 52 mmol) in dry diethyl ether (100 mL) cooled to 0 ºC (water-ice bath). The mixture was allowed to warm to room temperature at which it was stirred for one additional hour. After cooling to 0 ºC, excess of $LiAlH_4$ was quenched using saturated NH_4Cl, after which the solution was acidified to pH 1 using 3 M HCl. The organic layer was extracted (2x50 mL distilled water), washed with brine (50 mL) and dried using $MgSO_4$. Purification using flash chromatography (100% hexanes, Rf = 0.7) yielded 7-tridecanethiol as a pale tan oil (2.93 g, 52%).

^{1}H NMR (400 MHz, $CDCl_3$) δ 2.83 – 2.73 (m, 1H, C*H*SH), 1.66 – 1.58 (m, 2H, C*H*CHSH), 1.52 – 1.41 (m, 4H, alk-CH_2), 1.38 – 1.19 (m, 14H, alk-CH_2), 0.89 (t, 6H, CH_2CH_3, J = 7.0 Hz).

^{13}C NMR (101 MHz, $CDCl_3$) δ 41.4 (CSH), 39.2 (*C*H2CSH), 31.9 (alk-CH2), 29.2 (alk-CH2), 27.2 (alk-CH2), 22.8 (alk-CH2), 14.2 (CH2*C*H3).

5-Mercapto-2-nitrobenzoic Acid (**4**):



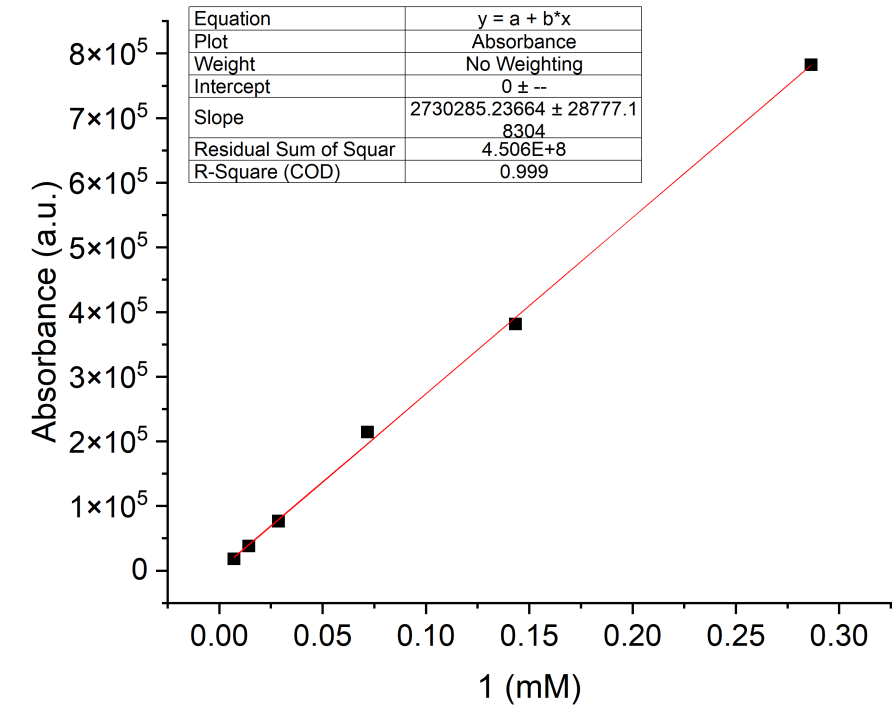
5,5'-Dithiobis-(2-nitrobenzoic acid) (**3**, 1000 mg, 2.53 mmol) was dissolved in 10 mL of an EtOH : H2O (4:1) mixture. The solution was cooled to 0 ºC (ice bath) before $NaBH_4$ (800 mg, 21 mmol) was added carefully and slowly over ~10 min. The mixture was stirred for one hour, before 1M HCl (20 mL) was added and the solution was extracted by degassed CH_2Cl_2 (2 x 30 mL). The organic layer was quickly dried by (Na_2SO_4) and concentrated to dryness to afford bright orange solid (0.80 g, 79%).

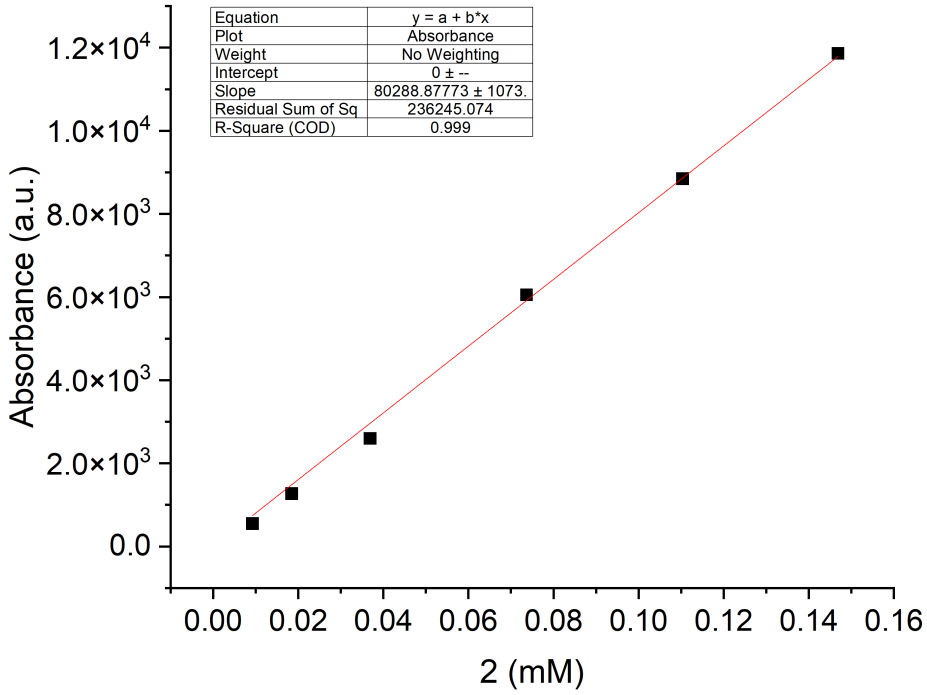
^{1}H NMR (400 MHz, DMSO) δ 14.08 (s, 1H, CO_2H), 8.04 (d, J = 8.6 Hz, 1H, $CHCNO_2$), 7.96 (d, J = 2.2 Hz, 1H, SCC*H*CO_2H), 7.89 (dd, J = 8.6, 2.2 Hz, 1H, SCC*H*CH), 3.36 (s, 1H, SH).

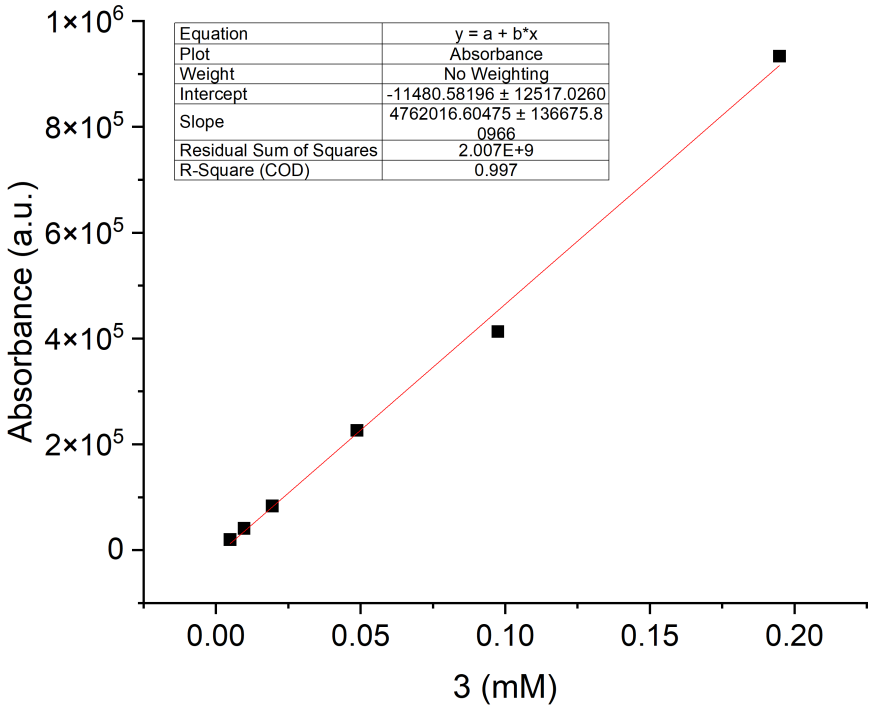
^{13}C NMR (101 MHz, DMSO) δ 165.37 (CO_2H), 146.52 (CNO_2), 141.66 (CSH), 128.97 (*C*CSH), 128.92 (CSH*C*CO_2H), 126.67 (*C*CO_2H), 125.30 (*C*CNO_2).

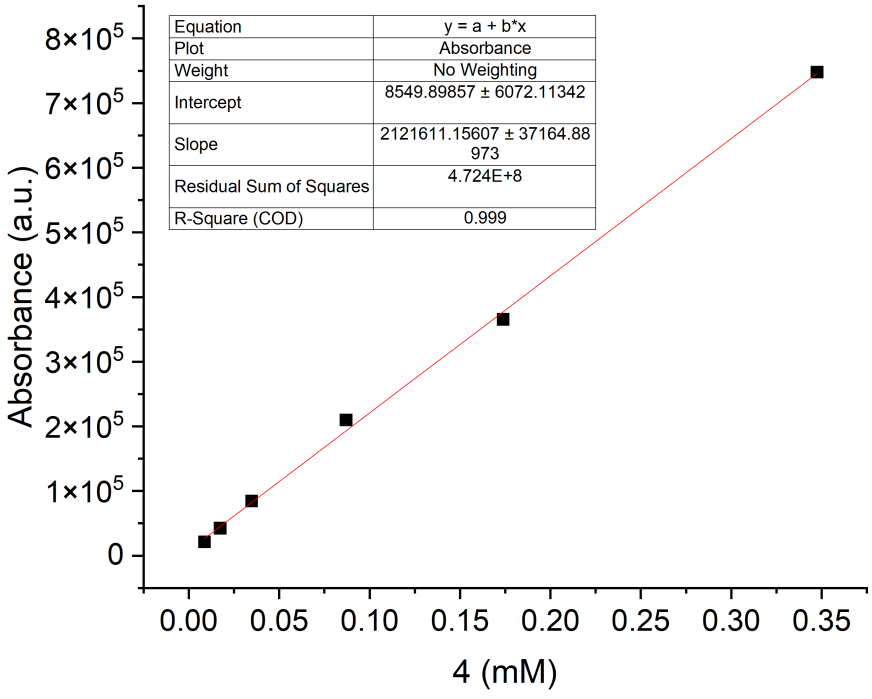
5.1.6 UPLC Calibration

The concentrations of the different UV-active species that were analysed using UPLC (see methods section) were calculated based on the calibration curves of Figure S 1.All samples were diluted by maleimide solution (62 mM, 3:1 H2O: MeCN) in gradient and measured immediately except thiol **2**, which was left overnight 12 hours to be fully quenched and dissolved.


Equation y = a + b*x
Plot Absorbance
Weight No Weighting
Intercept 0 ± --
Slope 2730285.23664 ± 28777.18304
Residual Sum of Squar 4.506E+8
R-Square (COD) 0.999
Absorbance (a.u.)
8×10^5
7×10^5
6×10^5
5×10^5
4×10^5
3×10^5
2×10^5
1×10^5
0
0.00
0.05
0.10
0.15
0.20
0.25
0.30
1 (mM)


Equation y = a + b*x
Plot Absorbance
Weight No Weighting
Intercept 0 ± --
Slope 80288.87773 ± 1073.
Residual Sum of Sq 236245.074
R-Square (COD) 0.999
Absorbance (a.u.)
1.2×10^4
1.0×10^4
8.0×10^3
6.0×10^3
4.0×10^3
2.0×10^3
0.0
0.00
0.02
0.04
0.06
0.08
0.10
0.12
0.14
0.16
2 (mM)


Equation y = a + b*x
Plot Absorbance
Weight No Weighting
Intercept -11480.58196 ± 12517.0260
Slope 4762016.60475 ± 136675.80966
Residual Sum of Squares 2.007E+9
R-Square (COD) 0.997
Absorbance (a.u.)
1×10^6
8×10^5
6×10^5
4×10^5
2×10^5
0
0.00
0.05
0.10
0.15
0.20
3 (mM)


Equation y = a + b*x
Plot Absorbance
Weight No Weighting
Intercept 8549.89857 ± 6072.11342
Slope 2121611.15607 ± 37164.88973
Residual Sum of Squares 4.724E+8
R-Square (COD) 0.999
Absorbance (a.u.)
8×10^5
7×10^5
6×10^5
5×10^5
4×10^5
3×10^5
2×10^5
1×10^5
0
0.00
0.05
0.10
0.15
0.20
0.25
0.30
0.35
4 (mM)

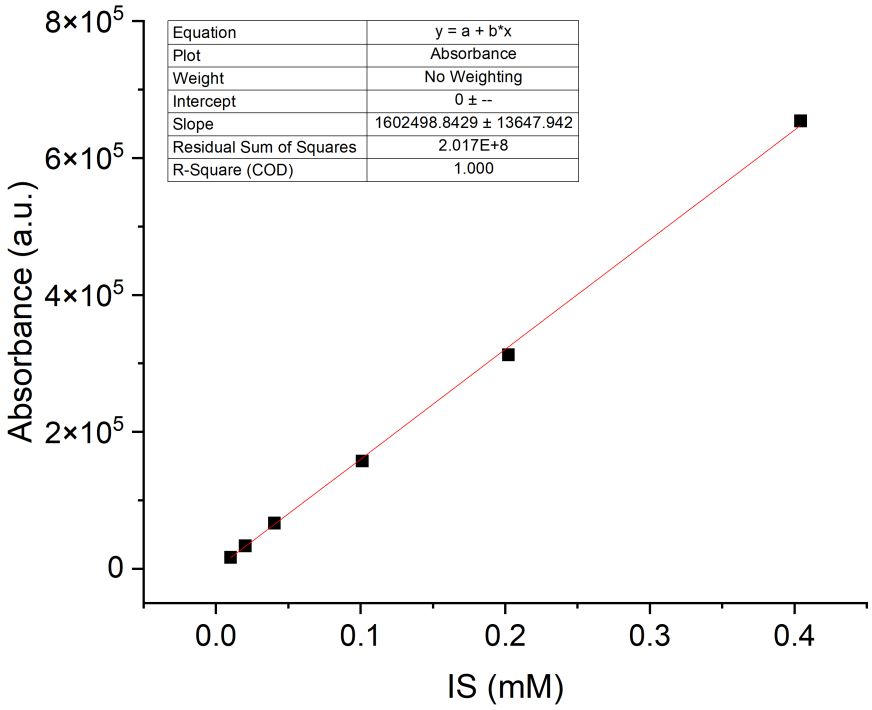


Figure S 1. UPLC calibration curves for compounds 1-4 and the internal standard.

5.1.7 Contrast-to-mass calibration of iSCAT

Contrast-to-mass (C2M) calibration was performed in commercial PBS buffer solution. The calibration protocol included measurement of a standard protein oligomer solution, with masses of 90, 180, 360, 540 and 720 kDa. Each calibration experiment was analysed using same software as described above. The mean peak contrast was determined in the software using Gaussian fitting. The mean contrast values from the calibration protein solution were then plotted and fitted to a line, $y=a + bx$, with y-contrast, x-mass, a-intercept and b-C2M calibration factor (Figure S 2).

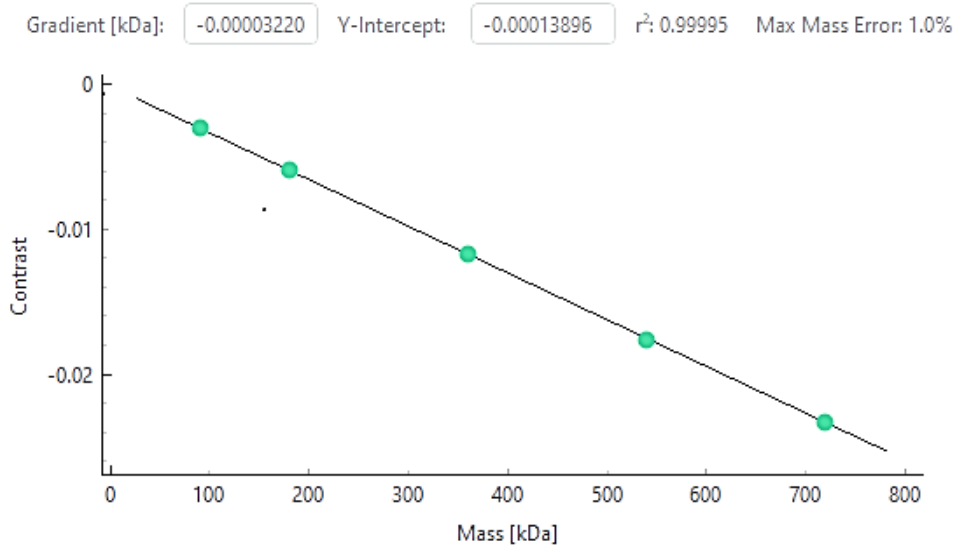


Figure S 2. Calibration curve for the conversion of ratiometric contrast to mass for a known protein oligomer standard, with masses of 90, 180, 360, 540 and 720 kDa. This calibration curve was used to estimate the average mass of the vesicles of **1**.

5.1.8 DLS measurements of 1

Measurements on **1** in pH 9 TRIS buffer gave varying size distribution depending on the concentration. From 2 mM to 0.01 mM, the sizes of vesicles dropped slightly over dilution. The vesicles fully decompose when monomer concentration at < 0.01 mM.

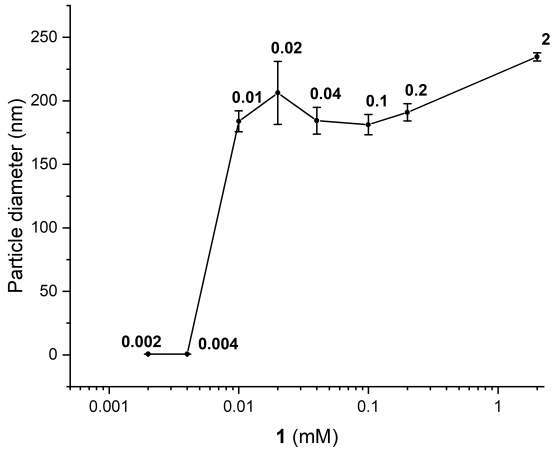
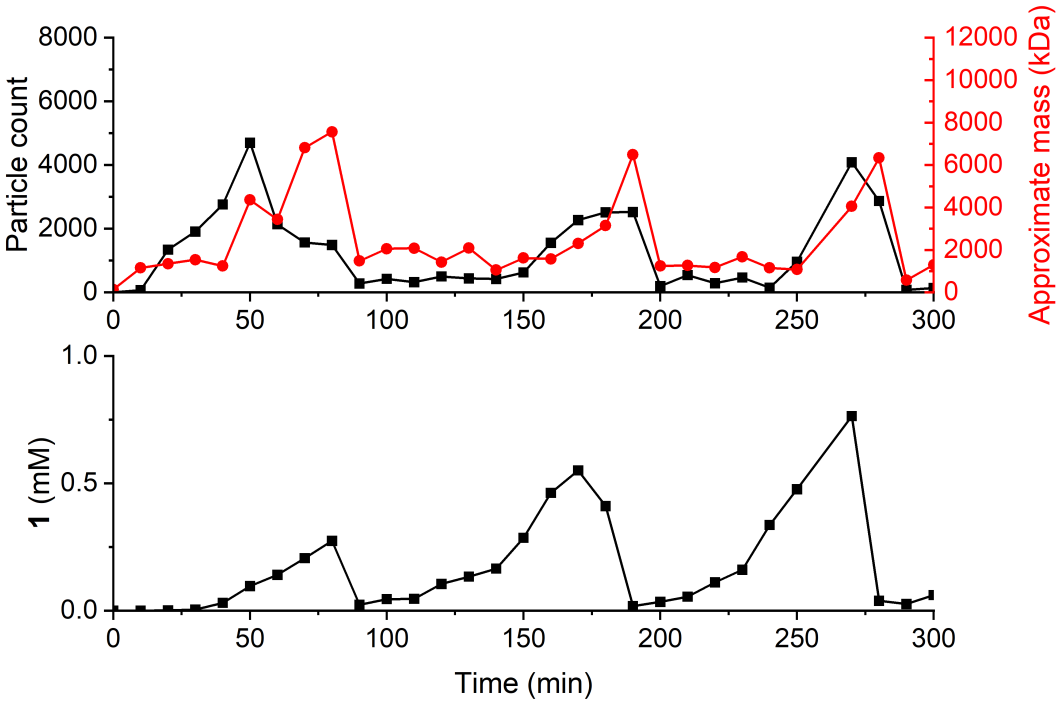


Figure S 3. Number mean diameters for various concentrations of **1** at pH 9.00. Error bars correspond to the standard deviation of the means of three experiments.

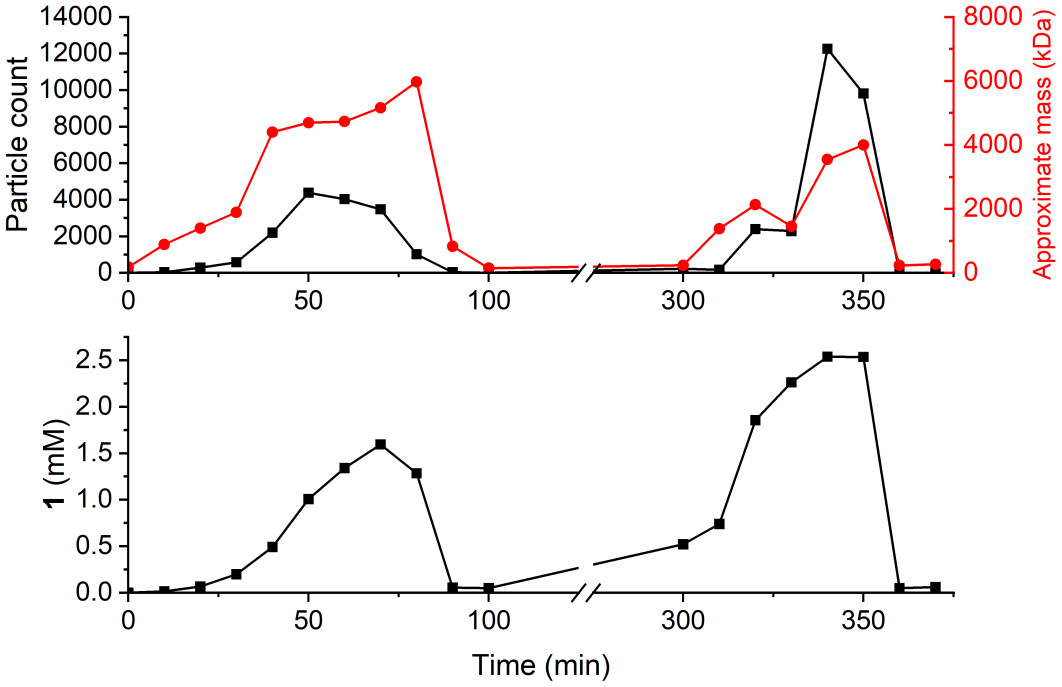
5.1.9 Replications of iSCAT measurements shown in Fig 5

Three repeats of the experiment presented in Figure 20 were conducted. One was done under the same set of measurements, and the other two were allowed to run longer. The four total experiments are consisted with observing four supramolecular stages as shown in Figure 20 in this oscillating vesicular system. All 4 trials in Figure 20 and here are conducted under as close as possible to identical conditions as described in "oscillation conditions" section above.

Experiment A:



Experiment B:



Experiment C:

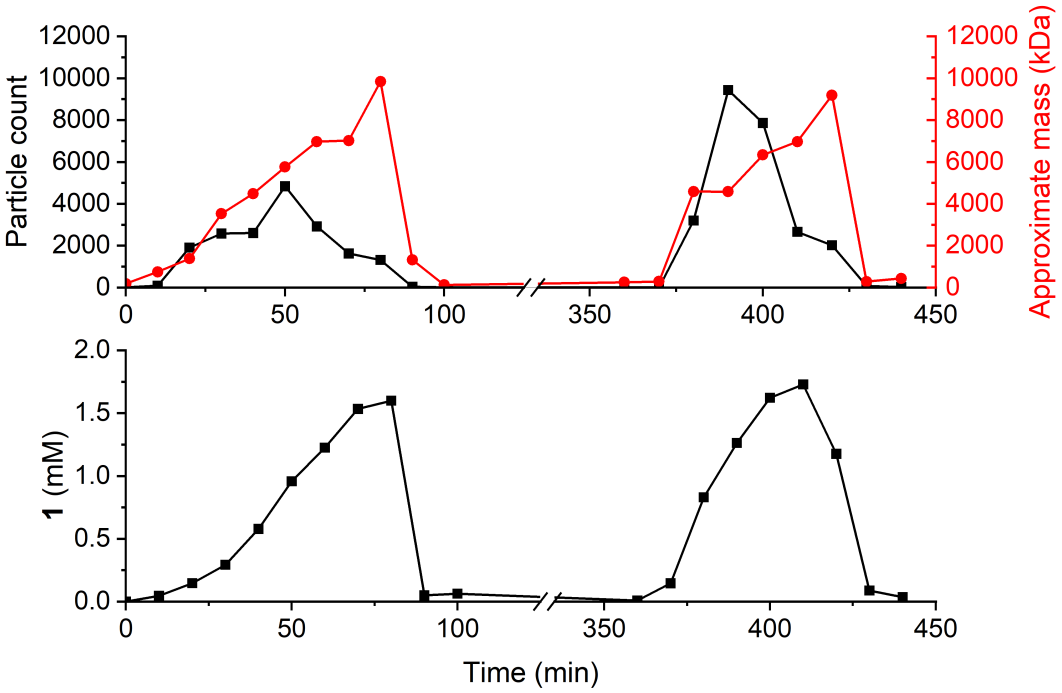


Figure S 4. Three repeating experiments of Figure 20.

5.1.10 iSCAT of the vesicles of 1 in steady state

In order to show the population cycling of vesicles only occurs in oscillation state, the counts and contrast distribution of vesicles of **1** were measured in steady state to make comparison. The preparation of the vesicles is from the procedure by Engwerda et al.[109] **3** was dissolved in pH 9.0 TRIS buffer to 2.5 mM. Then 2 mL of solution was injected into 10 mL round bottom flask with an oval stirring bar (L= 15 mm, ø= 5 mm). 5.4 mg (5 equiv.) of **2** was added after the solution was heated to 50 °C and stirred to 1200 rpm. The concentration of **1** and **3** was monitored by UPLC (Figure S 5). After the concentration of **1** went stable, three 10 µL aliquots were taken at 80, 100 and 130min, diluted by 0.5 mL pH 9.0 TRIS buffer and measured by iSCAT (Figure S 6, Figure S 7). Figure S 6 shows that the count and contrast (approximate mass) of assemblies grew up gradually, without showing population cycling.

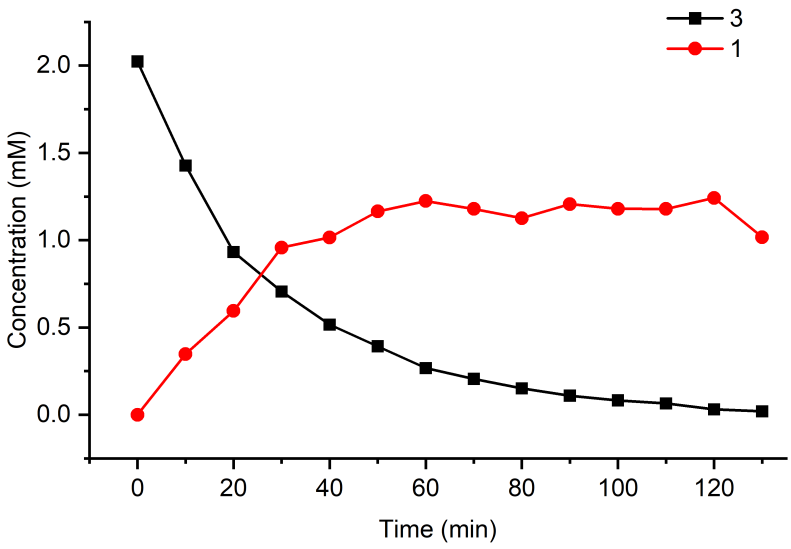


Figure S 5. The concentration changes of **1** and **3** measured by UPLC.

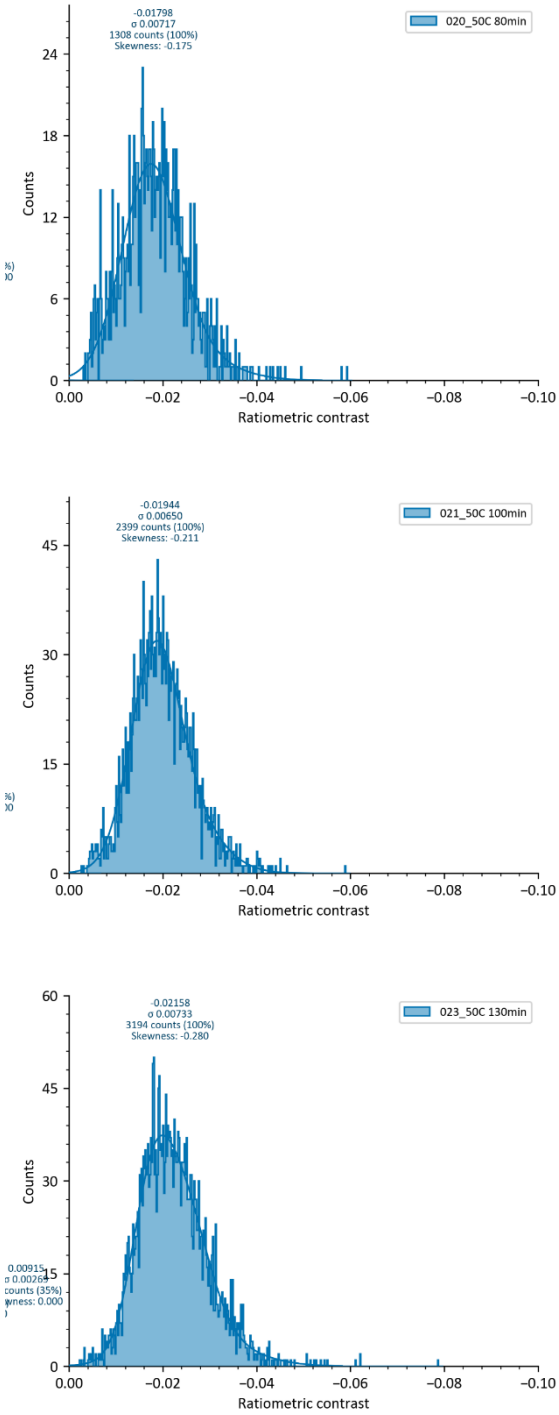


Figure S 6. Counts and contrast distributions of vesicles at different times measured by iSCAT.

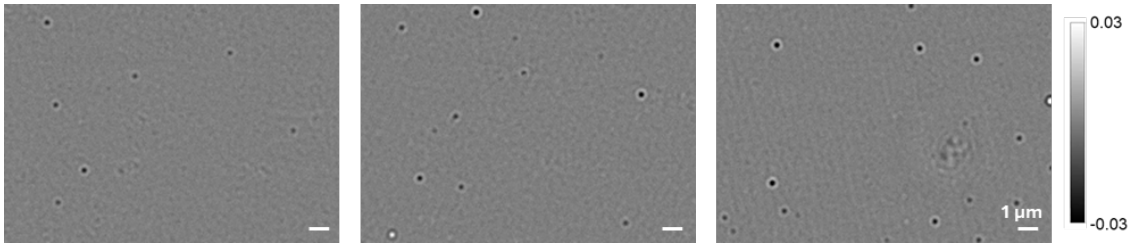


Figure S 7. iSCAT images of vesicles at different times, in which contrast scale is set to ± 0.03. The images are taken at 80, 100 and 130 min from left to right.

5.1.11 Replication of chemical oscillation with extended time

The experiment in Figure 16b was replicated with longer monitoring time to show reproducibility (Figure S 8).

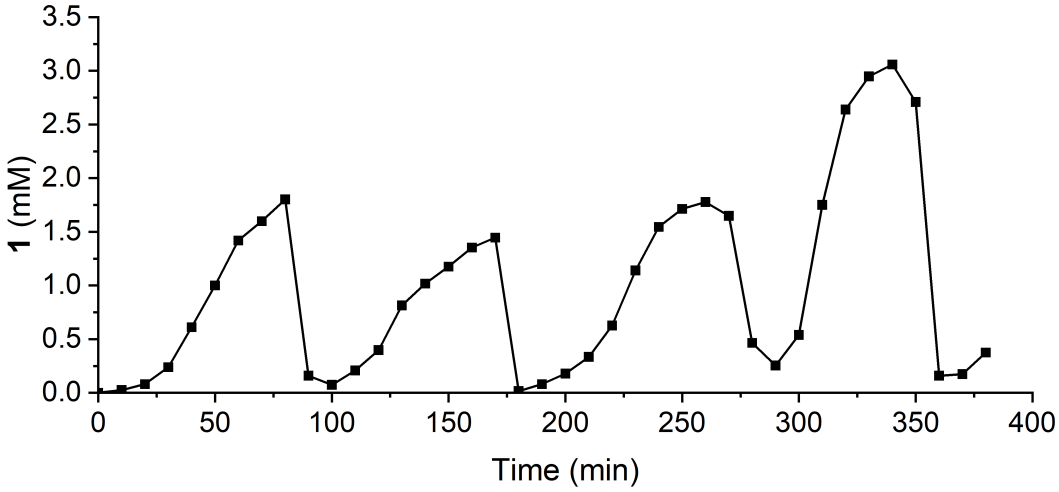


Figure S 8. Duplicate of Figure 16b. Lines are drawn to guide the eye.

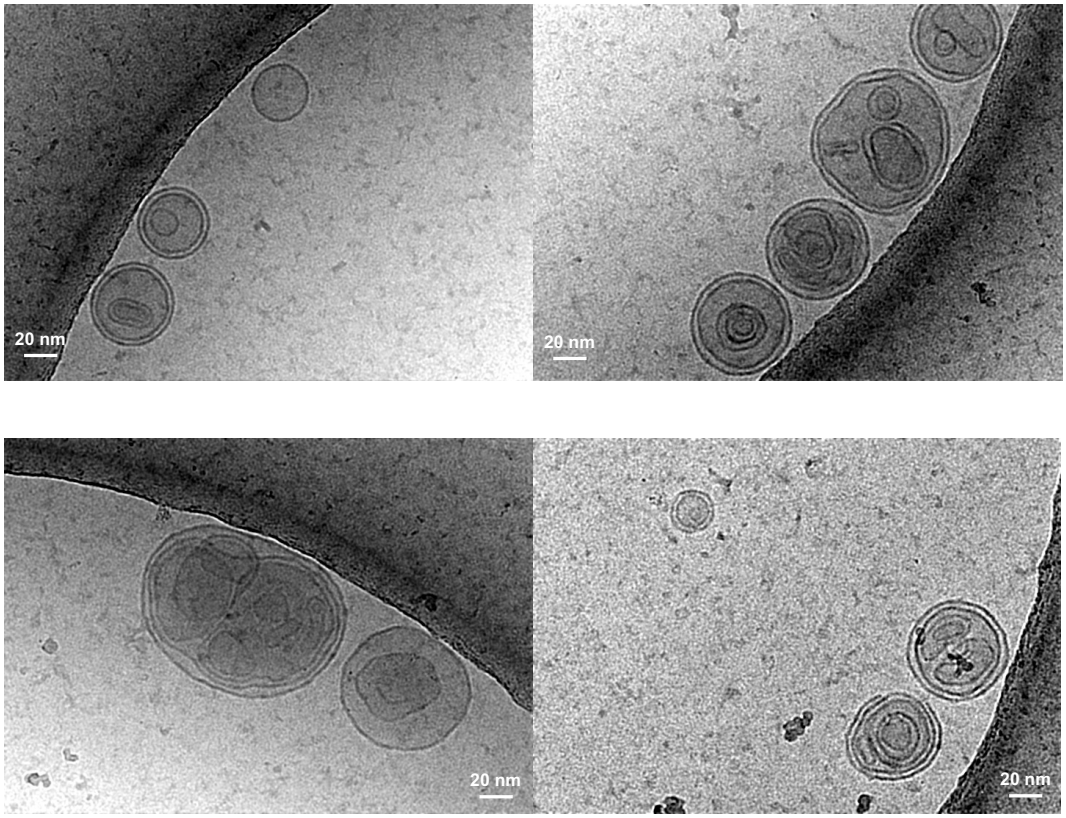
5.1.12 Cryo-TEM measurements of vesicles of 1

Plunge Freezing

2.5 mM samples of surfactant **1** were prepared for cryoEM imaging. 4 µL samples were applied to freshly plasma-cleaned Quantifoil 2/1 holey carbon copper-mesh grids (Agar Scientific). Excess sample was blotted away by hand before plunging into a reservoir of propane/ethane with a manual plunger. Grids were stored under liquid nitrogen until imaging.

CryoEM

CryoEM data were recorded on a Titan Krios microscope (FEI, Thermofisher), equipped with a K3 direct electron detector (Gatan) and Quantum energy filter (Gatan). Projection images were collected with SerialEM[207] with a pixel size of 1.1A˚/pixel and the energy-selection slit set to 20 eV. 50 image frames (0.04s exposure/frame) in counting mode were collected at a dose rate of 15 e^-/unbinned pixel/second, giving an overall dose of ~25 $e^-/Å^2$. A defocus of 4 μm under focus was used to record data. Frames were aligned on the fly in SerialEM. Images were subsequently processed for viewing in FIJI[208].



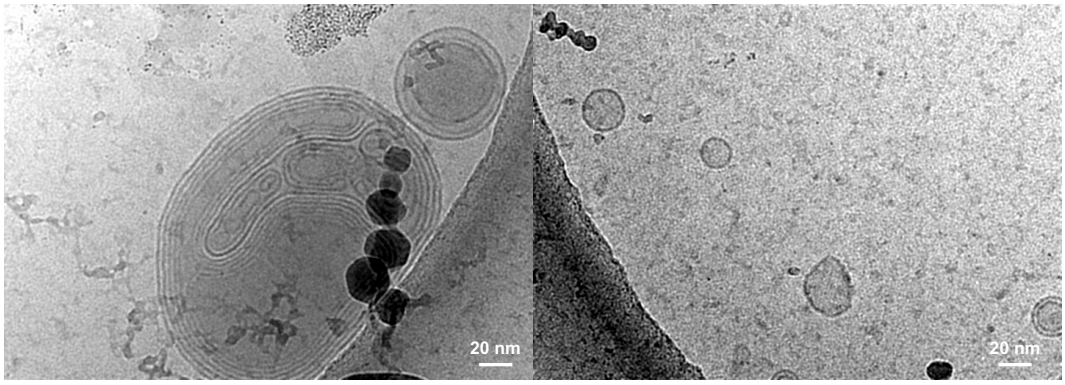
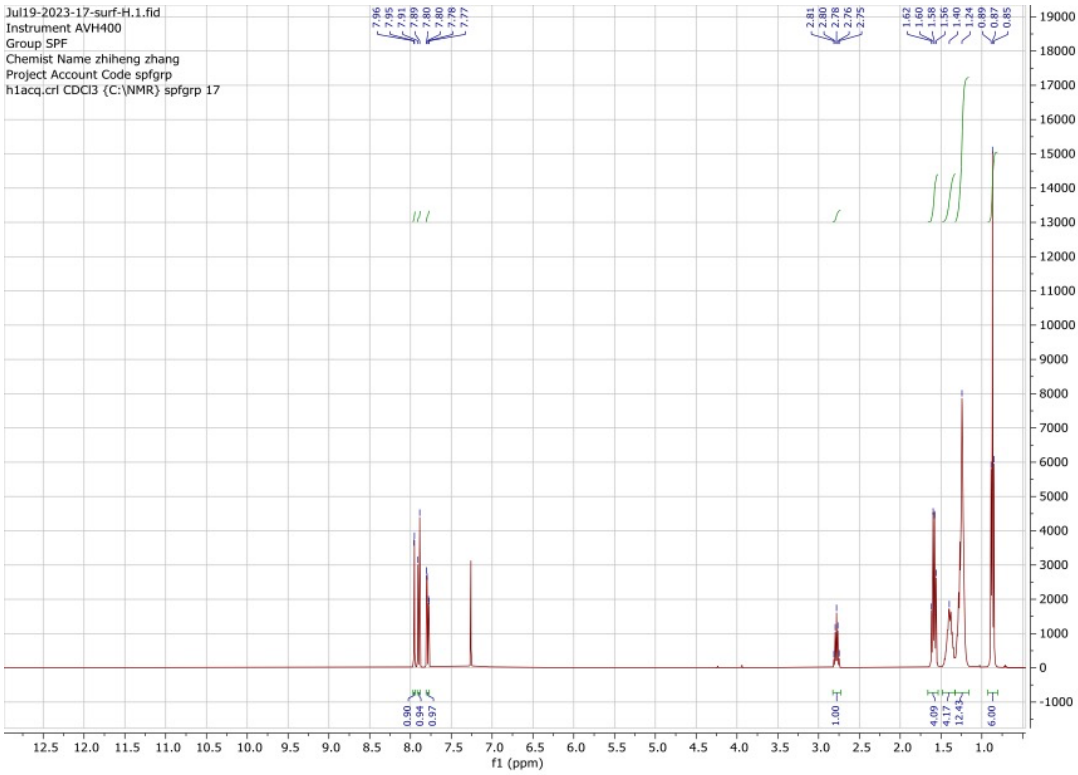
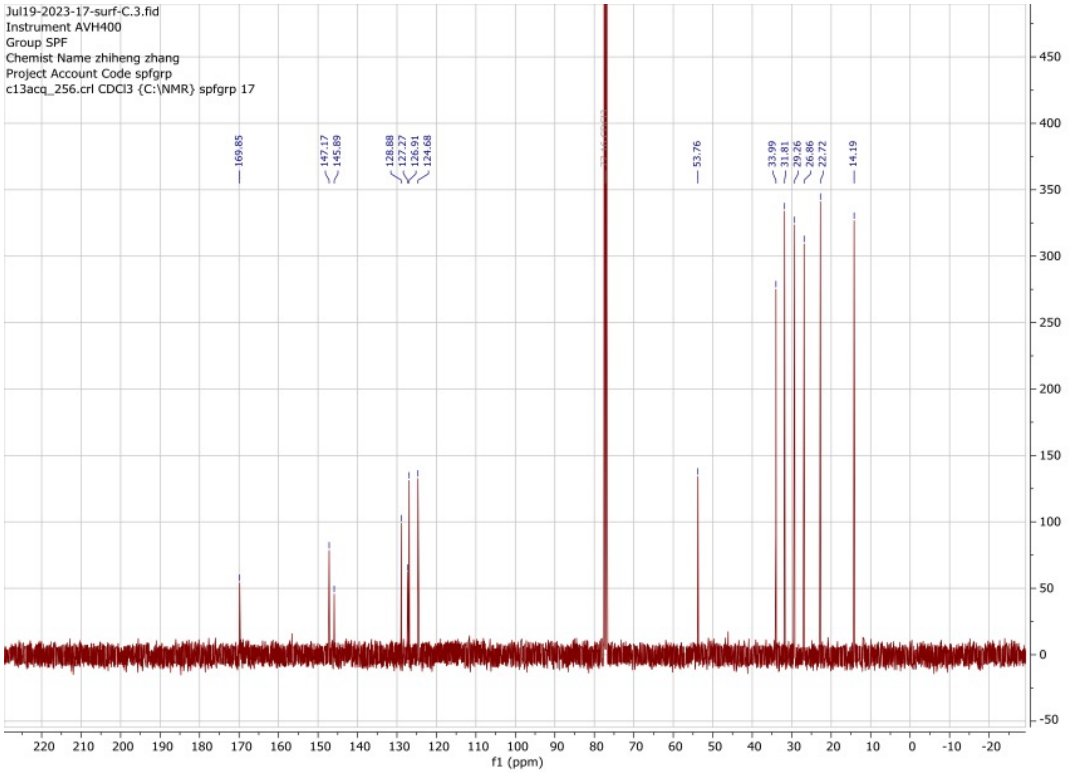


Figure S 9. Cryo-TEM images of vesicles composed of surfactants **1**. Images were recorded for 2.5 mM samples of compound **1** in TRIS buffer (0.5M, pH 9.00), showing vesicles of approximately 20 ~ 190 nm in size.

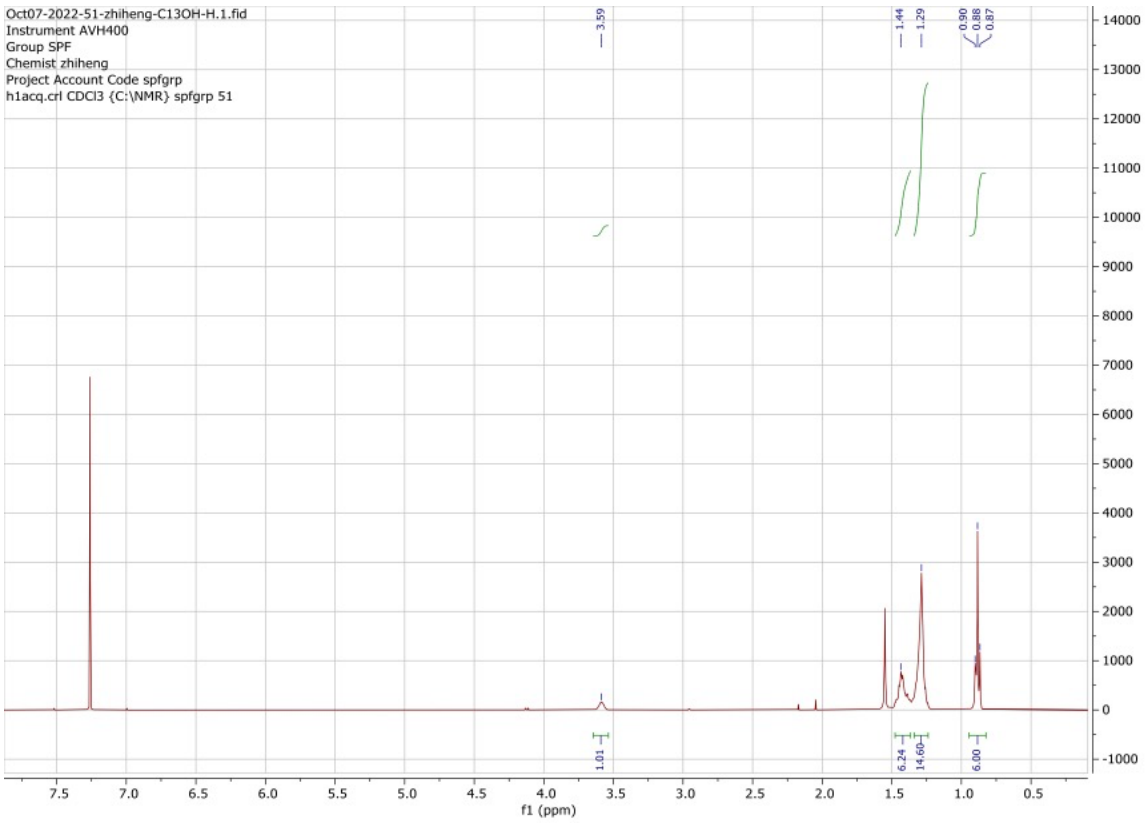
5.1.13 NMR spectra

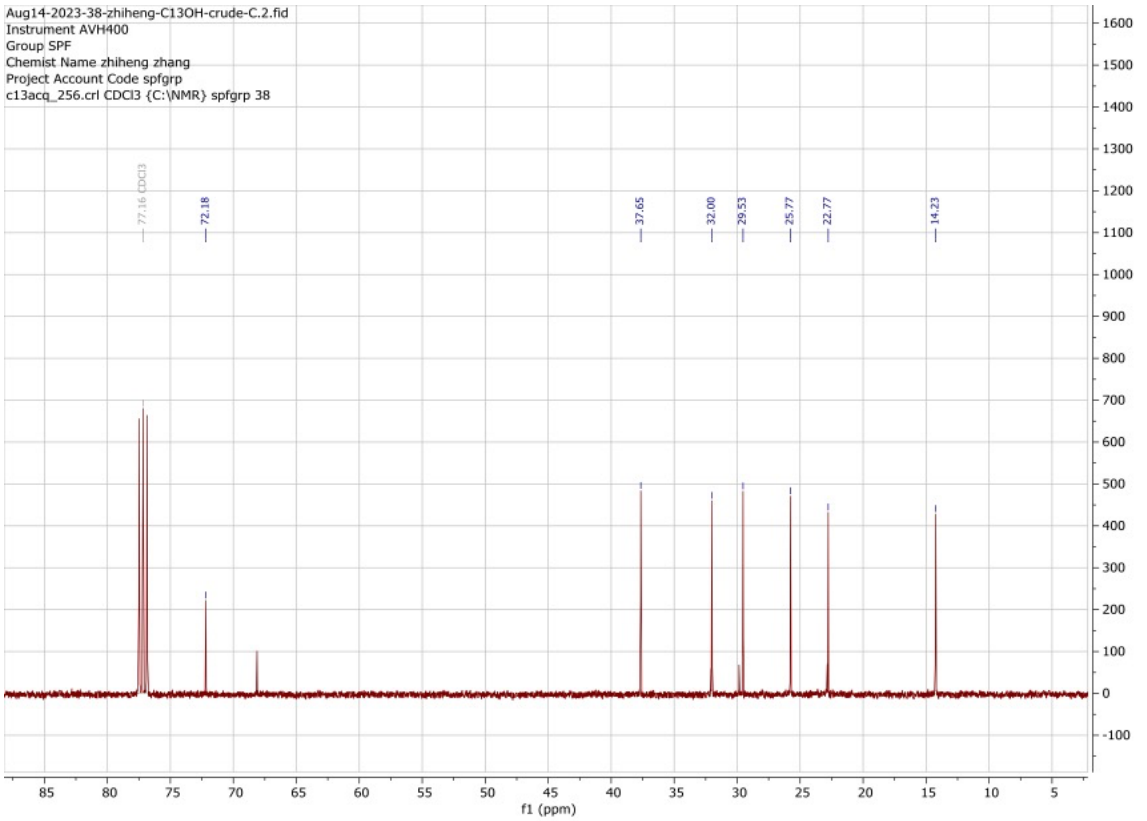
2-nitro-5-(tridecan-7-yldisulfaneyl)benzoic acid (**1**):



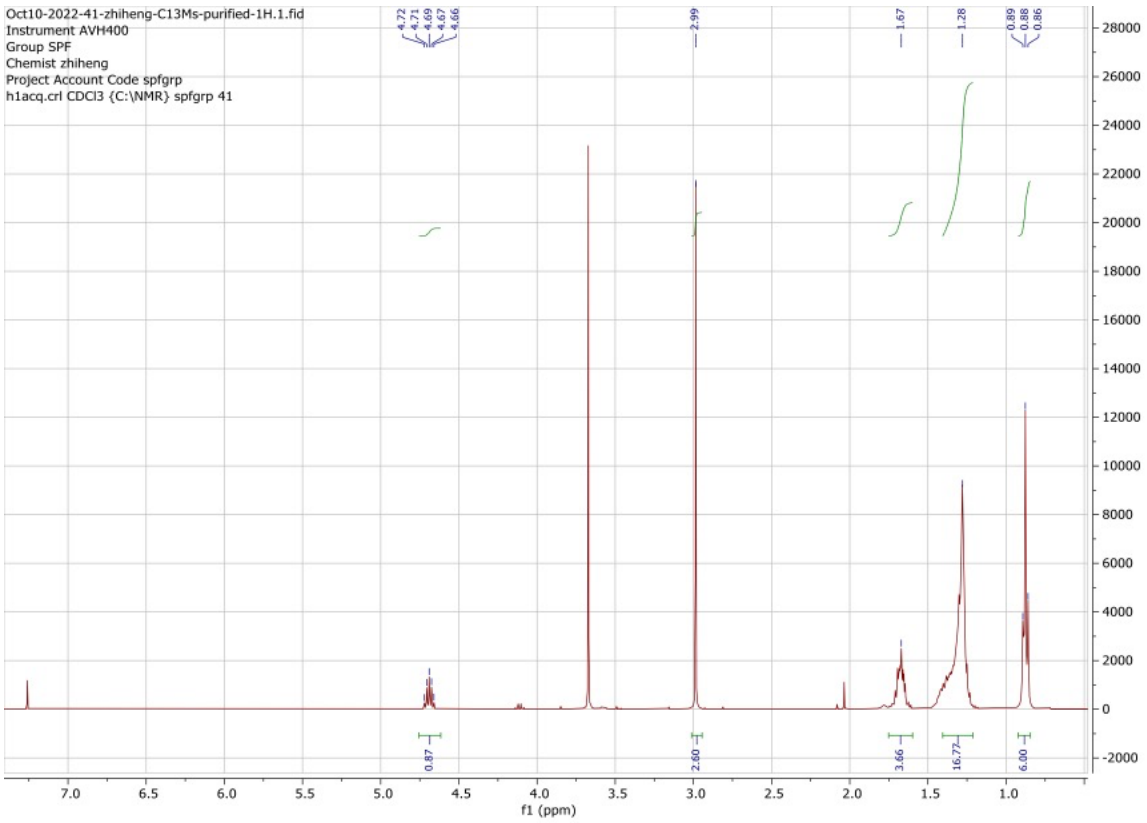


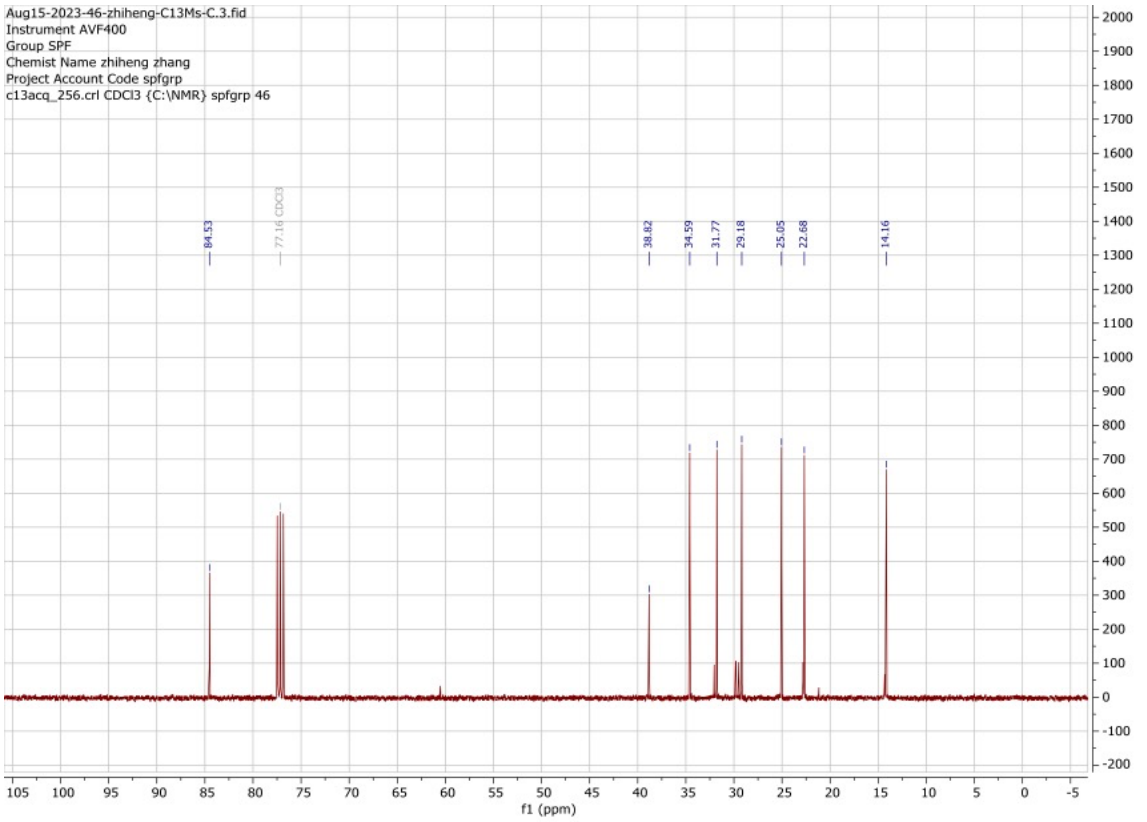
7-tridecanol (**2a**):



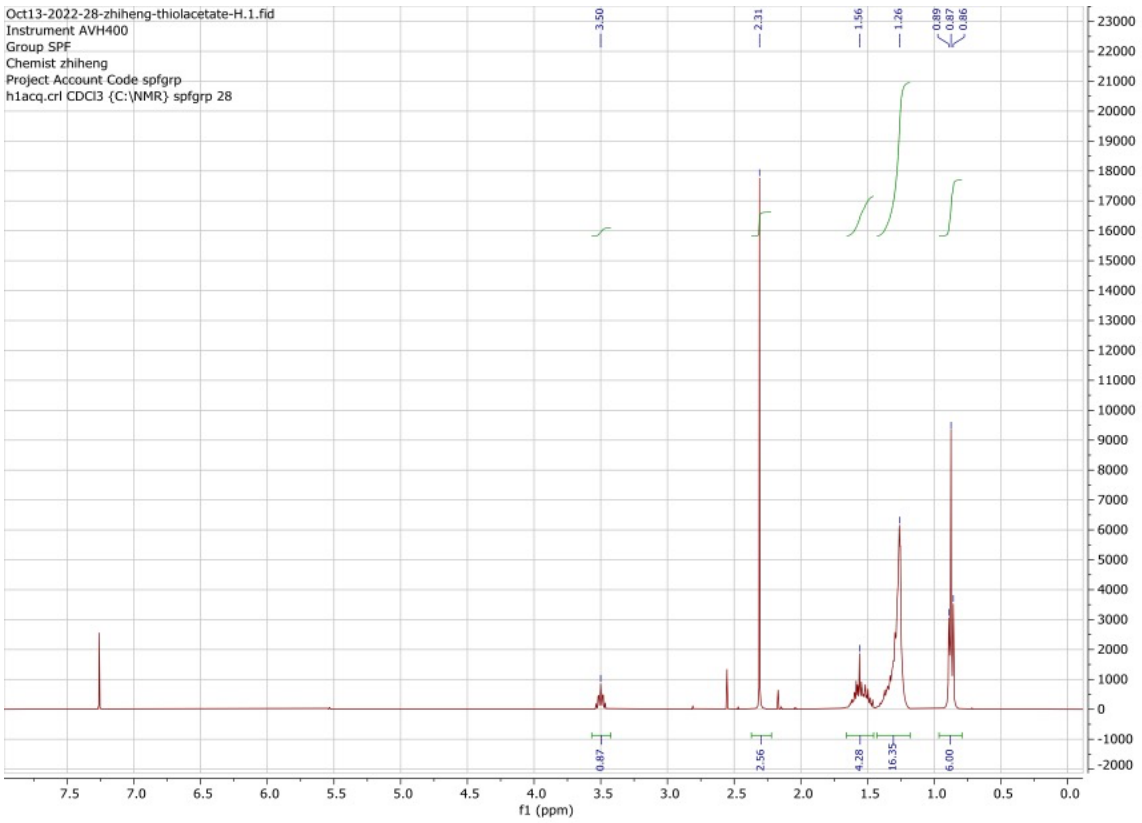


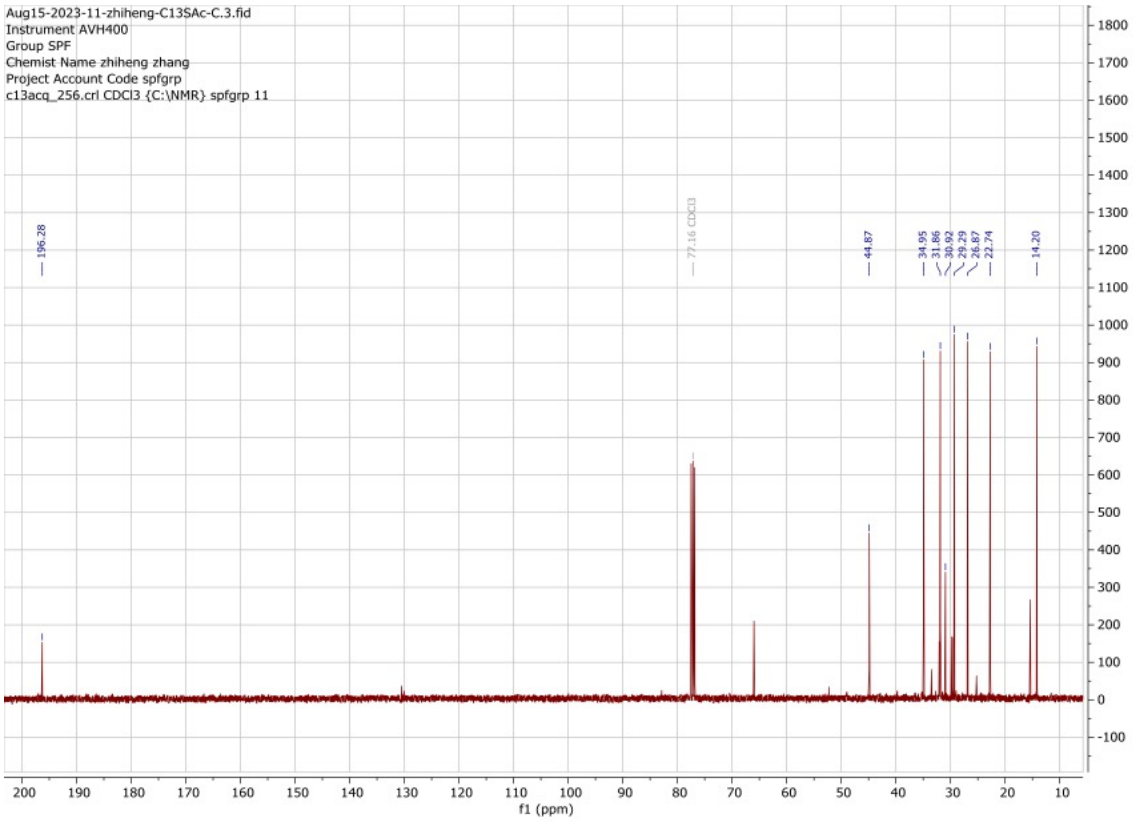
Tridecan-7-yl methanesulfonate (**2b**):



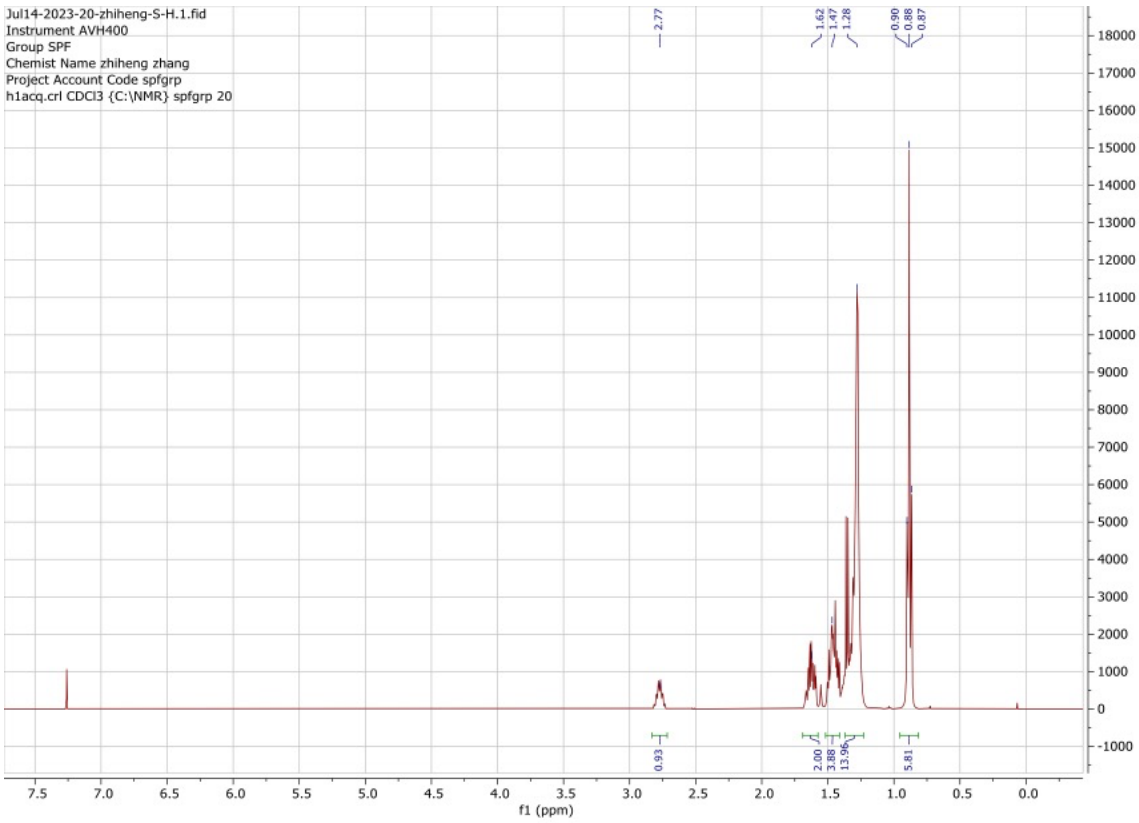


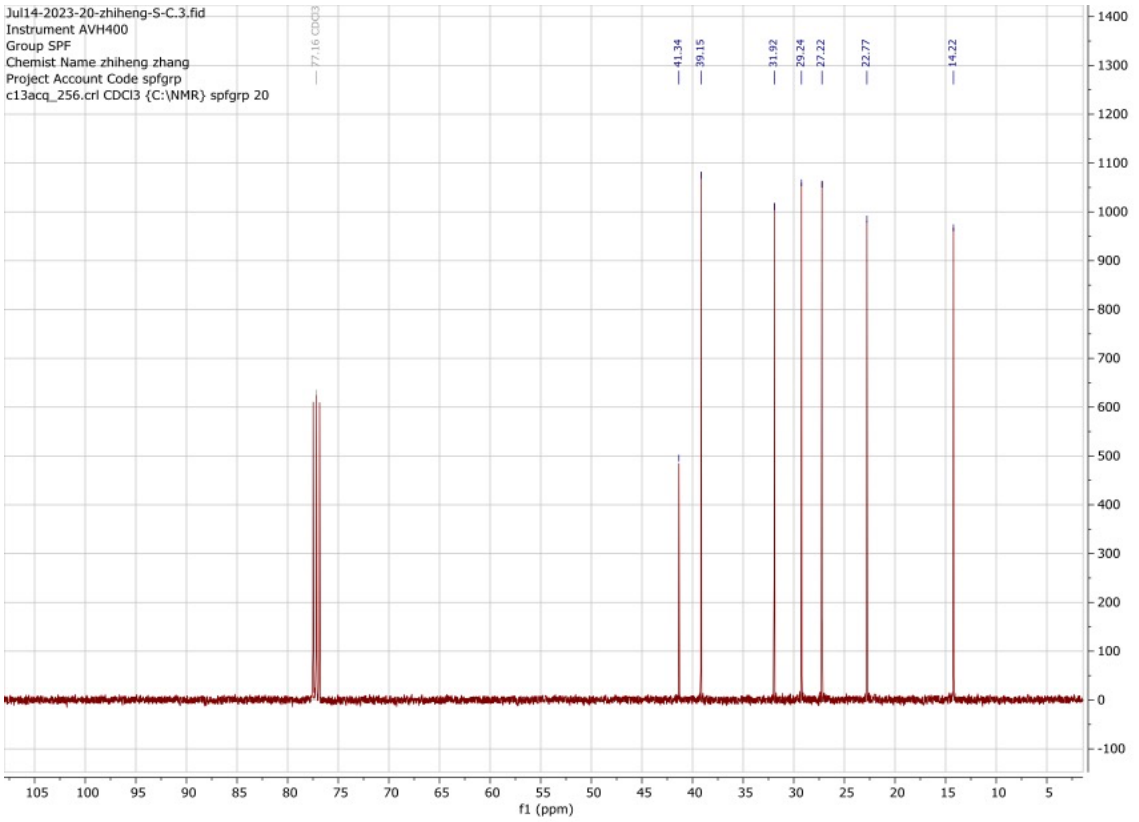
S-(tridecan-7-yl) ethanethioate (**2c**):



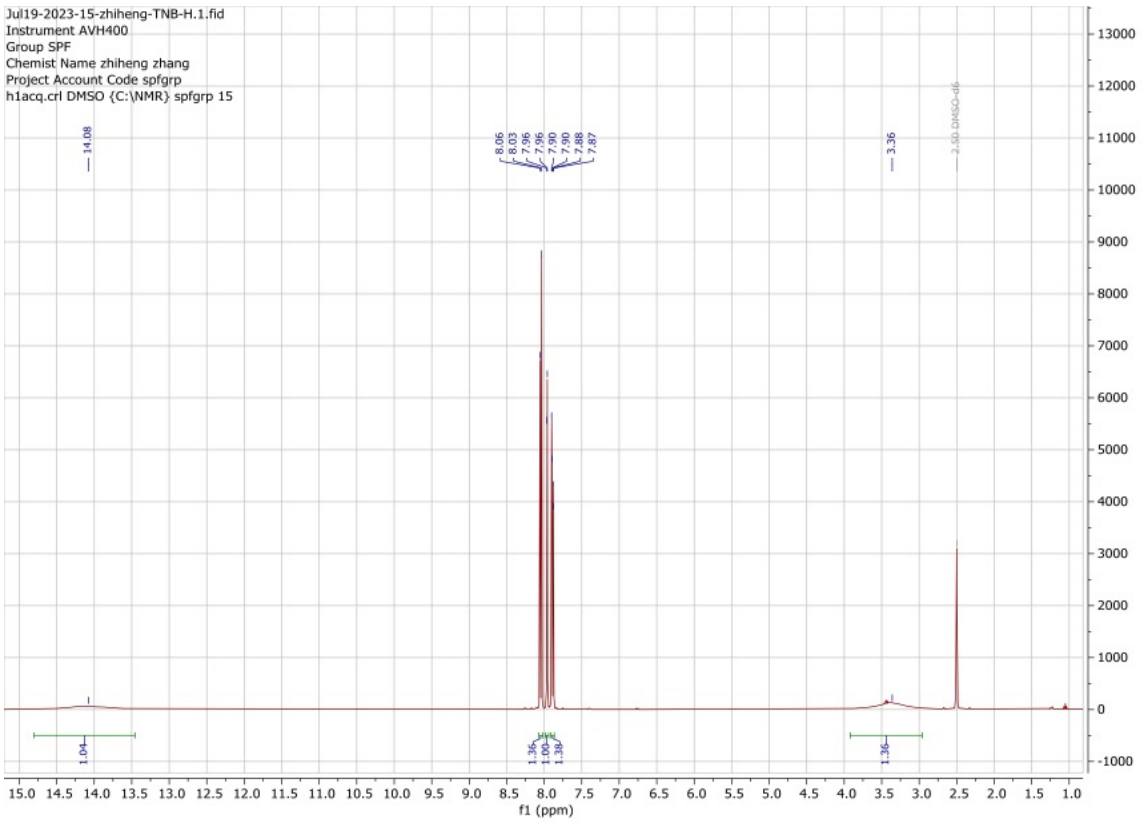


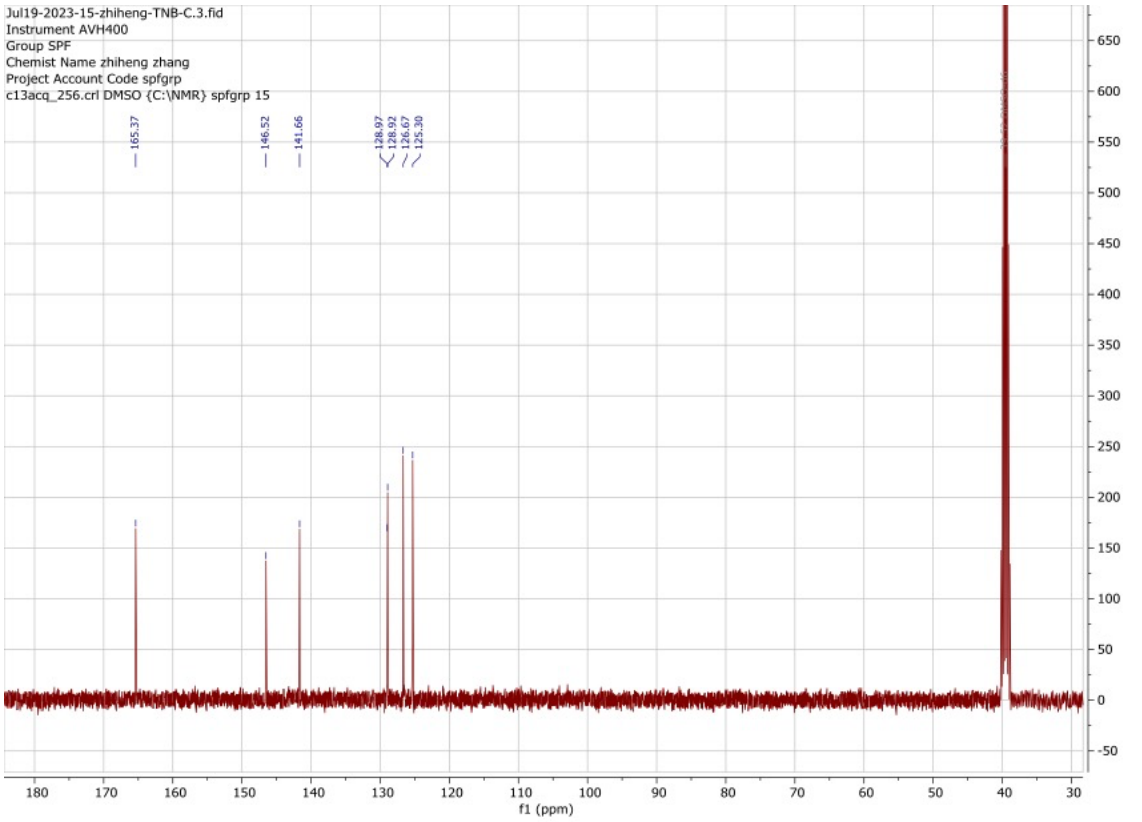
7-tridecanethiol (**2**):





5-Mercapto-2-nitro-benzoic acid (**4**):





5.2 Supplementary methods and data of chapter 3

5.2.1 Derivation of non-dimensionalised rate equations

For convenience in the analysis and simulations, the rate equation (1.8) is reduced and non-dimensionalised. The conservation of matter is $c_A = 2(\mathbf{C}_{A_2} - c_{A_2}) - c_S - nc_M$, and the micellisation-dissociation equilibrium gives $k_M \mathbf{C}_{CMC}^m = k_{dM}(\frac{\mathbf{C}_{CMC}}{n})$. Where $\mathbf{C}_{A_2}$ is the starting concentration of A_2. When the starting material is A, $\frac{1}{2}\mathbf{C}_A = \mathbf{C}_{A_2}$ can also be used. $\mathbf{C}_{CMC}$ is the critical micelle concentration of the surfactant S, which is the concentration of the surfactant when the micellisation rate equals the dissociation rate. So, the non-dimensionalised concentrations and time are (1.9). $\mathbf{C}_O$ and τ are scales of the hydrogen peroxide concentration and time.

$$\begin{aligned}
c_{A_2} &\mapsto \mathbf{C}_{A_2} c_{A_2} \\
c_O &\mapsto \mathbf{C}_O c_O \qquad \mathbf{C}_O = \frac{r_{ext}}{k_O \mathbf{C}_{A_2}} \\
c_S &\mapsto \mathbf{C}_{CMC} c_S \\
c_M &\mapsto \frac{\mathbf{C}_{CMC}}{n} c_M \\
t &\mapsto \tau t \qquad \tau = \frac{\mathbf{C}_{A_2}}{r_{ext}}
\end{aligned} \tag{1.9}$$

The non-dimensionalised form of the rate equation is (1.10).

$$
\begin{aligned}
\frac{dc_{A_2}}{dt} &= c_O c_A - \alpha c_M c_{A_2} - \theta c_{A_2} \\
\frac{dc_S}{dt} &= \frac{\alpha}{\lambda} c_M c_{A_2} + \frac{\theta}{\lambda} c_{A_2} - \phi c_S - \delta(c_S^m - c_M) \\
\frac{dc_O}{dt} &= \varepsilon(1 - c_O c_A) \\
\frac{dc_M}{dt} &= \delta(c_S^m - c_M) - \beta c_M \\
c_A &= 2(1 - c_{A_2}) - \lambda(c_S + c_M)
\end{aligned}
\tag{1.10}
$$

The dimensionless parameters are shown below. The hydrogen peroxide injection rate, r_{ext}, is a control factor in all parameters except λ.

$$
\lambda = \frac{\mathbf{C}_{CMC}}{\mathbf{C}_{A_2}} \qquad \varepsilon = \frac{k_O \mathbf{C}_{A_2}^2}{r_{ext}} = \frac{\mathbf{r}_O}{r_{ext}} \qquad \delta = \frac{k_{dM} \mathbf{C}_{A_2}}{r_{ext}} = \frac{\mathbf{r}_{dM}}{r_{ext}}
$$

$$
\alpha = \frac{k_S^* \mathbf{C}_{CMC} \mathbf{C}_{A_2}}{n r_{ext}} = \frac{\mathbf{r}_S^*}{r_{ext}} \qquad \beta = \frac{k_{dS}^* \mathbf{C}_{A_2}}{r_{ext}} = \frac{\mathbf{r}_{dS}^*}{r_{ext}} \qquad \theta = \frac{k_S \mathbf{C}_{A_2}}{r_{ext}} = \frac{\mathbf{r}_S}{r_{ext}} \qquad \phi = \frac{k_{dS} \mathbf{C}_{A_2}}{r_{ext}} = \frac{\mathbf{r}_{dS}}{r_{ext}}
$$

5.2.2 The time-delayed kinetic model

The kinetics of biphasic reactions are different from homogeneous reactions. The diffusion of reactants between phases and micelles causes time delays. There are two theories for the biphasic physical autocatalysis. The first one is the phase transfer catalysis, which means the non-soluble organic reactants are taken into the micelles and then released to the aqueous phase, while the second one is micellar catalysis, where the reaction occurs at the surface of the micelle without the release (Figure S 10).

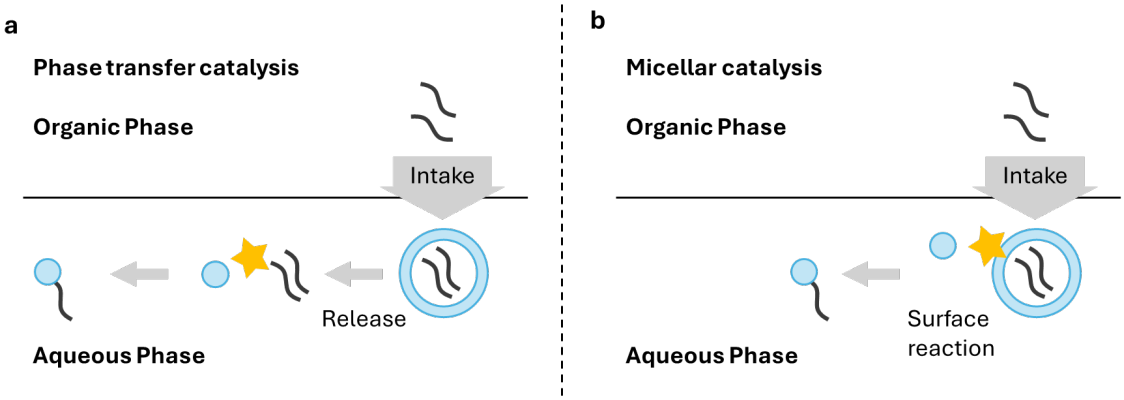


Figure S 10. Mechanistic overview of the physical autocatalysis. a) Phase transfer catalysis. The reactants are taken and released to the aqueous phase. b) Micellar catalysis. The reaction occurs at the surface of the micelle instead of being released.

In the theory of phase transfer catalysis, we assume the time of intake t_{d_1}, and the sum of intake and release time t_{d_2} ($t_{d_1} < t_{d_2}$). So, the micelle concentration terms become $c_{M,td1}$ in the micelle decomposition step βc_M and $c_{M,td2}$ in the surfactant formation step $\alpha c_M c_{A_2}$. In the theory of micellar catalysis, there is no release time, so we have $t_{d_1} = t_{d_2}$. The final time-delayed model is (1.11).

$$
\begin{aligned}
\frac{dc_{A_2}}{dt} &= c_O c_A - \alpha c_{M,td2} c_{A_2} - \theta c_{A_2} \\
\frac{dc_S}{dt} &= \frac{\alpha}{\lambda} c_{M,td2} c_{A_2} + \frac{\theta}{\lambda} c_{A_2} - \phi c_S - \delta(c_S^m - c_M) \\
\frac{dc_O}{dt} &= \varepsilon(1 - c_O c_A) \\
\frac{dc_M}{dt} &= \delta(c_S^m - c_M) - \beta c_{M,td1} \\
c_A &= 2(1 - c_{A_2}) - \lambda(c_S + c_M)
\end{aligned}
\tag{1.11}
$$

5.2.3 Simulation details

The models are simulated numerically by Python 3.10.16, in which the non-delayed part is solved by LSODA method in Scipy 1.15.1, and the time-delayed part is solved by JiTCDDE

1.8.2. All codes for the simulations can be found on the author's GitHub page https://github.com/Zhiheng419/Chemical_Oscillation_Model.git

5.2.3.1 The parameter settings in 3.2.2

$$\mathbf{r}_S^* = 3815mM/h \quad \mathbf{r}_{dS}^* = 280mM/h \quad r_{ext} = 12.6mM/h \quad \mathbf{C}_{A_2} = 14.5mM$$
$$\mathbf{r}_S = 10mM/h \quad \mathbf{r}_{dS} = 500mM/h \quad t_{d1} = 0.03 \quad \mathbf{C}_{CMC} = 1.56mM$$
$$\mathbf{r}_O = 10^4 mM/h \quad \mathbf{r}_M = 10^4 mM/h \quad t_{d2} = 0.03$$
$$\lambda = 0.11 \quad m = 2$$

5.2.3.2 The parameter settings in 3.2.3

Figure 22a:

$$\mathbf{r}_S^* = 220mM/h \quad \mathbf{r}_{dS}^* = 30mM/h \quad r_{ext} = 2mM/h$$
$$\mathbf{r}_S = 5.5mM/h \quad \mathbf{r}_{dS} = 180mM/h \quad \mathbf{C}_{A_2} = 14.5mM$$
$$\mathbf{r}_O = 10^4 mM/h \quad \mathbf{r}_M = 10^4 mM/h \quad \mathbf{C}_{CMC} = 1.56mM$$
$$\lambda = 0.11 \quad m = 2$$

Figure 22b:

$$\mathbf{r}_S^* = 220mM/h \quad \mathbf{r}_{dS}^* = 30mM/h \quad r_{ext} = 10mM/h$$
$$\mathbf{r}_S = 5.5mM/h \quad \mathbf{r}_{dS} = 180mM/h \quad \mathbf{C}_{A_2} = 14.5mM$$
$$\mathbf{r}_O = 10^4 mM/h \quad \mathbf{r}_M = 10^4 mM/h \quad \mathbf{C}_{CMC} = 1.56mM$$
$$\lambda = 0.11 \quad m = 2$$

Figure 22c:

$$\mathbf{r}_S^* = 220mM/h \quad \mathbf{r}_{dS}^* = 30mM/h \quad r_{ext} = 200mM/h$$
$$\mathbf{r}_S = 5.5mM/h \quad \mathbf{r}_{dS} = 180mM/h \quad \mathbf{C}_{A_2} = 14.5mM$$
$$\mathbf{r}_O = 10^4 mM/h \quad \mathbf{r}_M = 10^4 mM/h \quad \mathbf{C}_{CMC} = 1.56mM$$
$$\lambda = 0.11 \quad m = 2$$

5.2.3.3 The parameter settings in 3.2.4

H_2O_2 injection rates:

$$\mathbf{r}_S^* = 330mM/h \quad \mathbf{r}_{dS}^* = 350mM/h \quad r_{ext} = 7,14,28mM/h \quad \mathbf{C}_{A_2} = 14.5mM$$
$$\mathbf{r}_S = 6mM/h \quad \mathbf{r}_{dS} = 280mM/h \quad t_{d1} = 0.015, 0.03, 0.06 \quad \mathbf{C}_{CMC} = 1.56mM$$
$$\mathbf{r}_O = 10^4 mM/h \quad \mathbf{r}_M = 10^4 mM/h \quad t_{d2} = 0.015, 0.03, 0.06$$
$$\lambda = 0.11 \qquad m = 2$$

In fact, the real values of delays t_{d1}, t_{d2} are not changed here. Because the time unit $\tau = \mathbf{C}_{A_2} / r_{ext}$ changes when r_{ext} is changed, the values of the delays are different at different time units.

Stirring rates:

$$\mathbf{r}_S^* = 1320 \cdot k_1 \ mM/h \quad \mathbf{r}_{dS}^* = 870 \cdot k_2 \ mM/h \quad r_{ext} = 14mM/h \quad \mathbf{C}_{A_2} = 14.5mM$$
$$\mathbf{r}_S = 12.5 \cdot k_1 \ mM/h \quad \mathbf{r}_{dS} = 210 \cdot k_2 \ mM/h \quad t_{d1} = \frac{0.03}{n} \quad \mathbf{C}_{CMC} = 1.56mM$$
$$\mathbf{r}_O = 10^4 mM/h \quad \mathbf{r}_M = 10^4 mM/h \quad t_{d2} = \frac{0.03}{n}$$
$$\lambda = 0.11 \qquad m = 2$$

For 300, 600 and 900 rpm, $k_1 = 1,\ 1.1,\ 1.6$, $k_2 = 1,\ 1.4,\ 1.8$, $n = 1,\ 2,\ 2.5$.

Catalyst (DMAP) concentrations:

$$\mathbf{r}_S^* = 315 \cdot k_1 \ mM/h \quad \mathbf{r}_{dS}^* = 75 \cdot k_2 \ mM/h \quad r_{ext} = 12.6mM/h \quad \mathbf{C}_{A_2} = 14.5mM$$
$$\mathbf{r}_S = 5.3 \cdot k_1 \ mM/h \quad \mathbf{r}_{dS} = 280 \cdot k_2 \ mM/h \quad t_{d1} = 0.03 \quad \mathbf{C}_{CMC} = 1.56mM$$
$$\mathbf{r}_O = 10^4 mM/h \quad \mathbf{r}_M = 10^4 mM/h \quad t_{d2} = 0.03$$
$$\lambda = 0.11 \qquad m = 2$$

For 2, 20, 200 and 400 mol% DMAP, $k_1 = 1,\ 1.5,\ 2,\ 5$, $k_2 = 1,\ 1.2,\ 1.8, 2$.

5.2.3.4 The parameter settings in 3.3.2

Oscillator 1 (2-octanethiol):

$$\mathbf{r}_{S1}^{*} = 3360mM/h \quad \mathbf{r}_{dS1}^{*} = 672mM/h \quad r_{ext} = 11.2mM/h \quad \mathbf{C}_{A_2} = 15mM$$
$$\mathbf{r}_{S1} = 33.6mM/h \quad \mathbf{r}_{dS1} = 560mM/h \quad t_{d1} = 0.03 \quad \mathbf{C}_{CMC,1} = 1.56mM$$
$$\mathbf{r}_{O1} = 10^4 mM/h \quad \mathbf{r}_{M1} = 10^4 mM/h \quad t_{d2} = 0.03$$
$$\lambda_1 = 0.104 \quad m_1 = 2$$

Oscillator 2 (2-nonanethiol):

$$\mathbf{r}_{S2}^{*} = 112mM/h \quad \mathbf{r}_{dS2}^{*} = 336mM/h \quad r_{ext} = 11.2mM/h \quad \mathbf{C}_{A_2} = 15mM$$
$$\mathbf{r}_{S2} = 16.8mM/h \quad \mathbf{r}_{dS2} = 448mM/h \quad t_{d1} = 0.03 \quad \mathbf{C}_{CMC,2} = 0.29mM$$
$$\mathbf{r}_{O2} = 10^4 mM/h \quad \mathbf{r}_{M2} = 10^4 mM/h \quad t_{d2} = 0.03$$
$$\lambda_2 = 0.193 \quad m_2 = 2$$

5.2.4 Derivations of the kinetic model of mixed oscillators

This model describes the mixing of two chemical oscillators with different aliphatic thiols. The components and parameters in the two oscillators are labelled by 1 and 2 in the subscripts (such as T_1, T_2). The volume fraction of the thiols T_1 and T_2 are assumed to $\frac{1}{2}$, and the components in the aqueous phase have equal chance to contact and react with the both thiols. So, all thiol-related kinetic parameters are multiplied with the factor $\frac{1}{2}$.

The cross-terms (k_{dS12}, k_{dS21}) in the rate constants mean the cross reaction with T1 and S2 (or T2 and S1). They are assumed to equal to the averages of each rate constant in the pure systems ($k_{dS12} = k_{dS21} = \frac{k_{dS11} + k_{dS22}}{2}$). The cross-terms in the micelle decomposition steps are more complicated. The "partial concentration" of each surfactant is treated separately. We introduce $c_{M1} = \chi_{M1} c_M, c_{M2} = \chi_{M2} c_M$ to separate the two surfactants in the micelles in the kinetic equations, where χ is the mole fractions of the surfactants in the micelles. So, the micelle decomposition reaction can be decomposed to (1.12). The cross terms ($k_{dS21}^{*}, k_{dS12}^{*}$) are also calculated by averages.

$$
\begin{aligned}
&\mathrm{M1} + \mathrm{n_1T1} \xrightarrow{k^*_{dS11}} \mathrm{n_1A} + \mathrm{nW} \\
&\mathrm{M1} + \mathrm{n_1T2} \xrightarrow{k^*_{dS12}} \mathrm{n_1A} + \mathrm{nW} \\
&\mathrm{M2} + \mathrm{n_2T1} \xrightarrow{k^*_{dS21}} \mathrm{n_2A} + \mathrm{nW} \\
&\mathrm{M2} + \mathrm{n_2T2} \xrightarrow{k^*_{dS22}} \mathrm{n_2A} + \mathrm{nW}
\end{aligned}
\tag{1.12}
$$

The decomposition rate of M1 and M2 are (1.13) and (1.14).

$$
-\frac{k^*_{dS11}}{2} c_{M1,d1} - \frac{1}{2} \cdot \frac{k^*_{dS11} + k^*_{dS22}}{2} c_{M1,d1} = -(\frac{3}{4} k^*_{dS11} + \frac{1}{4} k^*_{dS22}) c_{M1,d1} \tag{1.13}
$$

$$
-\frac{k^*_{dS22}}{2} c_{M2,d1} - \frac{1}{2} \cdot \frac{k^*_{dS11} + k^*_{dS22}}{2} c_{M2,d1} = -(\frac{1}{4} k^*_{dS11} + \frac{3}{4} k^*_{dS22}) c_{M2,d1} \tag{1.14}
$$

By using the same forms of dimensionless parameters in (1.9), the final dimensionless form of the mixed kinetic model is (1.15). r is $\dfrac{\mathbf{C}_{CMC,2}}{\mathbf{C}_{CMC,1}}$, which appears naturally in the non-dimensionalisation.

$$
\begin{aligned}
&\frac{dc_{A_2}}{dt} = c_O c_A - \frac{\alpha_1}{2}(c_{M1,d2} + r c_{M2,d2}) c_{A_2} - \frac{\alpha_2}{2}(\frac{1}{r} c_{M1,d2} + c_{M2,d2}) c_{A_2} - \frac{(\theta_1 + \theta_2)}{2} c_{A_2} \\
&\frac{dc_{S1}}{dt} = \frac{\alpha_1}{2\lambda_1}(c_{M1,d2} + r c_{M2,d2}) c_{A_2} + \frac{\theta_1}{2\lambda_1} c_{A_2} - (\frac{3}{4}\phi_1 + \frac{1}{4}\phi_2) c_{S1} - \delta_1 (c_{S1}^{m_1} - c_{M1}) \\
&\frac{dc_{S2}}{dt} = \frac{\alpha_2}{2\lambda_2}(\frac{1}{r} c_{M1,d2} + c_{M2,d2}) c_{A_2} + \frac{\theta_2}{2\lambda_2} c_{A_2} - (\frac{1}{4}\phi_1 + \frac{3}{4}\phi_2) c_{S2} - \delta_2 (c_{S2}^{m_2} - c_{M2}) \\
&\frac{dc_{M1}}{dt} = \delta_1 (c_{S1}^{m_1} - c_{M1}) - (\frac{3}{4}\beta_1 + \frac{1}{4}\beta_2) c_{M1,d1} \\
&\frac{dc_{M2}}{dt} = \delta_2 (c_{S2}^{m_2} - c_{M2}) - (\frac{1}{4}\beta_1 + \frac{3}{4}\beta_2) c_{M2,d1} \\
&\frac{dc_O}{dt} = \varepsilon (1 - c_O c_A) \\
&c_A = 2(1 - c_{A2}) - \lambda_1 (c_{S1} + c_{M1}) - \lambda_2 (c_{S2} + c_{M2})
\end{aligned}
\tag{1.15}
$$

6. References

(1) Pross, A.; Pascal, R. The Origin of Life: What We Know, What We Can Know and What We Will Never Know. *Open Biol.* **2013**, *3* (3), 120190. https://doi.org/10.1098/rsob.120190.

(2) Preiner, M.; Asche, S.; Becker, S.; Betts, H. C.; Boniface, A.; Camprubi, E.; Chandru, K.; Erastova, V.; Garg, S. G.; Khawaja, N.; Kostyrka, G.; Machné, R.; Moggioli, G.; Muchowska, K. B.; Neukirchen, S.; Peter, B.; Pichlhöfer, E.; Radványi, Á.; Rossetto, D.; Salditt, A.; Schmelling, N. M.; Sousa, F. L.; Tria, F. D. K.; Vörös, D.; Xavier, J. C. The Future of Origin of Life Research: Bridging Decades-Old Divisions. *Life* **2020**, *10* (3), 20. https://doi.org/10.3390/life10030020.

(3) Sharma, A.; Czégel, D.; Lachmann, M.; Kempes, C. P.; Walker, S. I.; Cronin, L. Assembly Theory Explains and Quantifies Selection and Evolution. *Nature* **2023**, *622* (7982), 321–328. https://doi.org/10.1038/s41586-023-06600-9.

(4) Jirasek, M.; Sharma, A.; Bame, J. R.; Mehr, S. H. M.; Bell, N.; Marshall, S. M.; Mathis, C.; MacLeod, A.; Cooper, G. J. T.; Swart, M.; Mollfulleda, R.; Cronin, L. Investigating and Quantifying Molecular Complexity Using Assembly Theory and Spectroscopy. *ACS Cent. Sci.* **2024**, *10* (5), 1054–1064. https://doi.org/10.1021/acscentsci.4c00120.

(5) Tsokolov, S. A. Why Is the Definition of Life So Elusive? Epistemological Considerations. *Astrobiology* **2009**, *9* (4), 401–412. https://doi.org/10.1089/ast.2007.0201.

(6) Gayon, J. Defining Life: Synthesis and Conclusions. *Orig. Life Evol. Biospheres* **2010**, *40* (2), 231–244. https://doi.org/10.1007/s11084-010-9204-3.

(7) Tirard, S.; Morange, M.; Lazcano, A. The Definition of Life: A Brief History of an Elusive Scientific Endeavor. *Astrobiology* **2010**, *10* (10), 1003–1009. https://doi.org/10.1089/ast.2010.0535.

(8) Schrödinger, E. *What Is Life? The Physical Aspect of the Living Cell*, Repr.; Cambridge paperbacks Science; Cambridge Univ. Press: Cambridge, 2010.

(9) Lynn, M.; Carl, S.; Dorion, S. Life. In *Encyclopedia Britannica*; 2025.

(10) Muller, H. J. *Panel One: The Origin of Life, w: Evolution after Darwin: Issues in Evolution, t. 3, Red. S. Tax, C. Callender*; Chicago: The University of Chicago Press, 1959.

(11) Ebenhöh, O.; Ebeling, J.; Meyer, R.; Pohlkotte, F.; Nies, T. Microbial Pathway Thermodynamics: Stoichiometric Models Unveil Anabolic and Catabolic Processes. *Life* **2024**, *14* (2), 247. https://doi.org/10.3390/life14020247.

(12) Prigogine, I.; Lefever, R.; Goldbeter, A.; Herschkowitz-Kaufman, M. Symmetry Breaking Instabilities in Biological Systems. *Nature* **1969**, *223* (5209), 913–916. https://doi.org/10.1038/223913a0.

(13) Prigogine, I.; Lefever, R. Theory of Dissipative Structures. In *Synergetics: Cooperative Phenomena in Multi-Component Systems*; Haken, H., Ed.; Vieweg+Teubner Verlag: Wiesbaden, 1973; pp 124–135. https://doi.org/10.1007/978-3-663-01511-6_10.

(14) Goldbeter, A. Dissipative Structures in Biological Systems: Bistability, Oscillations, Spatial Patterns and Waves. *Philos. Trans. R. Soc. Math. Phys. Eng. Sci.* **2018**, *376* (2124), 20170376. https://doi.org/10.1098/rsta.2017.0376.

(15) *Chemical waves in a Belousov-Zhabotinsky (BZ) Reaction | College of Art and Design | RIT*. https://www.rit.edu/artdesign/spotlights/chemical-waves-belousov-zhabotinsky-bz-reaction (accessed 2025-05-11).

(16) Tyson, J. J.; Novák, B. Functional Motifs in Biochemical Reaction Networks. *Annu. Rev. Phys. Chem.* **2010**, *61*, 219–240. https://doi.org/10.1146/annurev.physchem.012809.103457.

(17) Alon, U. *An Introduction to Systems Biology: Design Principles of Biological Circuits*, Second edition.; CRC Press, Taylor & Francis Group: Boca Raton London New York, 2020. https://doi.org/10.1201/9780429283321.

(18) Mitrophanov, A. Y.; Groisman, E. A. Positive Feedback in Cellular Control Systems. *BioEssays* **2008**, *30* (6), 542–555. https://doi.org/10.1002/bies.20769.

(19) Cardelli, L.; Csikász-Nagy, A.; Dalchau, N.; Tribastone, M.; Tschaikowski, M. Noise Reduction in Complex Biological Switches. *Sci. Rep.* **2016**, *6* (1), 20214. https://doi.org/10.1038/srep20214.

(20) Veloz, T.; Flores, D. Reaction Network Modeling of Complex Ecological Interactions: Endosymbiosis and Multilevel Regulation. *Complexity* **2021**, *2021* (1), 8760937. https://doi.org/10.1155/2021/8760937.

(21) Roush, R. T.; McKenzie, J. A. Ecological Genetics of Insecticide and Acaricide Resistance. *Annu. Rev. Entomol.* **1987**, *32* (Volume 32, 1987), 361–380. https://doi.org/10.1146/annurev.en.32.010187.002045.

(22) Hoffmann, A. A.; Hercus, M. J. Environmental Stress as an Evolutionary Force. *BioScience* **2000**, *50* (3), 217. https://doi.org/10.1641/0006-3568(2000)050[0217:ESAAEF]2.3.CO;2.

(23) Lehninger, A. L.; Nelson, D. L.; Cox, M. M. *Lehninger Principles of Biochemistry*, 4th ed.; W.H. Freeman: New York, 2005.

(24) Leslie E., O. Prebiotic Chemistry and the Origin of the RNA World. *Crit. Rev. Biochem. Mol. Biol.* **2004**, *39* (2), 99–123. https://doi.org/10.1080/10409230490460765.

(25) Robertson, M. P.; Joyce, G. F. The Origins of the RNA World. *Cold Spring Harb. Perspect. Biol.* **2012**, *4* (5), a003608. https://doi.org/10.1101/cshperspect.a003608.

(26) Koonin, E. V.; Starokadomskyy, P. Are Viruses Alive? The Replicator Paradigm Sheds Decisive Light on an Old but Misguided Question. *Stud. Hist. Philos. Biol. Biomed. Sci.* **2016**, *59*, 125–134. https://doi.org/10.1016/j.shpsc.2016.02.016.

(27) Peters, J. W.; Williams, L. D. The Origin of Life: Look Up and Look Down. *Astrobiology* **2012**, *12* (11), 1087–1092. https://doi.org/10.1089/ast.2012.0818.

(28) Podolsky, K. A.; Devaraj, N. K. Synthesis of Lipid Membranes for Artificial Cells. *Nat. Rev. Chem.* **2021**, *5* (10), 676–694. https://doi.org/10.1038/s41570-021-00303-3.

(29) Szostak, J. W.; Bartel, D. P.; Luisi, P. L. Synthesizing Life. *Nature* **2001**, *409* (6818), 387–390. https://doi.org/10.1038/35053176.

(30) Elani, Y.; Seddon, J. M. What It Means to Be Alive: A Synthetic Cell Perspective. *Interface Focus* **2023**, *13* (5), 20230036. https://doi.org/10.1098/rsfs.2023.0036.

(31) Desai, A.; Mitchison, T. J. MICROTUBULE POLYMERIZATION DYNAMICS. *Annu. Rev. Cell Dev. Biol.* **1997**, *13* (Volume 13, 1997), 83–117. https://doi.org/10.1146/annurev.cellbio.13.1.83.

(32) de Forges, H.; Bouissou, A.; Perez, F. Interplay between Microtubule Dynamics and Intracellular Organization. *Int. J. Biochem. Cell Biol.* **2012**, *44* (2), 266–274. https://doi.org/10.1016/j.biocel.2011.11.009.

(33) Whitesides, G. M.; Grzybowski, B. Self-Assembly at All Scales. *Science* **2002**, *295* (5564), 2418–2421. https://doi.org/10.1126/science.1070821.

(34) Fialkowski, M.; Bishop, K. J. M.; Klajn, R.; Smoukov, S. K.; Campbell, C. J.; Grzybowski, B. A. Principles and Implementations of Dissipative (Dynamic) Self-Assembly. *J. Phys. Chem. B* **2006**, *110* (6), 2482–2496. https://doi.org/10.1021/jp054153q.

(35) Boekhoven, J.; Brizard, A. M.; Kowlgi, K. N. K.; Koper, G. J. M.; Eelkema, R.; van Esch, J. H. Dissipative Self-Assembly of a Molecular Gelator by Using a Chemical Fuel. *Angew. Chem. Int. Ed.* **2010**, *49* (28), 4825–4828. https://doi.org/10.1002/anie.201001511.

(36) Boekhoven, J.; Hendriksen, W. E.; Koper, G. J. M.; Eelkema, R.; van Esch, J. H. Transient Assembly of Active Materials Fueled by a Chemical Reaction. *Science* **2015**, *349* (6252), 1075–1079. https://doi.org/10.1126/science.aac6103.

(37) Cheng, G.; Perez-Mercader, J. Dissipative Self-Assembly of Dynamic Multicompartmentalized Microsystems with Light-Responsive Behaviors. *Chem* **2020**, *6* (5), 1160–1171. https://doi.org/10.1016/j.chempr.2020.02.009.

(38) Weißenfels, M.; Gemen, J.; Klajn, R. Dissipative Self-Assembly: Fueling with Chemicals versus Light. *Chem* **2021**, *7* (1), 23–37. https://doi.org/10.1016/j.chempr.2020.11.025.

(39) Grzelczak, M.; Liz-Marzán, L. M.; Klajn, R. Stimuli-Responsive Self-Assembly of Nanoparticles. *Chem. Soc. Rev.* **2019**, *48* (5), 1342–1361. https://doi.org/10.1039/C8CS00787J.

(40) Bian, T.; Chu, Z.; Klajn, R. The Many Ways to Assemble Nanoparticles Using Light. *Adv. Mater.* **2020**, *32* (20), 1905866. https://doi.org/10.1002/adma.201905866.

(41) Klajn, R.; Wesson, P. J.; Bishop, K. J. M.; Grzybowski, B. A. Writing Self-Erasing Images Using Metastable Nanoparticle "Inks." *Angew. Chem. Int. Ed.* **2009**, *48* (38), 7035–7039. https://doi.org/10.1002/anie.200901119.

(42) Sentürk, O. I.; Chervyachkova, E.; Ji, Y.; Wegner, S. V. Independent Blue and Red Light Triggered Narcissistic Self-Sorting Self-Assembly of Colloidal Particles. *Small* **2019**, *15* (25), 1901801. https://doi.org/10.1002/smll.201901801.

(43) Manna, D.; Udayabhaskararao, T.; Zhao, H.; Klajn, R. Orthogonal Light-Induced Self-Assembly of Nanoparticles Using Differently Substituted Azobenzenes. *Angew. Chem. Int. Ed.* **2015**, *54* (42), 12394–12397. https://doi.org/10.1002/anie.201502419.

(44) Kassem, S.; Leeuwen, T. van; Lubbe, A. S.; Wilson, M. R.; Feringa, B. L.; Leigh, D. A. Artificial Molecular Motors. *Chem. Soc. Rev.* **2017**, *46* (9), 2592–2621. https://doi.org/10.1039/C7CS00245A.

(45) Iino, R.; Kinbara, K.; Bryant, Z. Introduction: Molecular Motors. *Chem. Rev.* **2020**, *120* (1), 1–4. https://doi.org/10.1021/acs.chemrev.9b00819.

(46) Spudich, J. A. The Myosin Swinging Cross-Bridge Model. *Nat. Rev. Mol. Cell Biol.* **2001**, *2* (5), 387–392. https://doi.org/10.1038/35073086.

(47) Block, S. M. Kinesin Motor Mechanics: Binding, Stepping, Tracking, Gating, and Limping. *Biophys. J.* **2007**, *92* (9), 2986–2995. https://doi.org/10.1529/biophysj.106.100677.

(48) Koumura, N.; Zijlstra, R. W. J.; van Delden, R. A.; Harada, N.; Feringa, B. L. Light-Driven Monodirectional Molecular Rotor. *Nature* **1999**, *401* (6749), 152–155. https://doi.org/10.1038/43646.

(49) Ragazzon, G.; Baroncini, M.; Silvi, S.; Venturi, M.; Credi, A. Light-Powered Autonomous and Directional Molecular Motion of a Dissipative Self-Assembling System. *Nat. Nanotechnol.* **2015**, *10* (1), 70–75. https://doi.org/10.1038/nnano.2014.260.

(50) de Jong, J. J. D.; Lucas, L. N.; Kellogg, R. M.; van Esch, J. H.; Feringa, B. L. Reversible Optical Transcription of Supramolecular Chirality into Molecular Chirality. *Science* **2004**, *304* (5668), 278–281. https://doi.org/10.1126/science.1095353.

(51) Hernández, J. V.; Kay, E. R.; Leigh, D. A. A Reversible Synthetic Rotary Molecular Motor. *Science* **2004**, *306* (5701), 1532–1537. https://doi.org/10.1126/science.1103949.

(52) Wilson, M. R.; Solà, J.; Carlone, A.; Goldup, S. M.; Lebrasseur, N.; Leigh, D. A. An Autonomous Chemically Fuelled Small-Molecule Motor. *Nature* **2016**, *534* (7606), 235–240. https://doi.org/10.1038/nature18013.

(53) Amano, S.; Fielden, S. D. P.; Leigh, D. A. A Catalysis-Driven Artificial Molecular Pump. *Nature* **2021**, *594* (7864), 529–534. https://doi.org/10.1038/s41586-021-03575-3.

(54) Binks, L.; Tian, C.; Fielden, S. D. P.; Vitorica-Yrezabal, I. J.; Leigh, D. A. Transamidation-Driven Molecular Pumps. *J. Am. Chem. Soc.* **2022**, *144* (34), 15838–15844. https://doi.org/10.1021/jacs.2c06807.

(55) Craddock, T. J. A.; Tuszynski, J. A.; Chopra, D.; Casey, N.; Goldstein, L. E.; Hameroff, S. R.; Tanzi, R. E. The Zinc Dyshomeostasis Hypothesis of Alzheimer's Disease. *PLOS ONE* **2012**, *7* (3), e33552. https://doi.org/10.1371/journal.pone.0033552.

(56) Freeman, S. Biological Science. 2: Evolution, Diversity and Ecology; Pearson Prentice Hall: Upper Saddle River, N.J, 2005.

(57) Wong, A. S. Y.; Huck, W. T. S. Grip on Complexity in Chemical Reaction Networks. *Beilstein J. Org. Chem.* **2017**, *13* (1), 1486–1497. https://doi.org/10.3762/bjoc.13.147.

(58) Niederholtmeyer, H.; Stepanova, V.; Maerkl, S. J. Implementation of Cell-Free Biological Networks at Steady State. *Proc. Natl. Acad. Sci.* **2013**, *110* (40), 15985–15990. https://doi.org/10.1073/pnas.1311166110.

(59) Dubuc, E.; Pieters, P. A.; van der Linden, A. J.; van Hest, J. C.; Huck, W. T.; de Greef, T. F. Cell-Free Microcompartmentalised Transcription–Translation for the Prototyping of Synthetic Communication Networks. *Curr. Opin. Biotechnol.* **2019**, *58*, 72–80. https://doi.org/10.1016/j.copbio.2018.10.006.

(60) Genot, A. J.; Baccouche, A.; Sieskind, R.; Aubert-Kato, N.; Bredeche, N.; Bartolo, J. F.; Taly, V.; Fujii, T.; Rondelez, Y. High-Resolution Mapping of Bifurcations in Nonlinear Biochemical Circuits. *Nat. Chem.* **2016**, *8* (8), 760–767. https://doi.org/10.1038/nchem.2544.

(61) Turing, A. M. The Chemical Basis of Morphogenesis. *Philos. Trans. R. Soc. Lond. B. Biol. Sci.* **1952**, *237* (641), 37–72. https://doi.org/10.1098/rstb.1952.0012.

(62) Kondo, S.; Miura, T. Reaction-Diffusion Model as a Framework for Understanding Biological Pattern Formation. *Science* **2010**, *329* (5999), 1616–1620. https://doi.org/10.1126/science.1179047.

(63) Vittadello, S. T.; Leyshon, T.; Schnoerr, D.; Stumpf, M. P. H. Turing Pattern Design Principles and Their Robustness. *Philos. Trans. R. Soc. Math. Phys. Eng. Sci.* **2021**, *379* (2213), 20200272. https://doi.org/10.1098/rsta.2020.0272.

(64) Paul, S.; Adetunji, J.; Hong, T. Widespread Biochemical Reaction Networks Enable Turing Patterns without Imposed Feedback. *Nat. Commun.* **2024**, *15* (1), 8380. https://doi.org/10.1038/s41467-024-52591-0.

(65) Zaikin, A. N.; Zhabotinsky, A. M. Concentration Wave Propagation in Two-Dimensional Liquid-Phase Self-Oscillating System. *Nature* **1970**, *225* (5232), 535–537. https://doi.org/10.1038/225535b0.

(66) Epstein, I. R.; Xu, B. Reaction–Diffusion Processes at the Nano- and Microscales. *Nat. Nanotechnol.* **2016**, *11* (4), 312–319. https://doi.org/10.1038/nnano.2016.41.

(67) Leathers, A.; Walczak, M.; Brady, R. A.; Al Samad, A.; Kotar, J.; Booth, M. J.; Cicuta, P.; Di Michele, L. Reaction–Diffusion Patterning of DNA-Based Artificial Cells. *J. Am. Chem. Soc.* **2022**, *144* (38), 17468–17476. https://doi.org/10.1021/jacs.2c06140.

(68) Semenov, S. N.; Kraft, L. J.; Ainla, A.; Zhao, M.; Baghbanzadeh, M.; Campbell, V. E.; Kang, K.; Fox, J. M.; Whitesides, G. M. Autocatalytic, Bistable, Oscillatory Networks of Biologically Relevant Organic Reactions. *Nature* **2016**, *537* (7622), 656–660. https://doi.org/10.1038/nature19776.

(69) Epstein, I. R.; Showalter, K. Nonlinear Chemical Dynamics: Oscillations, Patterns, and Chaos. *J. Phys. Chem.* **1996**, *100* (31), 13132–13147. https://doi.org/10.1021/jp953547m.

(70) Semenov, S. N.; Wong, A. S. Y.; van der Made, R. M.; Postma, S. G. J.; Groen, J.; van Roekel, H. W. H.; de Greef, T. F. A.; Huck, W. T. S. Rational Design of Functional and Tunable Oscillating Enzymatic Networks. *Nat. Chem.* **2015**, *7* (2), 160–165. https://doi.org/10.1038/nchem.2142.

(71) Wong, A. S. Y.; Pogodaev, A. A.; Vialshin, I. N.; Helwig, B.; Huck, W. T. S. Molecular Engineering of Robustness and Resilience in Enzymatic Reaction Networks. *J. Am. Chem. Soc.* **2017**, *139* (24), 8146–8151. https://doi.org/10.1021/jacs.7b00632.

(72) ter Harmsel, M.; Maguire, O. R.; Runikhina, S. A.; Wong, A. S. Y.; Huck, W. T. S.; Harutyunyan, S. R. A Catalytically Active Oscillator Made from Small Organic Molecules. *Nature* **2023**, *621* (7977), 87–93. https://doi.org/10.1038/s41586-023-06310-2.

(73) Novichkov, A. I.; Hanopolskyi, A. I.; Miao, X.; Shimon, L. J. W.; Diskin-Posner, Y.; Semenov, S. N. Autocatalytic and Oscillatory Reaction Networks That Form Guanidines and Products of Their Cyclization. *Nat. Commun.* **2021**, *12* (1), 2994. https://doi.org/10.1038/s41467-021-23206-9.

(74) Semenov, S. N.; Ainla, A.; Skorb, E. V.; Postma, S. G. J. Four-Variable Model of an Enzymatic Oscillator Based on Trypsin. *Isr. J. Chem.* **2018**, *58* (6–7), 781–786. https://doi.org/10.1002/ijch.201700146.

(75) van Duppen, P.; Daines, E.; Robinson, W. E.; Huck, W. T. S. Dynamic Environmental Conditions Affect the Composition of a Model Prebiotic Reaction Network. *J. Am. Chem. Soc.* **2023**, *145* (13), 7559–7568. https://doi.org/10.1021/jacs.3c00908.

(76) Baltussen, M. G.; de Jong, T. J.; Duez, Q.; Robinson, W. E.; Huck, W. T. S. Chemical Reservoir Computation in a Self-Organizing Reaction Network. *Nature* **2024**, *631* (8021), 549–555. https://doi.org/10.1038/s41586-024-07567-x.

(77) Sharma, K. *Krebs Cycle- Definition, Reactions, and Steps*. https://scienceinfo.com/krebs-cycle-reactions-steps/ (accessed 2025-05-07).

(78) *How Did Animals Get Their Spots and Stripes?*. Discover Magazine. https://www.discovermagazine.com/planet-earth/how-did-animals-get-their-spots-and-stripes (accessed 2025-05-07).

(79) Robinson, W. E.; Daines, E.; van Duppen, P.; de Jong, T.; Huck, W. T. S. Environmental Conditions Drive Self-Organization of Reaction Pathways in a Prebiotic Reaction Network. *Nat. Chem.* **2022**, *14* (6), 623–631. https://doi.org/10.1038/s41557-022-00956-7.

(80) Graur, D.; Li, W.-H. *Fundamentals of Molecular Evolution*, 2nd ed.; Sinauer: Sunderland (Mass.), 2000.

(81) Rich, A. On the Problems of Evolution and Biochemical Information Transfer. *Horiz. Biochem.* **1962**, 103–126.

(82) Joyce, G. F. RNA Evolution and the Origins of Life. *Nature* **1989**, *338* (6212), 217–224. https://doi.org/10.1038/338217a0.

(83) Gilbert, W. Origin of Life: The RNA World. *Nature* **1986**, *319* (6055), 618–618. https://doi.org/10.1038/319618a0.

(84) Lincoln, T. A.; Joyce, G. F. Self-Sustained Replication of an RNA Enzyme. *Science* **2009**, *323* (5918), 1229–1232. https://doi.org/10.1126/science.1167856.

(85) Neveu, M.; Kim, H.-J.; Benner, S. A. The "Strong" RNA World Hypothesis: Fifty Years Old. *Astrobiology* **2013**, *13* (4), 391–403. https://doi.org/10.1089/ast.2012.0868.

(86) Benner, S. A. Paradoxes in the Origin of Life. *Orig. Life Evol. Biospheres* **2014**, *44* (4), 339–343. https://doi.org/10.1007/s11084-014-9379-0.

(87) Tanford, C. The Hydrophobic Effect and the Organization of Living Matter. *Science* **1978**, *200* (4345), 1012–1018. https://doi.org/10.1126/science.653353.

(88) Bachmann, P. A.; Walde, P.; Luisi, P. L.; Lang, J. Self-Replicating Reverse Micelles and Chemical Autopoiesis. *J. Am. Chem. Soc.* **1990**, *112* (22), 8200–8201. https://doi.org/10.1021/ja00178a073.

(89) Bachmann, P. A.; Luisi, P. L.; Lang, J. Autocatalytic Self-Replicating Micelles as Models for Prebiotic Structures. *Nature* **1992**, *357* (6373), 57–59. https://doi.org/10.1038/357057a0.

(90) Smokers, I. B. A.; Visser, B. S.; Slootbeek, A. D.; Huck, W. T. S.; Spruijt, E. How Droplets Can Accelerate Reactions─Coacervate Protocells as Catalytic Microcompartments. *Acc. Chem. Res.* **2024**, *57* (14), 1885–1895. https://doi.org/10.1021/acs.accounts.4c00114.

(91) Kahana, A.; Lancet, D. Self-Reproducing Catalytic Micelles as Nanoscopic Protocell Precursors. *Nat. Rev. Chem.* **2021**, *5* (12), 870–878. https://doi.org/10.1038/s41570-021-00329-7.

(92) Howlett, M. G.; Fletcher, S. P. From Autocatalysis to Survival of the Fittest in Self-Reproducing Lipid Systems. *Nat. Rev. Chem.* **2023**, *7* (10), 673–691. https://doi.org/10.1038/s41570-023-00524-8.

(93) Segré, D.; Ben-Eli, D.; Deamer, D. W.; Lancet, D. The Lipid World. *Orig. Life Evol. Biosph.* **2001**, *31* (1), 119–145. https://doi.org/10.1023/A:1006746807104.

(94) Bag, B. G.; Kiedrowski, G. von. Templates, Autocatalysis and Molecular Replication. *Pure Appl. Chem.* **1996**, *68* (11), 2145–2152. https://doi.org/10.1351/pac199668112145.

(95) Bissette, A. J.; Fletcher, S. P. Mechanisms of Autocatalysis. *Angew. Chem. Int. Ed.* **2013**, *52* (49), 12800–12826. https://doi.org/10.1002/anie.201303822.

(96) Bissette, A. J.; Fletcher, S. P. Novel Applications of Physical Autocatalysis. *Orig. Life Evol. Biospheres* **2015**, *45* (1), 21–30. https://doi.org/10.1007/s11084-015-9404-y.

(97) Soai, K.; Shibata, T.; Morioka, H.; Choji, K. Asymmetric Autocatalysis and Amplification of Enantiomeric Excess of a Chiral Molecule. *Nature* **1995**, *378* (6559), 767–768. https://doi.org/10.1038/378767a0.

(98) Carnall, J. M. A.; Waudby, C. A.; Belenguer, A. M.; Stuart, M. C. A.; Peyralans, J. J.-P.; Otto, S. Mechanosensitive Self-Replication Driven by Self-Organization. *Science* **2010**, *327* (5972), 1502–1506. https://doi.org/10.1126/science.1182767.

(99) Malakoutikhah, M.; Peyralans, J. J.-P.; Colomb-Delsuc, M.; Fanlo-Virgós, H.; Stuart, M. C. A.; Otto, S. Uncovering the Selection Criteria for the Emergence of Multi-Building-Block Replicators from Dynamic Combinatorial Libraries. *J. Am. Chem. Soc.* **2013**, *135* (49), 18406–18417. https://doi.org/10.1021/ja4067805.

(100) Liu, B.; Wu, J.; Geerts, M.; Markovitch, O.; Pappas, C. G.; Liu, K.; Otto, S. Out-of-Equilibrium Self-Replication Allows Selection for Dynamic Kinetic Stability in a System of Competing Replicators. *Angew. Chem. Int. Ed.* **2022**, *61* (18), e202117605. https://doi.org/10.1002/anie.202117605.

(101) Sadownik, J. W.; Mattia, E.; Nowak, P.; Otto, S. Diversification of Self-Replicating Molecules. *Nat. Chem.* **2016**, *8* (3), 264–269. https://doi.org/10.1038/nchem.2419.

(102) Ottelé, J.; Hussain, A. S.; Mayer, C.; Otto, S. Chance Emergence of Catalytic Activity and Promiscuity in a Self-Replicator. *Nat. Catal.* **2020**, *3* (7), 547–553. https://doi.org/10.1038/s41929-020-0463-8.

(103) Bachmann, P. A.; Walde, P.; Luisi, P. L.; Lang, J. Self-Replicating Micelles: Aqueous Micelles and Enzymatically Driven Reactions in Reverse Micelles. *J. Am. Chem. Soc.* **1991**, *113* (22), 8204–8209. https://doi.org/10.1021/ja00022a002.

(104) Bissette, A. J.; Odell, B.; Fletcher, S. P. Physical Autocatalysis Driven by a Bond-Forming Thiol–Ene Reaction. *Nat. Commun.* **2014**, *5* (1), 4607. https://doi.org/10.1038/ncomms5607.

(105) Post, E. A. J.; Bissette, A. J.; Fletcher, S. P. Self-Reproducing Micelles Coupled to a Secondary Catalyst. *Chem. Commun.* **2018**, *54* (63), 8777–8780. https://doi.org/10.1039/C8CC02136H.

(106) Post, E. A. J.; Fletcher, S. P. Controlling the Kinetics of Self-Reproducing Micelles by Catalyst Compartmentalization in a Biphasic System. *J. Org. Chem.* **2019**, *84* (5), 2741–2755. https://doi.org/10.1021/acs.joc.8b03149.

(107) Colomer, I.; Morrow, S. M.; Fletcher, S. P. A Transient Self-Assembling Self-Replicator. *Nat. Commun.* **2018**, *9* (1), 2239. https://doi.org/10.1038/s41467-018-04670-2.

(108) Morrow, S. M.; Colomer, I.; Fletcher, S. P. A Chemically Fuelled Self-Replicator. *Nat. Commun.* **2019**, *10* (1), 1011. https://doi.org/10.1038/s41467-019-08885-9.

(109) Engwerda, A. H. J.; Southworth, J.; Lebedeva, M. A.; Scanes, R. J. H.; Kukura, P.; Fletcher, S. P. Coupled Metabolic Cycles Allow Out-of-Equilibrium Autopoietic Vesicle Replication. *Angew. Chem. Int. Ed.* **2020**, *59* (46), 20361–20366. https://doi.org/10.1002/anie.202007302.

(110) Post, E. A. J.; Fletcher, S. P. Dissipative Self-Assembly, Competition and Inhibition in a Self-Reproducing Protocell Model. *Chem. Sci.* **2020**, *11* (35), 9434–9442. https://doi.org/10.1039/D0SC02768E.

(111) Colomer, I.; Borissov, A.; Fletcher, S. P. Selection from a Pool of Self-Assembling Lipid Replicators. *Nat. Commun.* **2020**, *11* (1), 176. https://doi.org/10.1038/s41467-019-13903-x.

(112) Howlett, M. G.; Scanes, R. J. H.; Fletcher, S. P. Selection between Competing Self-Reproducing Lipids: Succession and Dynamic Activation. *JACS Au* **2021**, *1* (9), 1355–1361. https://doi.org/10.1021/jacsau.1c00138.

(113) Ortega-Arroyo, J.; Bissette, A. J.; Kukura, P.; Fletcher, S. P. Visualization of the Spontaneous Emergence of a Complex, Dynamic, and Autocatalytic System. *Proc. Natl. Acad. Sci.* **2016**, *113* (40), 11122–11126. https://doi.org/10.1073/pnas.1602363113.

(114) Engwerda, A. H. J.; Fletcher, S. P. A Molecular Assembler That Produces Polymers. *Nat. Commun.* **2020**, *11* (1), 4156. https://doi.org/10.1038/s41467-020-17814-0.

(115) Lebedeva, M. A.; Palmieri, E.; Kukura, P.; Fletcher, S. P. Emergence and Rearrangement of Dynamic Supramolecular Aggregates Visualized by Interferometric Scattering Microscopy. *ACS Nano* **2020**, *14* (9), 11160–11168. https://doi.org/10.1021/acsnano.0c02414.

(116) Patke, A.; Young, M. W.; Axelrod, S. Molecular Mechanisms and Physiological Importance of Circadian Rhythms. *Nat. Rev. Mol. Cell Biol.* **2020**, *21* (2), 67–84. https://doi.org/10.1038/s41580-019-0179-2.

(117) Dupont, G.; Combettes, L.; Bird, G. S.; Putney, J. W. Calcium Oscillations. *Cold Spring Harb. Perspect. Biol.* **2011**, *3* (3), a004226. https://doi.org/10.1101/cshperspect.a004226.

(118) Cao, Y.; Wang, H.; Ouyang, Q.; Tu, Y. The Free-Energy Cost of Accurate Biochemical Oscillations. *Nat. Phys.* **2015**, *11* (9), 772–778. https://doi.org/10.1038/nphys3412.

(119) Novak, B.; Tyson, J. J. Design Principles of Biochemical Oscillators. *Nat. Rev. Mol. Cell Biol.* **2008**, *9* (12), 981–991. https://doi.org/10.1038/nrm2530.

(120) Lotka, A. J. Contribution to the Theory of Periodic Reactions. *J. Phys. Chem.* **1910**, *14* (3), 271–274. https://doi.org/10.1021/j150111a004.

(121) Mackey, M. C.; Glass, L. Oscillation and Chaos in Physiological Control Systems. *Science* **1977**, *197* (4300), 287–289. https://doi.org/10.1126/science.267326.

(122) Yamaguchi, I.; Ogawa, Y.; Jimbo, Y.; Nakao, H.; Kotani, K. Reduction Theories Elucidate the Origins of Complex Biological Rhythms Generated by Interacting Delay-Induced Oscillations. *PLOS ONE* **2011**, *6* (11), e26497. https://doi.org/10.1371/journal.pone.0026497.

(123) Prigogine, I.; Lefever, R. Symmetry Breaking Instabilities in Dissipative Systems. II. *J. Chem. Phys.* **1968**, *48* (4), 1695–1700. https://doi.org/10.1063/1.1668896.

(124) Bray, W. C. A PERIODIC REACTION IN HOMOGENEOUS SOLUTION AND ITS RELATION TO CATALYSIS. *J. Am. Chem. Soc.* **1921**, *43* (6), 1262–1267. https://doi.org/10.1021/ja01439a007.

(125) Bray, W. C.; Liebhafsky, H. A. REACTIONS INVOLVING HYDROGEN PEROXIDE, IODINE AND IODATE ION. I. INTRODUCTION. *J. Am. Chem. Soc.* **1931**, *53* (1), 38–44. https://doi.org/10.1021/ja01352a006.

(126) Briggs, T. S.; Rauscher, W. C. An Oscillating Iodine Clock. *Journal of Chemical Education*, 1973, *50*, 496. https://doi.org/10.1021/ed050p496.

(127) Pechenkin, A. On the Origin of the Belousov-Zhabotinsky Reaction. *Biol. Theory* **2009**, *4* (2), 196–206. https://doi.org/10.1162/biot.2009.4.2.196.

(128) Nicolis, G.; Portnow, J. Chemical Oscillations. *Chem. Rev.* **1973**, *73* (4), 365–384. https://doi.org/10.1021/cr60284a003.

(129) De Kepper, P.; Epstein, I. R.; Kustin, K. A Systematically Designed Homogeneous Oscillating Reaction: The Arsenite-Iodate-Chlorite System. *J. Am. Chem. Soc.* **1981**, *103* (8), 2133–2134. https://doi.org/10.1021/ja00398a061.

(130) Orbán, M.; De Kepper, P.; Epstein, I. R.; Kustin, K. New Family of Homogeneous Chemical Oscillators: Chlorite–Iodate–Substrate. *Nature* **1981**, *292* (5826), 816–818. https://doi.org/10.1038/292816a0.

(131) Jensen, J. H. New Type of Oscillating Reaction: Air Oxidation of Benzaldehyde. *J. Am. Chem. Soc.* **1983**, *105* (9), 2639–2641. https://doi.org/10.1021/ja00347a020.

(132) Burger, M.; Field, R. J. A New Chemical Oscillator Containing Neither Metal nor Oxyhalogen Ions. *Nature* **1984**, *307* (5953), 720–721. https://doi.org/10.1038/307720a0.

(133) Orban, M.; Epstein, I. R. A New Halogen-Free Chemical Oscillator: The Reaction between Sulfide Ion and Hydrogen Peroxide in a CSTR. *J. Am. Chem. Soc.* **1985**, *107* (8), 2302–2305. https://doi.org/10.1021/ja00294a016.

(134) Kovacs, K.; McIlwaine, R. E.; Scott, S. K.; Taylor, A. F. pH Oscillations and Bistability in the Methylene Glycol–Sulfite–Gluconolactone Reaction. *Phys. Chem. Chem. Phys.* **2007**, *9* (28), 3711–3716. https://doi.org/10.1039/B704407K.

(135) Epstein, I. R. The Role of Flow Systems in Far-from-Equilibrium Dynamics. *J. Chem. Educ.* **1989**, *66* (3), 191. https://doi.org/10.1021/ed066p191.

(136) Szántó, T. G.; Rábai, G. pH Oscillations in the BrO3-−SO32-/HSO3- Reaction in a CSTR. *J. Phys. Chem. A* **2005**, *109* (24), 5398–5402. https://doi.org/10.1021/jp050833h.

(137) De Kepper, P.; Epstein, I. R.; Kustin, K. Bistability in the Oxidation of Arsenite by Iodate in a Stirred Flow Reactor. *J. Am. Chem. Soc.* **1981**, *103* (20), 6121–6127. https://doi.org/10.1021/ja00410a023.

(138) Dateo, C. E.; Orban, M.; De Kepper, P.; Epstein, I. R. Bistability and Oscillations in the Autocatalytic Chlorite-Iodide Reaction in a Stirred-Flow Reactor. *J. Am. Chem. Soc.* **1982**, *104* (2), 504–509. https://doi.org/10.1021/ja00366a021.

(139) Dolnik, M.; Abbott, L. F.; Epstein, I. R. Concentration-Dependent Regulation of Flow Rate in a Chemical Oscillator. *J. Phys. Chem.* **1994**, *98* (40), 10124–10130. https://doi.org/10.1021/j100091a030.

(140) Dolnik, M.; Banks, A. S.; Epstein, I. R. Oscillatory Chemical Reaction in a CSTR with Feedback Control of Flow Rate. *J. Phys. Chem. A* **1997**, *101* (28), 5148–5154. https://doi.org/10.1021/jp970728a.

(141) Boissonade, J.; De Kepper, P. Transitions from Bistability to Limit Cycle Oscillations. Theoretical Analysis and Experimental Evidence in an Open Chemical System. *J. Phys. Chem.* **1980**, *84* (5), 501–506. https://doi.org/10.1021/j100442a009.

(142) Aubel, D.; Fussenegger, M. Watch the Clock—Engineering Biological Systems to Be on Time. *Curr. Opin. Genet. Dev.* **2010**, *20* (6), 634–643. https://doi.org/10.1016/j.gde.2010.09.003.

(143) Maguire, O. R.; Huck, W. T. S. On the Importance of Reaction Networks for Synthetic Living Systems. *Emerg. Top. Life Sci.* **2019**, *3* (5), 517–527. https://doi.org/10.1042/ETLS20190016.

(144) Roekel, H. W. H. van; Rosier, B. J. H. M.; Meijer, L. H. H.; Hilbers, P. A. J.; Markvoort, A. J.; Huck, W. T. S.; Greef, T. F. A. de. Programmable Chemical Reaction Networks: Emulating Regulatory Functions in Living Cells Using a Bottom-up Approach. *Chem. Soc. Rev.* **2015**, *44* (21), 7465–7483. https://doi.org/10.1039/C5CS00361J.

(145) Cafferty, B. J.; Wong, A. S. Y.; Semenov, S. N.; Belding, L.; Gmür, S.; Huck, W. T. S.; Whitesides, G. M. Robustness, Entrainment, and Hybridization in Dissipative Molecular Networks, and the Origin of Life. *J. Am. Chem. Soc.* **2019**, *141* (20), 8289–8295. https://doi.org/10.1021/jacs.9b02554.

(146) Li, X.; Fomitskaya, P.; Smaliak, V. A.; Smith, B. S.; Skorb, E. V.; Semenov, S. N. Selenium Catalysis Enables Negative Feedback Organic Oscillators. *Nat. Commun.* **2024**, *15* (1), 3316. https://doi.org/10.1038/s41467-024-47714-6.

(147) Pogodaev, A. A.; Wong, A. S. Y.; Huck, W. T. S. Photochemical Control over Oscillations in Chemical Reaction Networks. *J. Am. Chem. Soc.* **2017**, *139* (43), 15296–15299. https://doi.org/10.1021/jacs.7b08109.

(148) Pogodaev, A. A.; Lap, T. T.; Huck, W. T. S. The Dynamics of an Oscillating Enzymatic Reaction Network Is Crucially Determined by Side Reactions. *ChemSystemsChem* **2021**, *3* (1), e2000033. https://doi.org/10.1002/syst.202000033.

(149) Maguire, O. R.; Wong, A. S. Y.; Baltussen, M. G.; van Duppen, P.; Pogodaev, A. A.; Huck, W. T. S. Dynamic Environments as a Tool to Preserve Desired Output in a Chemical Reaction Network. *Chem. – Eur. J.* **2020**, *26* (7), 1676–1682. https://doi.org/10.1002/chem.201904725.

(150) Lagzi, I.; Wang, D.; Kowalczyk, B.; Grzybowski, B. A. Vesicle-to-Micelle Oscillations and Spatial Patterns. *Langmuir* **2010**, *26* (17), 13770–13772. https://doi.org/10.1021/la102635w.

(151) Lagzi, I.; Kowalczyk, B.; Wang, D.; Grzybowski, B. A. Nanoparticle Oscillations and Fronts. *Angew. Chem. Int. Ed.* **2010**, *49* (46), 8616–8619. https://doi.org/10.1002/anie.201004231.

(152) Kim, Y. S.; Tamate, R.; Akimoto, A. M.; Yoshida, R. Recent Developments in Self-Oscillating Polymeric Systems as Smart Materials: From Polymers to Bulk Hydrogels. *Mater. Horiz.* **2017**, *4* (1), 38–54. https://doi.org/10.1039/C6MH00435K.

(153) Yoshida, R.; Sakai, T.; Ito, S.; Yamaguchi, T. Self-Oscillation of Polymer Chains with Rhythmical Soluble-Insoluble Changes. *J. Am. Chem. Soc.* **2002**, *124* (27), 8095–8098. https://doi.org/10.1021/ja012584q.

(154) Ueki, T.; Yoshida, R. Recent Aspects of Self-Oscillating Polymeric Materials: Designing Self-Oscillating Polymers Coupled with Supramolecular Chemistry and Ionic Liquid Science. *Phys. Chem. Chem. Phys.* **2014**, *16* (22), 10388–10397. https://doi.org/10.1039/C4CP00980K.

(155) Tamate, R.; Ueki, T.; Shibayama, M.; Yoshida, R. Self-Oscillating Vesicles: Spontaneous Cyclic Structural Changes of Synthetic Diblock Copolymers. *Angew. Chem. Int. Ed.* **2014**, *53* (42), 11248–11252. https://doi.org/10.1002/anie.201406953.

(156) Yoshida, R.; Takahashi, T.; Yamaguchi, T.; Ichijo, H. Self-Oscillating Gel. *J. Am. Chem. Soc.* **1996**, *118* (21), 5134–5135. https://doi.org/10.1021/ja9602511.

(157) Howlett, M. G.; Engwerda, A. H. J.; Scanes, R. J. H.; Fletcher, S. P. An Autonomously Oscillating Supramolecular Self-Replicator. *Nat. Chem.* **2022**, *14* (7), 805–810. https://doi.org/10.1038/s41557-022-00949-6.

(158) Avnir, D. Chemically Induced Pulsations of Interfaces: The Mercury Beating Heart. *J. Chem. Educ.* **1989**, *66* (3), 211. https://doi.org/10.1021/ed066p211.

(159) Lin, S.-W.; Keizer, J.; Rock, P. A.; Stenschke, H. On the Mechanism of Oscillations in the "Beating Mercury Heart." *Proc. Natl. Acad. Sci.* **1974**, *71* (11), 4477–4481. https://doi.org/10.1073/pnas.71.11.4477.

(160) He, X.; Aizenberg, M.; Kuksenok, O.; Zarzar, L. D.; Shastri, A.; Balazs, A. C.; Aizenberg, J. Synthetic Homeostatic Materials with Chemo-Mechano-Chemical Self-Regulation. *Nature* **2012**, *487* (7406), 214–218. https://doi.org/10.1038/nature11223.

(161) Aizawa, A.; Asakura, K. Theory of Turing Pattern Formation and Its Experimental Realization in the CIMA Reaction System in the Presence of Materials Lowering the Diffusivity of Activators. *Front. Phys.* **2024**, *12*. https://doi.org/10.3389/fphy.2024.1358766.

(162) De Kepper, P.; Epstein, I. R.; Kustin, K.; Orban, M. Batch Oscillations and Spatial Wave Patterns in Chlorite Oscillating Systems. *J. Phys. Chem.* **1982**, *86* (2), 170–171. https://doi.org/10.1021/j100391a007.

(163) Castets, V.; Dulos, E.; Boissonade, J.; De Kepper, P. Experimental Evidence of a Sustained Standing Turing-Type Nonequilibrium Chemical Pattern. *Phys. Rev. Lett.* **1990**, *64* (24), 2953–2956. https://doi.org/10.1103/PhysRevLett.64.2953.

(164) Asakura, K.; Konishi, R.; Nakatani, T.; Nakano, T.; Kamata, M. Turing Pattern Formation by the CIMA Reaction in a Chemical System Consisting of Quaternary Alkyl Ammonium Cationic Groups. *J. Phys. Chem. B* **2011**, *115* (14), 3959–3963. https://doi.org/10.1021/jp111584u.

(165) Vanag, V. K.; Epstein, I. R. Pattern Formation in a Tunable Medium: The Belousov-Zhabotinsky Reaction in an Aerosol OT Microemulsion. *Phys. Rev. Lett.* **2001**, *87* (22), 228301. https://doi.org/10.1103/PhysRevLett.87.228301.

(166) Howlett, M. G.; Engwerda, A. H. J.; Fletcher, S. P. Information Transduction via Fuel-Controlled Chemical Waves. *Chem* **2024**, *10* (9), 2861–2871. https://doi.org/10.1016/j.chempr.2024.05.010.

(167) Kuhnert, L.; Agladze, K. I.; Krinsky, V. I. Image Processing Using Light-Sensitive Chemical Waves. *Nature* **1989**, *337* (6204), 244–247. https://doi.org/10.1038/337244a0.

(168) Tóth, Á.; Showalter, K. Logic Gates in Excitable Media. *J. Chem. Phys.* **1995**, *103* (6), 2058–2066. https://doi.org/10.1063/1.469732.

(169) Stevens, W. M.; Adamatzky, A.; Jahan, I.; Costello, B. de L. Time-Dependent Wave Selection for Information Processing in Excitable Media. *Phys. Rev. E* **2012**, *85* (6), 066129. https://doi.org/10.1103/PhysRevE.85.066129.

(170) Parrilla-Gutierrez, J. M.; Sharma, A.; Tsuda, S.; Cooper, G. J. T.; Aragon-Camarasa, G.; Donkers, K.; Cronin, L. A Programmable Chemical Computer with Memory and Pattern Recognition. *Nat. Commun.* **2020**, *11* (1), 1442. https://doi.org/10.1038/s41467-020-15190-3.

(171) Sharma, A.; Ng, M. T.-K.; Parrilla Gutierrez, J. M.; Jiang, Y.; Cronin, L. A Programmable Hybrid Digital Chemical Information Processor Based on the Belousov-Zhabotinsky Reaction. *Nat. Commun.* **2024**, *15* (1), 1984. https://doi.org/10.1038/s41467-024-45896-7.

(172) Aguilar, W.; Santamaría-Bonfil, G.; Froese, T.; Gershenson, C. The Past, Present, and Future of Artificial Life, 2014, *1*, 8. https://doi.org/10.3389/frobt.2014.00008.

(173) Sasselov, D. D.; Grotzinger, J. P.; Sutherland, J. D. The Origin of Life as a Planetary Phenomenon. *Science Advances*, 2020, *6*, eaax3419. https://doi.org/ARTN eaax3419 10.1126/sciadv.aax3419.

(174) Miller, S. L. A Production of Amino Acids under Possible Primitive Earth Conditions. *Science*, 1953, *117*, 528–529. https://doi.org/DOI 10.1126/science.117.3046.528.

(175) Miller, S. L.; Urey, H. C. Organic Compound Synthesis on the Primitive Earth. *Science*, 1959, *130*, 245–251. https://doi.org/DOI 10.1126/science.130.3370.245.

(176) Termonia, Y.; Ross, J. Oscillations and Control Features in Glycolysis: Numerical Analysis of a Comprehensive Model. *Proceedings of the National Academy of Sciences of the United States of America*, 1981, *78*, 2952–2956. https://doi.org/10.1073/pnas.78.5.2952.

(177) Bar-Or, R. L.; Maya, R.; Segel, L. A.; Alon, U.; Levine, A. J.; Oren, M. Generation of Oscillations by the P53-Mdm2 Feedback Loop: A Theoretical and Experimental Study. *Proceedings of the National Academy of Sciences of the United States of America*, 2000, *97*, 11250–11255. https://doi.org/DOI 10.1073/pnas.210171597.

(178) Bell-Pedersen, D.; Cassone, V. M.; Earnest, D. J.; Golden, S. S.; Hardin, P. E.; Thomas, T. L.; Zoran, M. J. Circadian Rhythms from Multiple Oscillators: Lessons from Diverse Organisms. *Nature reviews. Genetics*, 2005, *6*, 544–556. https://doi.org/10.1038/nrg1633.

(179) Schafer, K. A. The Cell Cycle: A Review. *Veterinary Pathology*, 1998, *35*, 461–478. https://doi.org/Doi 10.1177/030098589803500601.

(180) Lu, Y.; Allegri, G.; Huskens, J. Vesicle-Based Artificial Cells: Materials, Construction Methods and Applications. *Materials Horizons*, 2022, *9*, 892–907. https://doi.org/10.1039/d1mh01431e.

(181) Fenz, S. F.; Sengupta, K. Giant Vesicles as Cell Models. *Integrative Biology*, 2012, *4*, 982–995. https://doi.org/10.1039/c2ib00188h.

(182) Dautel, D. R.; Heller, W. T.; Champion, J. A. Protein Vesicles with pH-Responsive Disassembly. *Biomacromolecules*, 2022, *23*, 3678–3687. https://doi.org/10.1021/acs.biomac.2c00562.

(183) Belluati, A.; Thamboo, S.; Najer, A.; Maffeis, V.; von Planta, C.; Craciun, I.; Palivan, C. G.; Meier, W. Multicompartment Polymer Vesicles with Artificial Organelles for Signal-Triggered Cascade Reactions Including Cytoskeleton Formation. *Advanced Functional Materials*, 2020, *30*, 2002949. https://doi.org/ARTN 2002949 10.1002/adfm.202002949.

(184) Martino, C.; deMello, A. J. Droplet-Based Microfluidics for Artificial Cell Generation: A Brief Review. *Interface Focus*, 2016, *6*, 20160011. https://doi.org/10.1098/rsfs.2016.0011.

(185) Wick, R.; Luisi, P. L. Enzyme-Containing Liposomes Can Endogenously Produce Membrane-Constituting Lipids. *Chemistry & Biology*, 1996, *3*, 277–285. https://doi.org/Doi 10.1016/S1074-5521(96)90107-6.

(186) Kruse, K.; Julicher, F. Oscillations in Cell Biology. *Current Opinion in Cell Biology*, 2005, *17*, 20–26. https://doi.org/10.1016/j.ceb.2004.12.007.

(187) Ragazzon, G.; Malferrari, M.; Arduini, A.; Secchi, A.; Rapino, S.; Silvi, S.; Credi, A. Autonomous Non-Equilibrium Self-Assembly and Molecular Movements Powered by Electrical Energy. *Angewandte Chemie International Edition*, 2023, *62*, e202214265. https://doi.org/10.1002/anie.202214265.

(188) Degn, H. Oscillating Chemical Reactions in Homogeneous Phase. *Journal of Chemical Education*, 1972, *49*, 302–307. https://doi.org/DOI 10.1021/ed049p302.

(189) Winfree, A. T. The Prehistory of the Belousov-Zhabotinsky Oscillator. *Journal of Chemical Education*, 1984, *61*, 661–663. https://doi.org/DOI 10.1021/ed061p661.

(190) Wojtowicz, J. Oscillatory Behavior in Electrochemical Systems. *Modern aspects of electrochemistry: No. 8*, 1972, 47–120. https://doi.org/10.1007/978-1-4615-7440-8_2.

(191) Leira-Iglesias, J.; Tassoni, A.; Adachi, T.; Stich, M.; Hermans, T. M. Oscillations, Travelling Fronts and Patterns in a Supramolecular System. *Nat. Nanotechnol.* **2018**, *13* (11), 1021–1027. https://doi.org/10.1038/s41565-018-0270-4.

(192) Helm, M. P. van der; Beun, T. de; Eelkema, R. On the Use of Catalysis to Bias Reaction Pathways in Out-of-Equilibrium Systems. *Chem. Sci.* **2021**, *12* (12), 4484–4493. https://doi.org/10.1039/D0SC06406H.

(193) Dzieciol, A. J.; Mann, S. Designs for Life: Protocell Models in the Laboratory. *Chemical Society Reviews*, 2012, *41*, 79–85. https://doi.org/10.1039/c1cs15211d.

(194) Budin, I.; Szostak, J. W. Physical Effects Underlying the Transition from Primitive to Modern Cell Membranes. *Proceedings of the National Academy of Sciences of the United States of America*, 2011, *108*, 5249–5254. https://doi.org/10.1073/pnas.1100498108.

(195) Lin, C.; Katla, S. K.; Pérez-Mercader, J. Photochemically Induced Cyclic Morphological Dynamics via Degradation of Autonomously Produced, Self-Assembled Polymer Vesicles. *Commun. Chem.* **2021**, *4* (1), 25. https://doi.org/10.1038/s42004-021-00464-8.

(196) Albertsen, A. N.; Szymański, J. K.; Pérez-Mercader, J. Emergent Properties of Giant Vesicles Formed by a Polymerization-Induced Self-Assembly (PISA) Reaction. *Sci. Rep.* **2017**, *7* (1), 41534. https://doi.org/10.1038/srep41534.

(197) Young, G.; Hundt, N.; Cole, D.; Fineberg, A.; Andrecka, J.; Tyler, A.; Olerinyova, A.; Ansari, A.; Marklund, E. G.; Collier, M. P.; Chandler, S. A.; Tkachenko, O.; Allen, J.; Crispin, M.; Billington, N.; Takagi, Y.; Sellers, J. R.; Eichmann, C.; Selenko, P.; Frey, L.; Riek, R.; Galpin, M. R.; Struwe, W. B.; Benesch, J. L. P.; Kukura, P. Quantitative Mass Imaging of Single Biological Macromolecules. *Science*, 2018, *360*, 423–427. https://doi.org/10.1126/science.aar5839.

(198) Stetefeld, J.; McKenna, S. A.; Patel, T. R. Dynamic Light Scattering: A Practical Guide and Applications in Biomedical Sciences. *Biophysical reviews*, 2016, *8*, 409–427. https://doi.org/10.1007/s12551-016-0218-6.

(199) Giuliano, C. B.; Cvjetan, N.; Ayache, J.; Walde, P. Multivesicular Vesicles: Preparation and Applications. *ChemSystemsChem* **2021**, *3* (2), e2000049. https://doi.org/10.1002/syst.202000049.

(200) Kiprijanov, K. S. Chaos and Beauty in a Beaker: The Early History of the Belousov-Zhabotinsky Reaction. *Ann. Phys.* **2016**, *528* (3–4), 233–237. https://doi.org/10.1002/andp.201600025.

(201) Lefever, R.; Nicolis, G.; Prigogine, I. On the Occurrence of Oscillations around the Steady State in Systems of Chemical Reactions Far from Equilibrium. *J. Chem. Phys.* **1967**, *47* (3), 1045–1047. https://doi.org/10.1063/1.1711987.

(202) Noyes, R. M.; Field, R. J. Oscillatory Chemical Reactions. *Annu. Rev. Phys. Chem.* **1974**, *25* (Volume 25,), 95–119. https://doi.org/10.1146/annurev.pc.25.100174.000523.

(203) Field, R. J.; Noyes, R. M. Oscillations in Chemical Systems. IV. Limit Cycle Behavior in a Model of a Real Chemical Reaction. *J. Chem. Phys.* **1974**, *60* (5), 1877–1884. https://doi.org/10.1063/1.1681288.

(204) O'Keeffe, K. P.; Hong, H.; Strogatz, S. H. Oscillators That Sync and Swarm. *Nat. Commun.* **2017**, *8* (1), 1504. https://doi.org/10.1038/s41467-017-01190-3.

(205) Lombardo, D.; Kiselev, M. A.; Magazù, S.; Calandra, P. Amphiphiles Self-Assembly: Basic Concepts and Future Perspectives of Supramolecular Approaches. *Adv. Condens. Matter Phys.* **2015**, *2015* (1), 151683. https://doi.org/10.1155/2015/151683.

(206) Yue, W.; Zhao, Y.; Shao, S.; Tian, H.; Xie, Z.; Geng, Y.; Wang, F. Novel NIR-Absorbing Conjugated Polymers for Efficient Polymer Solar Cells: Effect of Alkyl Chain Length on Device Performance. *J. Mater. Chem.* **2009**, *19* (15), 2199–2206. https://doi.org/10.1039/B818885H.

(207) Mastronarde, D. N. Automated Electron Microscope Tomography Using Robust Prediction of Specimen Movements. *J. Struct. Biol.* **2005**, *152* (1), 36–51. https://doi.org/10.1016/j.jsb.2005.07.007.

(208) Schindelin, J.; Arganda-Carreras, I.; Frise, E.; Kaynig, V.; Longair, M.; Pietzsch, T.; Preibisch, S.; Rueden, C.; Saalfeld, S.; Schmid, B.; Tinevez, J.-Y.; White, D. J.; Hartenstein, V.; Eliceiri, K.; Tomancak, P.; Cardona, A. Fiji: An Open-Source Platform for Biological-Image Analysis. *Nat. Methods* **2012**, *9* (7), 676–682. https://doi.org/10.1038/nmeth.2019.